

Circulation along the northern slope of the Greenland-Scotland Ridge

Stefanie Semper

Thesis for the degree of Philosophiae Doctor (PhD)
University of Bergen, Norway
2020

UNIVERSITY OF BERGEN



Circulation along the northern slope of the Greenland-Scotland Ridge

Stefanie Semper



Thesis for the degree of Philosophiae Doctor (PhD)
at the University of Bergen

Date of defense: 11.12.2020

© Copyright Stefanie Semper

The material in this publication is covered by the provisions of the Copyright Act.

Year: 2020

Title: Circulation along the northern slope of the Greenland-Scotland Ridge

Name: Stefanie Semper

Print: Skipnes Kommunikasjon / University of Bergen

Scientific environment

The research conducted for this work was carried out at the Geophysical Institute at the University of Bergen and the Bjerknes Centre for Climate Research. My position was associated with the project "Overturning in the Nordic Seas", which was funded by the Bergen Research Foundation (Grant BFS2016REK01) and led by my main advisor Kjetil Våge. My co-advisor Robert S. Pickart kindly hosted me for a six-month and a three-month research stay at the Woods Hole Oceanographic Institution, USA, in autumn 2017 and summer 2019, respectively. A shorter research visit in spring 2019 at the University of Akureyri, Iceland, was kindly hosted by Steingrímur Jónsson. These research stays were partly funded by the Ocean Outlook program and the Meltzer foundation at the University of Bergen. Throughout my PhD I have been enrolled in the Norwegian Research School on Changing Climates in the coupled Earth System (CHESS).



UNIVERSITY OF BERGEN
Faculty of Mathematics and Natural Sciences

BJERKNES CENTRE
for Climate Research



Woods Hole
Oceanographic
INSTITUTION



Research school on changing climates in the coupled earth system

Acknowledgements

What a journey – or cruise, I guess, is more appropriate. Surprisingly, sailing has mostly been smooth, and it's been exciting to explore unknown waters, anchor in various harbours for meetings, and get to know many fellow sailors along the way. It was crucial, however, to have a skilled navigator on board who knew how to avoid shipwrecking and getting stuck in the ice (or rather grounding on continental slopes). Kjetil, thanks for navigating me through this PhD! Thank you for always being available for questions and discussions, for providing thorough and immediate feedback on the numerous drafts I delivered, for enduring my arguments of not only science but also semantics and grammar, and for being dedicated to my research. I greatly appreciate that you taught me the Norwegian oceanographic terminology casually along the way, that you were patient with me on a certain downhill slope in Iceland, that you were always up for yet another ping-pong match, and that you were as eager as me to replace digital meetings with (sometimes less sciency) supervision-walks up Fløyen during corona times.

Bob, I'm extremely grateful for having had you as a co-advisor. Thanks for listening to my ideas and asking the right questions that forced me to think critically. Your experience is invaluable, and your enthusiasm for science is inspiring. Thanks for hosting me twice at WHOI and bringing me along on two *Healy* cruises to the Pacific Arctic – the weeks "in the bubble" at sea were some of my most productive periods.

Having two advisors that are into the Norwegian art of "friluftsliving" was wonderful. I very much enjoyed our hikes, and Mt. Washington was definitely a highlight! The scientific discussions among the three of us had their own dynamics and usually left me with more ideas than pages in my notebook. I have learned so much from both of you and could not have wished for a better pair of advisors. Thank you!

There were many more people who made important contributions to this thesis and in general my PhD work: Many thanks to Dan for teaching me heaps about LADCP processing and introducing me to the WHOI hoops gang. Steingrímur, thank you for many insightful discussions and hosting me in Akureyri. I enjoyed all my visits to Iceland and hope to be back at some point. I also want to thank all other co-authors for good input and contributions to the papers. Mirjam, thanks for creative hours in the lab, and Øyvind, thanks for funding many of my travels through Ocean Outlook and believing in Ailin and me making a movie that we can be proud of.

Ailin, thanks for being my companion on the PhD journey. It's been a lot of fun sharing offices, houses in Woods Hole, and state rooms on at least four different research vessels. You were always up for discussing scientific and not-so-scientific things, and I'm glad I had you and your positive attitude around me. Thanks also to the rest of the OVENS-group including Lisbeth for great meetings with as intense scientific

discussions as rounds of Hearts – I hope no one is suffering from long-term damages after the attacks by the queen of spades. I also want to thank Bob's lab at WHOI, I felt very welcome and enjoyed the stimulating discussions with all of you!

I'm grateful to the many people who made my PhD time as pleasant as it was, at and outside of work, in Bergen, Woods Hole, and remotely. In particular, thanks to Astrid P., Christian, Clemens, Elena S., Frank, Kjersti K., Kristine H., Matthias, Schafkopf-gjengen, Sebastian, Svenja, Tine, and Wilma for the countless outdoor adventures, rounds of card games, or regular calls across various oceans. Another thanks to Astrid and Seb for reading the thesis and for all the encouragement. Thanks also to Helene for being a reliable office mate during the long corona summer and to the lively PhD community at the Geophysical Institute and the Bjerknes Centre. Many thanks to my flatmates for taking my mind off work when I came home and for making me socialise; thanks for extensive discussions about anything and everything.

Finally, I'd like to thank my parents. Thank you for your interest in my work, for getting excited whenever I came "home" to Europe, and simply for always being there for me. Thank you, Anna, for good conversations and your support, and for being a sister more than just "in-law". Dirk, you may not have read my thesis, but I know you'd have been proud of your little sis'. This is for you.

Abstract

The Greenland-Scotland Ridge separates the subpolar North Atlantic from the Nordic Seas and constrains the flow of the upper and lower branches of the northern extremity of the Atlantic Meridional Overturning Circulation (AMOC). Warm, saline Atlantic Water flowing northward across the Greenland-Scotland Ridge into the Nordic Seas is transformed into cold, dense water, which returns to the south as overflow plumes through gaps in the ridge. The exchange flows across the ridge have been monitored for several decades, but gaps in our knowledge remain about where and how the dense waters are formed and transported toward the overflows. In this thesis, observational data are used to clarify the upstream pathways of the densest overflow waters and to examine the transformation of the Atlantic Water inflow through Denmark Strait.

Paper I focuses on the North Icelandic Jet (NIJ), which supplies the densest water to the overflow plume passing through Denmark Strait. The properties, structure, and transport of the NIJ are investigated for the first time along its entire pathway along the slope north of Iceland, using 13 high-resolution hydrographic/velocity surveys conducted between 2004 and 2018. The comprehensive data set reveals that the current originates northeast of Iceland and that its volume transport increases toward Denmark Strait. The bulk of the NIJ transport is confined to a small area in temperature-salinity space, and these hydrographic properties are not significantly modified along the NIJ's pathway. The transport of overflow water 300 km upstream of Denmark Strait exceeds 1.8 ± 0.3 Sv ($1 \text{ Sv} \equiv 10^6 \text{ m}^3 \text{ s}^{-1}$), which implies a more substantial contribution from the NIJ to the overflow plume than previously envisaged.

In paper II we present evidence of a previously unrecognised deep current following the slope from Iceland toward the Faroe Bank Channel, using a high-resolution hydrographic/velocity survey from 2011 along with long-term hydrographic and velocity measurements north of the Faroe Islands. We refer to this current as the Iceland-Faroe Slope Jet (IFSJ). The bulk of the IFSJ's volume transport occupies a small area in temperature-salinity space. The similarity of the hydrographic properties of the eastward-flowing IFSJ and the westward-flowing NIJ suggests that the densest components of the two major overflows across the Greenland-Scotland Ridge have a common source. We estimate that the IFSJ transports approximately 1.0 ± 0.1 Sv, which can account for roughly half of the total overflow transport through the Faroe Bank Channel. As such, the IFSJ is a significant component of the overturning circulation in the Nordic Seas.

In paper III we quantify the along-stream evolution of the North Icelandic Irminger Current (NIIC) as it progresses along the shelf break north of Iceland, using a high-resolution shipboard hydrographic/velocity survey, satellite and surface drifter data, and historical hydrographic measurements. The NIIC cools and freshens along its

pathway, predominantly due to mixing with cold, fresh offshore waters. Dense-water formation on the shelf is limited, occurring sporadically in only 7% of all historical winter profiles. The hydrographic properties of this locally formed water match the lighter, shallower portion of the NIJ. Along the northeast Iceland slope, enhanced eddy activity and variability in sea surface temperature indicate that locally formed eddies due to instability of the NIIC divert heat and salt into the interior Iceland Sea. The emergence of the NIJ in the same region suggests that there may be a dynamical link to the formation of the NIJ. As such, our results indicate that while the NIIC rarely supplies the NIJ directly, it may be dynamically important for the overturning circulation in the Nordic Seas.

The three papers advance our knowledge about the circulation along the northern slope of the Greenland-Scotland Ridge and highlight its significance for water mass transformation in the Nordic Seas and our understanding of the Nordic Seas–North Atlantic exchange. In particular, my results contribute to an improved understanding of the pathways of dense water feeding the overflows, which is imperative to accurately predict how the AMOC will respond to a changing climate.

List of papers

This thesis consists of an introduction and a discussion that form the framework for three scientific papers. In Chapter 1 the motivation for the project is presented, while in Chapter 2 the Nordic Seas and the circulation near the Greenland-Scotland Ridge are introduced. An overview of the data sets used is provided in Chapter 3 before a brief summary of the papers is presented in Chapter 4. The papers are included in Chapter 5. Finally, the conclusions are set into context in Chapter 6. The papers in this thesis are:

- I **Semper, S.**, K. Våge, R. S. Pickart, H. Valdimarsson, D. J. Torres, and S. Jónsson (2019): *The emergence of the North Icelandic Jet and its evolution from northeast Iceland to Denmark Strait*, Journal of Physical Oceanography, **49(10)**.
- II **Semper, S.**, R. S. Pickart, K. Våge, K. M. H. Larsen, H. Hátún, and B. Hansen (accepted): *The Iceland-Faroe Slope Jet: A conduit for dense water toward the Faroe Bank Channel overflow*, Nature Communications.
- III **Semper, S.**, K. Våge, R. S. Pickart, S. Jónsson, and H. Valdimarsson (manuscript in preparation): *The evolution and transformation of the North Icelandic Irminger Current along the north Iceland shelf*.

Other relevant contributions

- A) Zhao, J., J. Yang, **S. Semper**, R. S. Pickart, K. Våge, H. Valdimarsson, and S. Jónsson (2018): *A numerical study of interannual variability in the North Icelandic Irminger Current*, Journal of Geophysical Research: Oceans, **123**.
- B) Renfrew, I. A. and 65 others including **S. Semper** (2019): *The Iceland Greenland Seas Project*, Bulletin of the American Meteorological Society, **100**.

Contents

Scientific environment	i
Acknowledgements	iii
Abstract	v
List of papers	vii
1 Motivation	1
2 Introduction	3
2.1 The Atlantic Meridional Overturning Circulation	3
2.2 The Nordic Seas and the Greenland-Scotland Ridge	3
2.3 Hydrography of the Nordic Seas	5
2.3.1 The Thermodynamic Equation Of Seawater – 2010	6
2.3.2 Water masses	6
2.3.3 Water mass transformation	8
2.4 Exchange flows across the Greenland-Scotland Ridge	9
2.4.1 The Atlantic Water inflow into the Nordic Seas	11
2.4.2 Sources and pathways of water supplying the Denmark Strait overflow	13
2.4.3 Sources and pathways of water supplying the Faroe Bank Channel overflow	15
3 Data	17
3.1 Shipboard measurements	18
3.1.1 High-resolution hydrographic/velocity surveys	18
3.1.2 Historical hydrographic data	18
3.2 Moored measurements	18
3.3 Ancillary data	19
4 Summary of the papers	21
5 Scientific papers	23
Paper I: The emergence of the North Icelandic Jet and its evolution from northeast Iceland to Denmark Strait	25

Paper II: The Iceland-Faroe Slope Jet: A conduit for dense water toward the
Faroe Bank Channel overflow 51

Paper III: The evolution and transformation of the North Icelandic Irminger
Current along the north Iceland shelf 81

6 Concluding discussion 135

Bibliography 141

Chapter 1

Motivation

The Greenland-Scotland Ridge separates the subpolar North Atlantic from the Nordic Seas. This submarine ridge system constrains the exchange between the two regions, i.e., the flows of the upper and lower branches of the northern extremity of the Atlantic Meridional Overturning Circulation (AMOC). The AMOC is a system of ocean currents that is key for the redistribution of heat, freshwater, and carbon in the ocean, and thus constitutes a fundamental component of the global climate system (e.g., *Johnson et al.*, 2019; *McCarthy et al.*, 2020). The Nordic Seas, comprising the Norwegian, Greenland, and Iceland Seas (Fig. 2.1), are crucial for the state of the AMOC and the climate (e.g., *Lozier et al.*, 2019; *Chafik and Rossby*, 2019; *Drange et al.*, 2005).

The Nordic Seas are a region of transition and transformation, where warm subtropical water masses meet and interact with cold polar waters, and where intense water mass modification takes place (e.g., *Hansen and Østerhus*, 2000). They are also one of few regions where considerable amounts of atmospheric carbon dioxide (CO₂) are being taken up by the ocean throughout the year (*Skjelvan et al.*, 2005). The warm water inflow from the south keeps large areas of the Nordic Seas free of sea ice and maintains, along with the vast amounts of heat transported by the atmosphere, the mild climate in northern Europe that exceeds the mean temperatures at similar latitudes by more than 10 °C (*Árthun et al.*, 2018; *Drange et al.*, 2005). The nutrient-rich warm waters also create favourable conditions for primary production (e.g., *Stefánsson and Ólafsson*, 1991) and for fish stocks that are of great economic value (e.g., *Lehodey et al.*, 2006). Cold polar waters transit the Nordic Seas along the east Greenland shelf. This is one of the main export routes for sea ice and freshwater from the Arctic Ocean (*Haine et al.*, 2015). In the interior Nordic Seas, strong air-sea exchange of momentum, heat, freshwater, and gases such as CO₂ leads to significant water mass transformation, especially during winter (*Drange et al.*, 2005). In particular, the Nordic Seas are one of the key regions for the formation of dense water that fills the deep North Atlantic and spreads throughout the world ocean. *Gebbie and Huybers* (2010) estimated that more than half of the overturning in the North Atlantic occurs in the Nordic Seas. Recent observational studies emphasised the importance of water mass transformation east of Greenland (*Lozier et al.*, 2019), and especially north of the Greenland-Scotland Ridge (*Chafik and Rossby*, 2019), for sustaining the lower limb of the AMOC. As such, understanding where and how the warm, saline waters are transformed into cold, dense waters and transported across the Greenland-Scotland Ridge is imperative, especially in view of the warming climate.

Climate change is altering the processes and locations of dense-water formation in the Nordic Seas. Oceanic convection important for dense-water formation occurs mainly in the centres of the Greenland and Iceland Seas (*Marshall and Schott, 1999; Swift et al., 1980*). Convection is facilitated by strong heat fluxes that tend to be largest near the ice edge where cold and dry polar air meets the relatively warm surface waters (*Papritz and Spengler, 2017; Renfrew and Moore, 1999*). Over the past decades, the winter sea-ice extent in the Nordic Seas has dramatically declined, which, in turn, has increased the distance between the interior basins of the Greenland and Iceland Seas and the ice edge (e.g., *Moore et al., 2015*). Along with a general warming further reducing the temperature gradient between the atmosphere and the ocean, the retreat of the ice edge has resulted in a diminished heat loss and weakened convection in the interior basins, and hence the formation of less dense water masses (*Moore et al., 2015; Våge et al., in prep.*). However, a warming Arctic may lead to more favourable conditions for dense-water formation at other locations (*Lique and Thomas, 2018*). In particular, dense waters transported by the East Greenland Current that were previously insulated by the sea ice are now exposed to the atmosphere and can be further densified (*Våge et al., 2018*). These shifts in dense-water formation sites may affect the properties and the composition of the overflow waters that cross the Greenland-Scotland Ridge.

Furthermore, recent work has shown that enhanced water mass transformation occurs not only in the East Greenland Current, but also in the Atlantic Water boundary current branches flowing northward through Fram Strait and into the Barents Sea (*Moore et al., submitted*). Increased densification within these currents, along with reduced sea-ice cover, a weakened stratification, and enhanced vertical mixing, leads to the so-called "Atlantification" of the Barents Sea and parts of the Arctic Ocean (*Årthun et al., 2012; Lind et al., 2018; Polyakov et al., 2017*). The documented heat accumulation in the Nordic Seas and the Arctic Ocean since 2000 can to a large extent be explained by the increased ocean heat transport across the Greenland-Scotland Ridge (*Tsubouchi et al., accepted*). As such, the changes in the Arctic climate suggest of late a greater role for the Atlantic Water flowing into the Nordic Seas.

The focus of this thesis is to better understand three currents that are of central importance to the exchange across the Greenland-Scotland Ridge and the overturning in the Nordic Seas: the North Icelandic Jet (NIJ), which advects the densest water to the overflow through Denmark Strait (Paper I), the Iceland-Faroe Slope Jet (IFSJ), a previously unrecognised pathway supplying the densest water to the overflow through the Faroe Bank Channel (Paper II), and the North Icelandic Irminger Current (NIIC), which transports warm and saline water into the Nordic Seas (Paper III). In particular, each of the three papers in this study is concerned with an overarching research question regarding the circulation along the northern slope of the Greenland-Scotland Ridge:

- Paper I: How does the NIJ evolve along the Iceland slope toward Denmark Strait?
- Paper II: How does overflow water progress toward the Faroe Bank Channel?
- Paper III: How is the NIIC modified along the north Iceland shelf?

To address these research questions we employed a multitude of observational platforms. The data sets are described in Chapter 3.

Chapter 2

Introduction

2.1 The Atlantic Meridional Overturning Circulation

The large-scale, full-depth circulation system in the Atlantic Ocean consists of four main branches that constitute the AMOC: upwelling of water from the deep ocean to the near-surface, poleward transport of warm and light water by surface currents, formation of deep water that sinks to depth at high latitudes, and the equatorward return flow of cold and dense water at depth (e.g., *Rahmstorf, 2006*). This circulation stretches over both hemispheres in the Atlantic Ocean and can be divided into two overturning cells: The northward flow of dense Antarctic Bottom Water extends into the mid-latitude North Atlantic in the abyssal ocean. The northern part of the deep Atlantic Ocean, however, is filled by North Atlantic Deep Water, which is formed through densification of the poleward-flowing warm and saline surface water (*Kuhlbrodt et al., 2007*). While wind-driven upwelling and vertical mixing are important driving processes of the AMOC, the deep-water formation sets the interhemispheric shape and strength of the overturning cells (*Kuhlbrodt et al., 2007*). In the northern hemisphere, this overturning or transformation from the upper to the lower layer occurs in the high-latitude North Atlantic, where the water is substantially cooled and loses buoyancy (*Johnson et al., 2019*). These surface buoyancy fluxes are considered as necessary for the AMOC's existence (*Huang, 2004*). In particular, dense-water formation sustaining the lower limb of the AMOC takes place both in the subpolar North Atlantic and in the Nordic Seas (Fig. 2.1). Observational evidence has recently highlighted the importance of the region east of Greenland (*Lozier et al., 2019*), and especially the Nordic Seas (*Chafik and Rossby, 2019*) – contrary to previous understanding of the Labrador Sea as one of the key sites of the overturning. As such, the deepest and densest waters that supply the lower limb of the AMOC and constitute its main component are formed in the Nordic Seas (*Dickson and Brown, 1994; Gebbie and Huybers, 2010*).

2.2 The Nordic Seas and the Greenland-Scotland Ridge

The Nordic Seas comprise the Norwegian, Greenland, and Iceland Seas (Fig. 2.2). The region is the main gateway to the Arctic Ocean; the northern boundary is Fram Strait with a sill depth exceeding 2500 m (e.g., *Langehaug and Falck, 2012*). The southern boundary is the Greenland-Scotland Ridge, a submarine ridge extending from

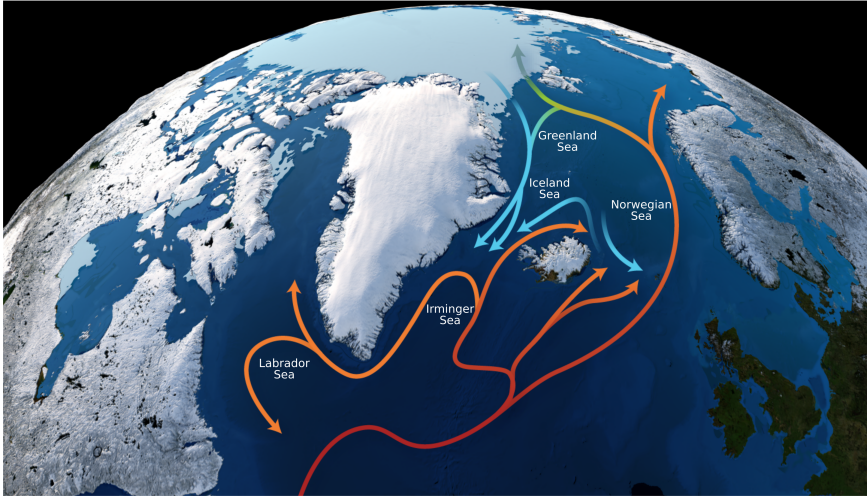


Figure 2.1: Schematic circulation of the Nordic Seas and subpolar North Atlantic. Colours of curves indicate approximate temperatures (warm–red, cold–blue). Courtesy of Woods Hole Oceanographic Institution.

Greenland via Iceland and the Faroe Islands to Scotland (Fig. 2.3). The Greenland-Scotland Ridge constrains the exchange of waters between the subpolar North Atlantic and the Nordic Seas as it provides a continuous barrier below approximately 850 m depth, which is the sill depth of the deepest gap, the Faroe Bank Channel (e.g., Hansen and Østerhus, 2000). All other passages across the ridge are at least 200 m shallower: Denmark Strait, located between Greenland and Iceland, has a sill depth of approximately 650 m. Progressing eastward, the Iceland-Faroe Ridge deepens from about 300 to 500 m toward the Faroe Islands and is intersected by several smaller channels. The southeasternmost gap in the Greenland-Scotland Ridge is the Wyville-Thompson Ridge, which diverts most of the overflow water passing through the wide, deep Faroe-Shetland Channel toward the Faroe Bank Channel (Hansen and Østerhus, 2000, Fig. 2.3).

Submarine ridges play also an important role in the interior of the Nordic Seas, where they separate the major basins and provide guidance for the deep flow, which generally follows the bathymetry (Nøst and Isachsen, 2003). As such, the Greenland Sea is bordered by the West Jan Mayen Ridge to the south and the Mohn Ridge to the east, while the Jan Mayen Ridge, a continuation of the Mohn Ridge, is the boundary between the Iceland Sea and the eastern basins (Fig. 2.2). The Kolbeinsey Ridge, an extension of the mid-Atlantic Ridge north of Iceland, separates the western Iceland Sea from the central basin of the Iceland Sea. The deep Greenland and Norwegian Seas exceed depths of 3500 m; steep continental slopes connect the basins to the shallow shelf areas along the margins. This complex and diverse bathymetry has major implications for the hydrography of the Nordic Seas, in particular the location and formation of different water masses.

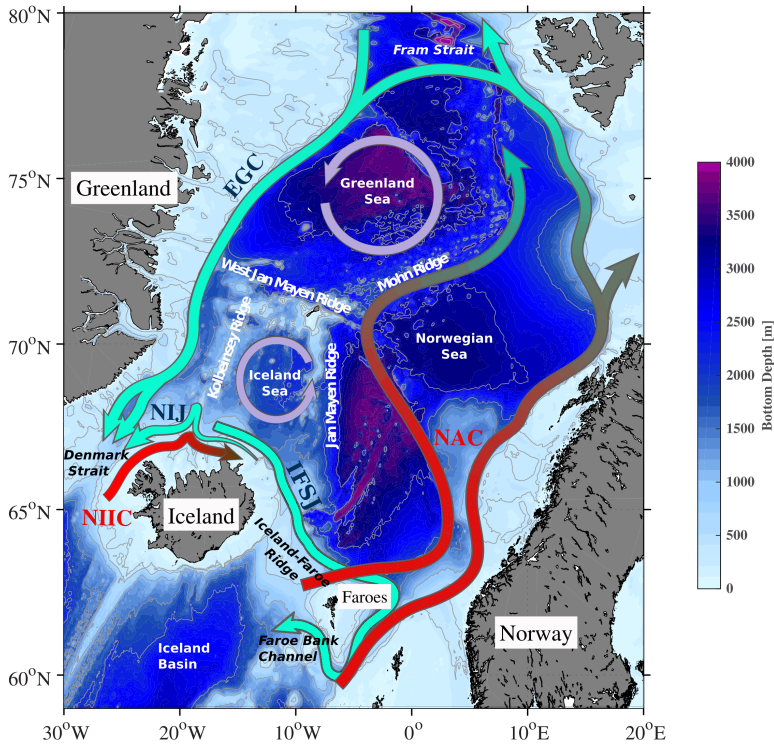


Figure 2.2: Schematic circulation of the Nordic Seas. The pathways of warm Atlantic inflow and dense outflow are shown by red and green arrows, respectively. Colours and grey contours represent the bathymetry from ETOPO2, and relevant topographic features and basins are named. The abbreviations are: EGC–East Greenland Current; IFSJ–Iceland-Faroe Slope Jet; NAC–Norwegian Atlantic Current; NIIC–North Icelandic Irminger Current; NIJ–North Icelandic Jet. Modified after Huang *et al.* (accepted).

2.3 Hydrography of the Nordic Seas

The Nordic Seas connect the Arctic Ocean with the subpolar North Atlantic and contain a large variety of water masses, which are being transported into the region. Furthermore, substantial air-sea exchange modifies the water within the different basins, creating additional water mass classes. While Rudels *et al.* (2002, 2005) have categorised the different water masses in detail, here we followed the approach by Våge *et al.* (2011), where the water mass definitions are simplified but remain sufficiently accurate for the context of this thesis. Before an overview of the water masses and their transformation is given, the standard used for the description of seawater properties is briefly introduced.

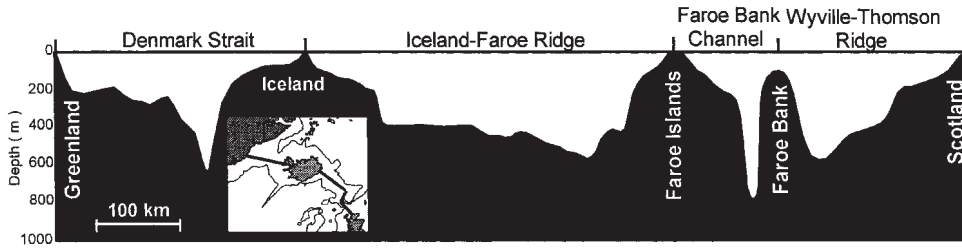


Figure 2.3: Bottom depth along the oceanic part of a section following the crest of the Greenland-Scotland Ridge (shown on the inset map). From Hansen and Østerhus (2000).

2.3.1 The Thermodynamic Equation Of Seawater – 2010

In this thesis the Thermodynamic Equation Of Seawater – 2010 (TEOS-10) standard was followed, a formulation from which the properties of seawater can be derived in a thermodynamically consistent manner (*IOC et al.*, 2010). Consequently, the boundaries of the water masses were converted to Conservative Temperature and Absolute Salinity (Table 2.1). As an example, for the hydrographic properties of the NIJ the Absolute Salinity is on average 0.167 larger than the practical salinity, while the temperature difference is smaller than the measurement accuracy (Chapter 3), and the potential density in TEOS-10 is $\mathcal{O}(0.001)$ kg m^{-3} greater than in ITS-90. Throughout the thesis Absolute Salinity, Conservative Temperature, and potential density are referred to as salinity, temperature, and density, respectively, unless otherwise specified.

2.3.2 Water masses

We consider six main water masses (Table 2.1). Their volumetric distribution in the Nordic Seas (Fig. 2.4) highlights the importance of the warm, saline Atlantic Water and the cold, dense overflow water (defined as waters denser than $\sigma_{\Theta} = 27.8 \text{ kg m}^{-3}$, *Dickson and Brown*, 1994). Note that this volumetric analysis is only based on winter-time hydrographic profiles. (In summer the properties will be spread even more, as the surface layer is warmed by the atmosphere and freshened by sea-ice melt in the western Nordic Seas.) The observations on the east Greenland shelf are sparse, which results in an underestimate of the Polar Surface Water volume.

Table 2.1: Water masses in the Nordic Seas, simplified after *Rudels et al.* (2005) following *Våge et al.* (2011). The water mass boundaries are converted to the TEOS-10 standard.

Water mass	Acronym	Boundaries
Surface Water	SW	$\Theta \geq 0^{\circ}\text{C}$; $S_A < 35.066 \text{ g kg}^{-1}$
Polar Surface Water	PSW	$\Theta < 0^{\circ}\text{C}$; $\sigma_0 < 27.7 \text{ kg m}^{-3}$
Atlantic Water	AW	$\Theta \geq 3^{\circ}\text{C}$; $S_A \geq 35.066 \text{ g kg}^{-1}$
Atlantic-origin water	Atow	$0 \leq \Theta < 3^{\circ}\text{C}$; $\sigma_0 \geq 27.7 \text{ kg m}^{-3}$; $\sigma_{0.5} < 30.44 \text{ kg m}^{-3}$
Arctic-origin water	Arow	$\Theta < 0^{\circ}\text{C}$; $\sigma_0 \geq 27.7 \text{ kg m}^{-3}$; $\sigma_{0.5} < 30.44 \text{ kg m}^{-3}$
Nordic Seas Deep Water	NDW	$\sigma_{0.5} \geq 30.44 \text{ kg m}^{-3}$

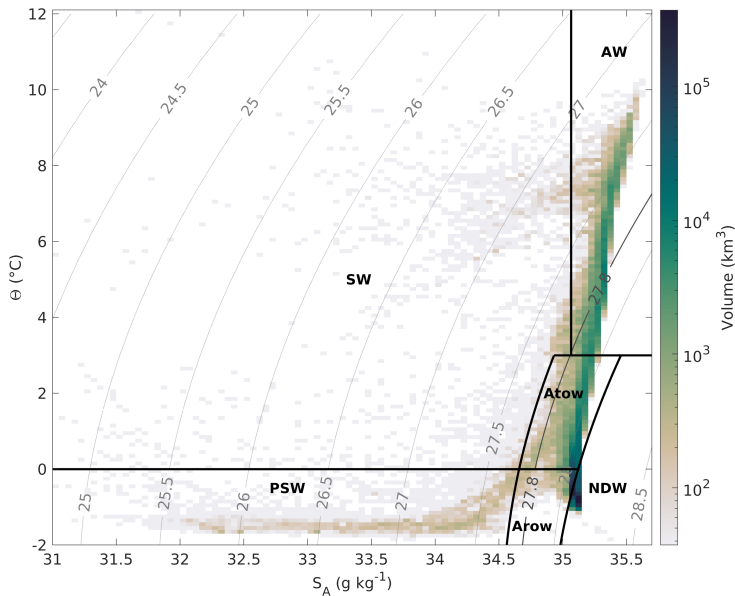


Figure 2.4: Volumetric Θ - S diagram of 0.5° longitude by 0.25° latitude binned winter hydrographic profiles in the Nordic Seas. The underlying data set, on which the gridded product is based, has been assembled by Huang *et al.* (accepted). The properties of the water masses are given in Table 2.1. The abbreviations are: Arow–Arctic-origin water; Atow–Atlantic-origin water; AW–Atlantic Water; NDW–Nordic Seas Deep Water; PSW–Polar Surface Water; SW–Surface Water.

The water masses can be roughly divided into the warm and saline Atlantic Water, the fresh surface waters, and the cold and dense overflow waters (Fig. 2.4). Atlantic Water enters the Nordic Seas from the south (Section 2.4.1) and is commonly defined by a temperature and salinity exceeding 3°C and 35.066 g kg^{-1} (Swift and Aagaard, 1981). The fresh Polar Surface Water originates mainly in the Arctic Ocean (Rudels *et al.*, 2005). The remaining broad range of fresh waters at the surface is collectively referred to as Surface Water. The surface water masses are separated from the intermediate water masses by the 27.7 kg m^{-3} isopycnal, while the intermediate Atlantic-origin and Arctic-origin waters are distinguished by temperatures above and below 0°C , respectively. Nordic Seas Deep Water, with densities exceeding $\sigma_{0.5} = 30.44\text{ kg m}^{-3}$, is the coldest and densest water mass that fills the deep basins of the Greenland, Iceland, and Norwegian Seas.

Geographically the Nordic Seas can be divided into three domains based on their near-surface salinities (Fig. 2.5). This partition was introduced by Helland-Hansen and Nansen (1909) and expanded by Swift and Aagaard (1981). In the eastern Nordic Seas the upper water column is dominated by Atlantic Water. This region, called the Atlantic domain, is always free of sea ice and characterised by intense heat loss to the atmosphere (Isachsen *et al.*, 2007). The Polar domain is located in the western Nordic Seas. Liquid and solid discharge from the Arctic Ocean and the Greenland ice sheet, in addition to locally formed sea ice in winter, are responsible for the dominance of the cold and fresh Polar Surface Water in this area (de Steur *et al.*, 2015; Haine *et al.*, 2015). The region between the Atlantic and Polar domains is characterised by

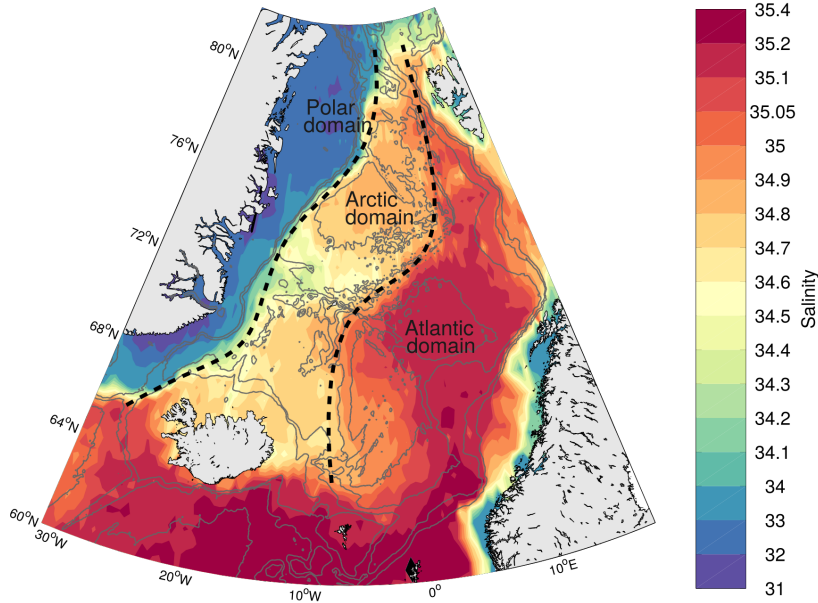


Figure 2.5: Average salinity at 50 m in the Nordic Seas based on around 100 000 CTD profiles from 1980–2014 (collected by Våge et al., 2013). The eastern dashed line indicates the Arctic Front between the Atlantic domain and the Arctic domain, and the western dashed line indicates the Polar Front between the Arctic domain and the Polar domain. The grey contours are the 500, 1000, 2000, and 3000 m isobaths. From Håvik (2018). Note that Håvik (2018) used practical salinity.

a distinct hydrographic regime of surface waters that are warmer and more saline than the Polar Surface Water, but colder and less saline than the Atlantic Water (Swift and Aagaard, 1981). To distinguish this region from regions under direct Polar and Atlantic influence, it is called the Arctic domain (Helland-Hansen and Nansen, 1909; Swift and Aagaard, 1981). The vertical stability in the Arctic domain is reduced compared to the adjacent domains, favouring the production of dense waters during winter through deep convection (Swift and Aagaard, 1981). The three domains are separated by strong horizontal gradients in hydrographic properties (Fig. 2.5). The Arctic Front, extending northward along the Jan Mayen Ridge and Mohn Ridge toward Svalbard, forms the border between the Atlantic and Arctic domains, while the Polar Front, which is located near the east Greenland shelf, separates the Arctic and Polar domains (e.g., Blindheim and Østerhus, 2005; Swift and Aagaard, 1981).

2.3.3 Water mass transformation

The three domains also differ in terms of water mass transformation, which occurs in the entire Nordic Seas due to substantial wintertime heat loss to the atmosphere (Isachsen et al., 2007). There are two main mechanisms of dense-water formation in the Nordic Seas: a gradual transformation along the boundary current and the eastern basins in the Atlantic domain and open-ocean convection in the Arctic domain, i.e., the interior basins of the Iceland and Greenland Seas.

Mauritzen (1996a) inferred that Atlantic Water is transformed to overflow water within the rim current system around the Nordic Seas and the Arctic Ocean (Section 2.4), with the Norwegian Sea (i.e., the Atlantic domain) as the most important site of dense-water formation (*Mauritzen*, 1996b). Her hypothesis was corroborated by *Eldevik et al.* (2009), who analysed the progression of thermohaline anomalies around the Nordic Seas, and by *Isachsen et al.* (2007), who estimated the water mass transformation from sea surface buoyancy fluxes over the different basins of the Nordic Seas. *Isachsen et al.* (2007) further suggest that the strong surface buoyancy loss in the Norwegian Sea is largely controlled by eddy dynamics. Atlantic Water that has been sufficiently cooled to exceed the density of overflow water is then classified as Atlantic-origin water (Table 2.1).

By contrast, Arctic-origin water is mainly formed in the Arctic domain. The weak stratification and strong atmospheric forcing favour transformation through open-ocean convection (*Marshall and Schott*, 1999). Especially in the Greenland Sea, where the winter atmospheric temperatures are low and the heat fluxes strong, the intense cooling of the surface layer erodes the weak near-surface stratification and results in an overturning of the water column. Before the end of the 1970s, wintertime convection extended almost to the bottom, which led to the formation of deep bottom waters (e.g., *Helland-Hansen and Nansen*, 1909; *Malmberg*, 1983). Thereafter, the convective activity in the Greenland Sea has been reduced, and mixed-layer depths have been limited to intermediate depths (< 1500 m; e.g., *Meincke et al.*, 1992; *Latarius and Quadfasel*, 2010; *Brakstad et al.*, 2019).

In the Iceland Sea typical late-winter mixed-layer depths extend to approximately 200 m and light overflow waters are regularly formed (*Swift and Aagaard*, 1981; *Våge et al.*, 2015). The deepest convection occurs in the northwestern part of the basin due to the proximity of the ice edge where the most intense heat fluxes prevail (*Våge et al.*, 2015). Recent observations from sea gliders revealed convection down to 400 m depth during winter 2016, re-ventilating the Atlantic-origin water that transits the western Iceland Sea in the East Greenland Current (*Våge et al.*, 2018, Section 2.4.2). The recent sea-ice retreat exposes the boundary current directly to the atmosphere and facilitates enhanced water mass transformation along its pathway (*Moore et al.*, submitted).

Finally, limited water mass transformation occurs on the shelf north of Iceland, where Atlantic Water is advected by the NIIC (Section 2.4.1). The north Iceland shelf as a possible source of overflow water is investigated in Paper III.

2.4 Exchange flows across the Greenland-Scotland Ridge

The Greenland-Scotland Ridge is the dominant gateway for exchange flows between the subpolar North Atlantic and the Arctic Mediterranean, the collective name for the Arctic Ocean, the Nordic Seas, and their adjacent shelf seas (Fig. 2.6; *Østerhus et al.*, 2019; *Tsubouchi et al.*, accepted). Three currents crossing the ridge northward constitute the majority of the Atlantic Water inflow into the Nordic Seas: the NIIC, entering through Denmark Strait, the Faroe Current, which combines all inflows across the Iceland-Faroe Ridge, and the Shetland Current, passing along the continental slope of the Shetland Islands (*Jónsson and Valdimarsson*, 2012; *Hansen et al.*, 2015; *Berx et al.*, 2013). The latter two currents form the Norwegian Atlantic Current system



Figure 2.6: The Arctic Mediterranean (roughly represented by the oceanic areas within the yellow curve) and its exchanges with the rest of the world ocean. Ocean areas shallower than 1000m are shown in light grey. Red, dark blue, and green arrows indicate inflow, overflow, and surface outflow branches, respectively. From Østerhus *et al.* (2019).

that follows the eastern rim of the Nordic Seas northward and extends into the Barents Sea and the Arctic Ocean (Fig. 2.2). The outflow of cold and fresh Polar Water across the Greenland-Scotland Ridge takes place primarily on the east Greenland shelf (Håvik *et al.*, 2017). By contrast, the outflow of overflow water is confined to the deep gaps in the ridge and occurs in four distinct branches, passing across Denmark Strait, the Iceland-Faroe Ridge, the Faroe Bank Channel, and the Wyville-Thompson Ridge (Figs. 2.3 and 2.6). The transports of overflow water across the Wyville-Thompson Ridge and the Iceland-Faroe Ridge are intermittent and, at least for the latter flow, not well constrained (Østerhus *et al.*, 2019). Denmark Strait and the Faroe Bank Channel, however, account for approximately 90% of the total supply of overflow water to the deep North Atlantic (Østerhus *et al.*, 2019); these two overflows are the focus of this thesis (Papers I–II). Since the Faroe Bank Channel is the deepest gap in the Greenland-Scotland Ridge, the densest water leaving the Nordic Seas exits there. However, due to extensive mixing downstream of the sill and modification in the subpolar North Atlantic, the resulting product (Northeast Atlantic Deep Water, Hopkins *et al.*, 2019) is less dense than the overflow water crossing Denmark Strait (Denmark Strait Overflow Water, Mauritzen *et al.*, 2005). The two water masses form the headwaters to the Deep Western Boundary Current in the Irminger Sea and follow the continental slope of Greenland into the Labrador Sea (Fig. 2.1). Along the way through the subpolar North Atlantic, the volume transport approximately doubles due to entrainment of am-

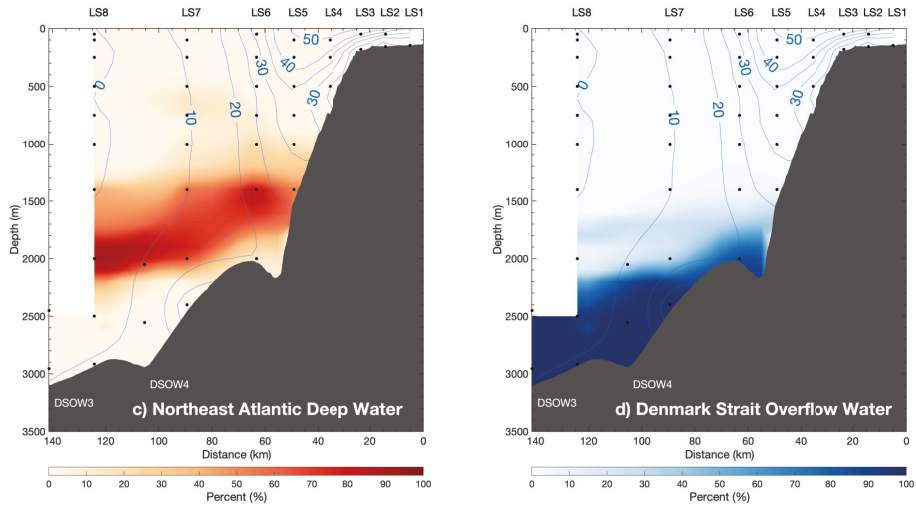


Figure 2.7: Locations of the Northeast Atlantic Deep Water and Denmark Strait Overflow Water at the OSNAP West mooring array. The percentage of the time that each grid point sampled a particular water mass over the four-year period is tallied. From Pacini *et al.* (2020).

bient water (Dickson and Brown, 1994; Rossby *et al.*, 2018). From the Overturning in the Subpolar North Atlantic Program (OSNAP) mooring arrays east and west of Greenland, the Denmark Strait Overflow Water and the Northeast Atlantic Deep Water were identified as the densest layers in the water column (Fig. 2.7), constituting the Deep Western Boundary Current (Hopkins *et al.*, 2019; Pacini *et al.*, 2020). In the Labrador Sea, these two water masses account for a volume transport of approximately 5 Sv each ($1 \text{ Sv} \equiv 10^6 \text{ m}^3 \text{ s}^{-1}$; Pacini *et al.*, 2020). This demonstrates the significance of the dense overflows from the Nordic Seas for filling the deep North Atlantic.

2.4.1 The Atlantic Water inflow into the Nordic Seas

Helland-Hansen and Nansen (1909) first identified the three main branches of Atlantic Water flow into the Nordic Seas and described their general features. While the major inflow of Atlantic Water takes place east of Iceland (Østerhus *et al.*, 2019), we focus here on the NIIC entering the Nordic Seas west of Iceland. The water mass transformation along the current and its fate northeast of Iceland, as well as the resulting implications for the NIIC's role for the overturning in the Nordic Seas, have only recently received more attention (Pickart *et al.*, 2017, Ypma *et al.*, 2019, Casanova-Masjoan *et al.*, 2020, Saberi *et al.*, 2020, Paper III).

The inflow east of Iceland

The inflow across the Iceland-Faroe Ridge accounts for most of the Atlantic Water transport into the Nordic Seas (Fig. 2.6). The ridge has its deepest gaps directly west of the Faroe Islands and east of Iceland (Fig. 2.3), where most of the inflow occurs. However, some water enters over the entire length of the ridge. Due to substantial

spatial and temporal variability (Meincke, 1983; Perkins *et al.*, 1998; Rossby *et al.*, 2009, 2018), the inflow has been monitored using a mooring array directly north of the Faroe Islands, where the flow merges into the Faroe Current, a relatively concentrated boundary current (Hansen *et al.*, 2015; Østerhus *et al.*, 2019). Between 1993 and 2015, the average transport of Atlantic Water in the Faroe Current was 3.8 ± 0.5 Sv (Hansen *et al.*, 2015).

The inflow between the Faroe Islands and Shetland occurs in the Shetland Current, which advects the warmest and most saline waters into the Nordic Seas (Hansen and Østerhus, 2000). Its volume transport was estimated to 2.7 ± 0.5 Sv between 1993 and 2015; a recirculating component of the Faroe Current has been accounted for in this transport estimate (Berx *et al.*, 2013; Østerhus *et al.*, 2019).

The inflow west of Iceland

The NIIC entering the Nordic Seas through Denmark Strait has the smallest volume transport of the three inflow branches (Fig. 2.6). It also has the lowest temperature and salinity and is the most variable branch (Jónsson and Valdimarsson, 2005). Nonetheless, the import of heat, salt, and nutrients to the Iceland shelf is crucial for the local ecosystem and climate (e.g., Jónsson and Valdimarsson, 2012). In particular, the nutrient-rich Atlantic Water favours the growth of phytoplankton and zooplankton, and the current transports eggs and larvae of the major Icelandic fish stocks from the spawning grounds southwest of Iceland to the nursery grounds north of Iceland. The reduced flow of Atlantic Water to the north Iceland shelf in combination with the presence of cold, fresh Polar Surface Water and sea ice on the shelf led to the so-called "ice-years" between 1965 and 1970 (Malmberg and Jónsson, 1997). Since the mid-1990s the volume, temperature, and salt transports have increased and Atlantic Water has prevailed on the shelf (Casanova-Masjoan *et al.*, 2020; Jónsson and Valdimarsson, 2012).

This variability is reflected in the estimates of the NIIC volume transport, which show a large range (though it is partly due to a dependence on the observational platform and applied method). Recent estimates vary between 0.9 and 1.4 Sv at the Hornbanki transect approximately 300 km northeast of Denmark Strait (Jónsson and Valdimarsson, 2012; Casanova-Masjoan *et al.*, 2020). The inflow decreases substantially directly north of Denmark Strait due to a recirculation that diverts a portion of the water offshore and back south through the passage (Casanova-Masjoan *et al.*, 2020; Saberi *et al.*, 2020). Along the north Iceland shelf the volume transport does not change significantly before reaching northeast of Iceland (Casanova-Masjoan *et al.*, 2020, Paper III).

These findings revise an earlier hypothesis of the gradual disintegration of the NIIC eastward and its importance as the upper limb of a local overturning loop responsible for the formation of overflow water in the Iceland Sea (Våge *et al.*, 2011). In particular, Våge *et al.* (2011) argued that the NIIC sheds warm and saline eddies into the Iceland Sea, where heat loss to the atmosphere densifies the water. The overflow water sinks near the slope and is advected back to Denmark Strait (Våge *et al.*, 2011). While the NIIC may be prone to instability along the entire shelf break (Casanova-Masjoan *et al.*, 2020, Paper I), the eddy kinetic energy appears to be enhanced northeast of Iceland, suggesting that eddy formation is one process that may cause a local reduction of the current's transport (Paper III). However, a recent study indicated that the Atlantic Water

in the NIIC contributes very little to the overflow water at Denmark Strait (*Ypma et al.*, 2019). Furthermore, we have shown that water mass transformation in the Iceland Sea is not important for the formation of overflow water in the present climate (*Våge et al.*, in prep.). As such, the dynamics and implications of the NIIC's role for the formation of overflow water remain unclear.

2.4.2 Sources and pathways of water supplying the Denmark Strait overflow

The existence of the Nordic Seas overflows has been known for about a century (*Helland-Hansen and Nansen*, 1909). However, the overflows' importance to the climate was only recognised much later (*Cooper*, 1955). The first hypotheses regarding the formation of Denmark Strait Overflow Water focused on the interior basins of the Iceland and Greenland Seas, where winter air-sea heat fluxes lead to convection down to intermediate depths (Section 2.3.3; *Swift et al.*, 1980; *Swift and Aagaard*, 1981; *Strass et al.*, 1993). Later, *Mauritzen* (1996a) proposed an alternative explanation for the formation of overflow water: In this scheme, the formation occurs through gradual transformation of the warm, saline Atlantic Water within the eastern part of the boundary current system of the Nordic Seas and the Arctic Ocean (Section 2.3.3). The East Greenland Current is then the major source of overflow water through Denmark Strait. Until recently, this has been the commonly accepted view, corroborated by quasi-synoptic measurements (*Rudels et al.*, 2002), historical data (*Eldevik et al.*, 2009), chemical tracers (*Tanhua et al.*, 2005), and high-resolution numerical simulations (*Köhl*, 2007). With the discovery of the NIJ (*Jónsson*, 1999; *Jónsson and Valdimarsson*, 2004), the interior basins of the Iceland and Greenland Seas regained focus as source regions of the densest overflow water passing through Denmark Strait. The most recent research identified the Greenland Sea as the main formation area of this densest component, while there are still open questions regarding the exact pathways and their transports (Paper II, *Huang et al.*, accepted).

By contrast, the total volume transport of overflow water through Denmark Strait is very well known. Since 1996, the current velocities have been monitored in the deep channel; the mean volume transport of overflow water was estimated to 3.2 Sv in the period 1996–2016, without a significant trend (*Jochumsen et al.*, 2017). As such, the outflow through Denmark Strait, jointly supplied by the East Greenland Current and the NIJ (*Harden et al.*, 2016), accounts for more than half of the total export of overflow water from the Nordic Seas (Fig. 2.6).

The East Greenland Current

The East Greenland Current advects both light surface water and dense intermediate water along the east Greenland shelf break toward Denmark Strait (*Håvik et al.*, 2017) and is a key export pathway for sea ice and liquid freshwater from the Arctic Ocean (*Haine et al.*, 2015). The East Greenland Current is surface-intensified, which partly results from the density difference between the fresh water on the east Greenland shelf and the dense water masses in the interior basins of the Greenland and Iceland Seas (*Håvik*, 2018). In the upper 1000 m the current carries primarily water of Atlantic origin, which is recognised by maxima in temperature and salinity at intermediate depths

and located below the cold, fresh Polar Surface Water (Mauritzen, 1996a; Håvik *et al.*, 2017; Mastropole *et al.*, 2017). Some of this Atlantic-origin water has encircled the Arctic Ocean, while another portion has recirculated in Fram Strait (Rudels *et al.*, 2002).

Along the pathway of the East Greenland Current two currents branch off to the east: the Jan Mayen Current following the West Jan Mayen Ridge (Bourke *et al.*, 1992) and farther south the East Icelandic Current (Macrander *et al.*, 2014; de Jong *et al.*, 2018). These currents divert fresh surface water into the interior of the Greenland and Iceland Seas, respectively. Approaching Denmark Strait, the East Greenland Current bifurcates into a shelfbreak and a separated branch (Fig. 2.2; Våge *et al.*, 2013; Harden *et al.*, 2016). The latter current is located seaward of the shelf break, near the base of the Iceland slope (Håvik *et al.*, 2017). From a year-long mooring array approximately 200 km upstream of Denmark Strait, Harden *et al.* (2016) estimated the transports of overflow water within the shelfbreak and separated East Greenland Current branches to 1.50 ± 0.16 Sv and 1.04 ± 0.15 Sv, respectively. This accounts for about two-thirds of the total overflow water transport, while the remaining portion is advected by the NIJ (Harden *et al.*, 2016).

The North Icelandic Jet

The NIJ was discovered about 20 years ago and shown to be distinct from the East Greenland Current (Jónsson, 1999; Jónsson and Valdimarsson, 2004). Along its pathway following the slope north of Iceland toward Denmark Strait (Fig. 2.2), the volume transport gradually increases until the Hornbanki transect, approximately 300 km upstream of Denmark Strait, where it exceeds 1.8 ± 0.3 Sv (Paper I). Thereafter, the current starts to merge with the separated East Greenland Current, which complicates the transport estimation and may lead to more uncertain results. The transport estimates are substantially lower: Based on the year-long mooring array at the Kögur transect approximately 200 km upstream of Denmark Strait, Harden *et al.* (2016) estimated that the NIJ transports 1.00 ± 0.17 Sv into Denmark Strait, while we estimated a transport of 1.3 ± 0.2 Sv based on ten hydrographic/velocity surveys at this transect (Paper I). The transport estimate upstream of the confluence thus indicates that the contribution from the NIJ to the Denmark Strait overflow may be larger than previously thought, exceeding 50 % of the total overflow volume (Paper I).

The water transported by the NIJ is predominantly classified as Arctic-origin water and Atlantic-origin water; on average the current carries only 10 % non-overflow water (Paper I). The NIJ transports the coldest and densest water toward Denmark Strait, which fills the bottom of the trough (Mastropole *et al.*, 2017). A division into Θ -S classes shows that the bulk of the transport is confined to a small range in hydrographic space (Paper I). This so-called transport mode is centred at the 28.05 kg m^{-3} isopycnal (within the class of Arctic-origin water) and is not significantly modified along the NIJ's pathway. This densest portion of the NIJ likely stems from the Greenland Sea, where sufficiently dense waters are regularly ventilated during winter (Brakstad *et al.*, 2019; Huang *et al.*, accepted). The previous hypothesis that the Iceland Sea is the main source region of Denmark Strait Overflow Water in general (Swift *et al.*, 1980), and the NIJ as part of a local overturning loop in particular (Section 2.4.1, Våge *et al.*, 2011), has lately been revised. Historical hydrographic measurements and recent sea glider

observations indicated that waters within the main density classes of the NIJ are not sufficiently ventilated in the Iceland Sea at present (Våge *et al.*, 2015, in prep.).

While the central Iceland Sea has been depreciated to a transit region for the dense waters supplying the NIJ, it does play a role as the location of the current's formation. One peculiarity of the NIJ is its sudden emergence northeast of Iceland (Våge *et al.*, 2011, Paper I), which is co-located with the region of enhanced eddy kinetic energy seaward of the shelf break where the NIIC disintegrates (Section 2.4.1, Paper III). The emergence of the NIJ could also be related to upstream effects of hydraulic control at the Denmark Strait sill. This mechanism has been shown to influence the flow near Denmark Strait (Nikolopoulos *et al.*, 2003; Lin *et al.*, accepted) and may determine the NIJ's location near the 600 m isobath, which coincides with the approximate sill depth of the strait (Paper II). Hydraulic control, however, cannot explain the existence of an outer core of the NIJ, which was first identified by Pickart *et al.* (2017). The outer core is located near the 800 m isobath and is present about 50 % of the time (Paper I). Both cores have a velocity maximum at mid-depth. This middepth intensification of the NIJ is related to the up-tilt of dense isopycnals along the Iceland slope (Jónsson and Valdimarsson, 2004; Våge *et al.*, 2011). Jónsson and Valdimarsson (2004) speculated that the uptilting isopycnals result from a bottom Ekman layer, but the dense water is present high up along both the entire slope north of Iceland and the Iceland-Faroe Ridge (Paper II), indicating that different processes may be at play. Despite the 20-year research efforts on the NIJ since its discovery, many aspects of the current's structure and dynamics remain unclear (Chapter 6).

2.4.3 Sources and pathways of water supplying the Faroe Bank Channel overflow

The overflow through the Faroe Bank Channel has been continuously monitored since 1995. The mean kinematic overflow, i.e., the volume transport derived only based on the velocity field, is 2.2 Sv (Hansen *et al.*, 2016). Applying the same density criterion for overflow water as in Denmark Strait ($\sigma_{\Theta} \geq 27.8 \text{ kg m}^{-3}$) reduces the transport to 1.9 Sv (Hansen *et al.*, 2016). This accounts for about one-third of the total overflow transport across the Greenland-Scotland Ridge, including the densest water that exits the Nordic Seas.

The overflow water in the Faroe Bank Channel is mainly composed of approximately equal portions of intermediate and deep waters (Fogelqvist *et al.*, 2003; McKenna *et al.*, 2016). These water masses are distinguished by their temperatures above and below -0.5°C , respectively (Hansen and Østerhus, 2000), based on the historical availability of only temperature measurements. The intermediate waters are ventilated in the Greenland and Iceland Seas and include a considerable contribution from the Arctic Ocean and a minor portion of Atlantic-origin water transformed within the boundary current system around the Nordic Seas (Jeansson *et al.*, 2017). The deep waters are old and have been formed in the shallow shelf regions surrounding the Arctic Ocean and by open-ocean convection in the Greenland Sea during times of vigorous deep-water formation (Hansen and Østerhus, 2000). They spread into the Norwegian Sea through a deep channel near Jan Mayen, where they are found beneath the intermediate waters (Østerhus and Gammelsrød, 1999; Somavilla, 2019). The advection of the intermediate and deep waters to the overflow results in mixing between the two lay-

ers in the Norwegian Sea. As such, the boundary of -0.5°C between the water masses is indistinct to some extent (*Hansen and Østerhus, 2000*).

The hydrographic properties and their interannual variability have been studied extensively in the Faroe-Shetland Channel, the passage directly upstream of the Faroe Bank Channel (e.g., *Turrell et al., 1999; Hansen et al., 2016*). However, only recently the pathways transporting the overflow water toward the channel have been identified. *Chafik et al. (2020)* used vessel-mounted velocity data in combination with output from a numerical model to demonstrate that the flow in the Faroe-Shetland Channel occurs along its eastern slope. The upstream pathways of overflow water feeding the channel, and thus ultimately the Faroe Bank Channel overflow, have been thought to originate in the interior Norwegian Sea (*Fogelqvist et al., 2003; Eldevik et al., 2009*). By contrast, drifter studies (*Søiland et al., 2008; de Jong et al., 2018*) and velocity records from deep moorings (*Hopkins et al., 1992*) indicated a westerly pathway along the Iceland-Faroe Ridge, whereas model studies (*Köhl, 2010; Serra et al., 2010*) suggested that, at times, the flow can also approach the Faroe-Shetland Channel along the Norwegian slope.

Lately, direct observational evidence has been provided of a current following the Iceland-Faroe Ridge from Iceland to the Faroe Islands, corroborating the pathway previously indicated by the drifters (Fig. 2.2, Paper II). This current, named the IFSJ, has a volume transport maximum in a small area in Θ - S space. The temperature of this transport mode coincides with the boundary between the intermediate and deep waters ($\approx -0.5^{\circ}\text{C}$), corresponding to Arctic-origin water in our classification (Fig. 2.4; Table 2.1). The density of the transport mode is not significantly different from the transport mode density of the NIJ (Paper II). As such, the hypothesis that both currents have the same source in the Greenland Sea seems plausible. *Huang et al. (accepted)* quantified the distances between the transport mode and all water in the entire Nordic Seas in terms of physical properties, based on potential density and potential spicity. In density-spicity space the isolines of these properties are orthogonal, and their gradients are of the same magnitude, as opposed to Θ - S space. This method is therefore effective in determining how close different water masses are to each other in terms of hydrographic properties. The findings by *Huang et al. (accepted)* confirm that the Greenland Sea is the main source within the Nordic Seas of this densest overflow water, and that the water follows the submarine ridge systems toward the overflows. This link between the two major overflows from the Nordic Seas suggests that changes in the process and location of deep-water formation may have large implications for the supply of the densest water to the lower limb of the AMOC (Chapter 1).

Chapter 3

Data

The two main types of observational oceanographic data analysed in this thesis are hydrographic/velocity shipboard measurements (Papers I–III) and moored measurements (Papers I–II). In addition, several ancillary data sets were used, which include historical profiles of conductivity, temperature, and depth (CTD), satellite altimetry and sea surface temperature data, and atmospheric reanalysis data. The data sets are introduced below; an overview is shown in Fig. 3.1.

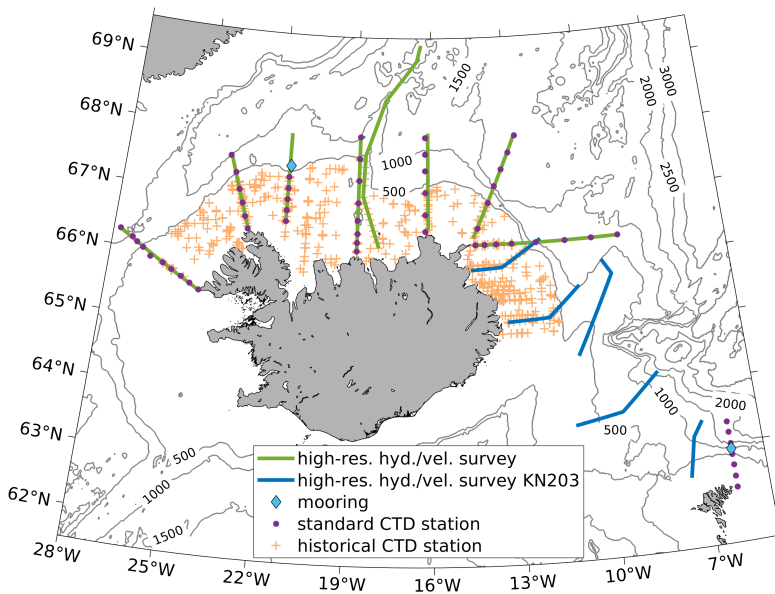


Figure 3.1: Main data sets used in the thesis. The high-resolution hydrographic/velocity surveys analysed in Paper I are shown in green, while additional transects surveyed during the KN203 cruise in autumn 2011 used in Paper II are presented in blue. Mooring locations (Papers I–II) are indicated by light blue diamonds. Standard and historical CTD stations used in Papers II and III are indicated in purple and orange, respectively. Isobaths from ETOPO1 (Amante and Eakins, 2009) are contoured every 500 m.

3.1 Shipboard measurements

3.1.1 High-resolution hydrographic/velocity surveys

In Paper I we used high-resolution hydrographic/velocity sections from 13 shipboard surveys conducted between 2004 and 2018, four of them during winter. Seven transects across the northern slope of Iceland were occupied during the surveys; six of them are repeated monitoring sections maintained by the Marine and Freshwater Research Institute (MFRI) in Iceland (Fig. 3.1). The typical station spacing over the slope is approximately 5 km, which is similar to the Rossby radius of deformation in the Iceland Sea (4–5 km; *Nurser and Bacon, 2014*). In addition to the CTD measurements, direct velocity measurements were obtained from acoustic Doppler current profiler (ADCP) instruments. On three of the surveys a vessel-mounted ADCP was used, while an upward- and downward-facing lowered ADCP system mounted on the rosette was employed on the remaining surveys. The direct current velocity was used to obtain the absolute geostrophic velocity by referencing the geostrophic velocity computed from the hydrographic fields. Details on the interpolation routines are provided in Papers I and II.

In Papers II and III we focused on one of these high-resolution hydrographic/velocity surveys, the cruise on R/V *Knorr* in September 2011 led by Robert Pickart at the Woods Hole Oceanographic Institution. This survey covered the region between Denmark Strait and the Faroe Islands. We used seven transects northeast of Iceland and across the Iceland-Faroe Ridge in Paper II. As this is also the first high-resolution survey that extended all the way to the coast for the repeat transects north of Iceland, those transects formed the basis for the analysis of the NIIC in Paper III.

3.1.2 Historical hydrographic data

Seven hydrographic stations from the standard monitoring section N north of the Faroe Islands maintained by the Faroe Marine Research Institute (FAMRI) were used in Paper II (Fig. 3.1). The stations are spaced 20 nautical miles (18.5 km) apart and were typically occupied three to four times per year. We analysed measurements from 120 surveys between 1987 and 2018.

In Paper III we used historical hydrographic observations on the north Iceland shelf between 1980 and 2015, a subset of the data set compiled by *Våge et al. (2015)* and updated by *Huang et al. (accepted)*. The profiles were obtained from the Unified Database for Arctic and Subarctic Hydrography (UDASH), the International Council for the Exploration of the Seas (ICES), the World Ocean Database (WOD), the Norwegian Iceland Seas Experiment (NISE) database, the Global Ocean Data Analysis Project version 2 (GLODAPv2), the Argo global program of profiling floats, and MFRI.

3.2 Moored measurements

We used data from a current meter mooring deployed 19 km north of the shelf break at the Hornbanki transect, approximately 300 km upstream of the Denmark Strait sill, from August 2005 to August 2006 (Paper I). The year-long time series of velocity in the

centre of the NIJ was analysed to address the variability in the current and its potential link to atmospheric forcing.

In Paper II velocity time series from two moorings at section N north of the Faroe Islands were analysed. One mooring was deployed at a bottom depth of 1210 m, i.e., near the centre of the deep core of the IFSJ. An ADCP instrument provided a year-long (June 2017 to May 2018) record of current velocities between 515 and 1185 m. The other mooring is part of a mooring array across the slope north of the Faroe Islands monitoring the Atlantic Water transport in the Faroe Current. This mooring is located 3.1 km farther inshore above a mean bottom depth of 960 m. While this mooring has been continuously deployed since 1997, we focused on the year 2017–2018, when we had concurrent near-bottom velocities, and the period 2006–2013, when the mooring was deployed at approximately the same bottom depth (956 ± 5 m). The velocities, recorded between 120 and 670 m depth, extended into the upper portion of the IFSJ and may be considered a longer-term proxy for the variability in the IFSJ.

When discussing the transport estimate of the NIJ near Denmark Strait in Paper I, we also used data from the Kögur mooring array approximately 200 km north of the Denmark Strait sill, compiled by *Harden et al.* (2016). The mooring array was deployed between September 2011 and August 2012 and consisted of 12 moorings covering the distance between the east Greenland and west Iceland shelves.

3.3 Ancillary data

In Paper I we used the mean sea level pressure and 10-m wind field from the ERA-Interim reanalysis data from the European Centre for Medium-Range Weather Forecast (ECMWF; *Dee et al.*, 2011) to assess the atmospheric conditions during the period of the mooring deployment at the Hornbanki transect (2005–2006). This product agrees well with observations in the study region (*Harden et al.*, 2011). (The new high-resolution reanalysis product ERA5 had not been released for the mooring deployment period during the time of analysis.)

Satellite altimetry and satellite sea surface temperature were employed to investigate the role of eddies shed from the NIIC (Paper III). We used along-track sea surface height anomalies from the Envisat satellite in the period 2002–2010 to calculate eddy kinetic energy northeast of Iceland. For sea surface temperature a reprocessed analysis product based on the Operational SST and Sea Ice Analysis (OSTIA) system was used. The data are on a global regular grid at 0.05° resolution and provide an estimate of the daily average temperature at 20 cm depth. We considered the data for 2002–2010, the same time period as for the sea surface height anomalies. Both products are distributed by E.U. Copernicus Marine Service Information (<http://marine.copernicus.eu/>).

To elucidate the pathway of the NIIC, annual mean near-surface velocities from both undrogued and 15-m drogued drifters of the Global Drifter Program (GDP) were used in Paper III. This global 0.25° by 0.25° climatology is archived and distributed by the Atlantic Oceanographic and Meteorological Laboratory of the National Oceanic and Atmospheric Administration (AOML/NOAA; https://www.aoml.noaa.gov/phod/gdp/mean_velocity.php).

Chapter 4

Summary of the papers

Paper I: The emergence of the North Icelandic Jet and its evolution from north-east Iceland to Denmark Strait

Semper, S., K. Våge, R. S. Pickart, H. Valdimarsson, D. J. Torres, and S. Jónsson (2019), Journal of Physical Oceanography, 49(10)

In Paper I the properties, structure, and transport of the North Icelandic Jet (NIJ) were investigated for the first time along the entire pathway of the current. We used 13 hydrographic/velocity surveys of high spatial resolution covering seven repeat transects across the continental slope north of Iceland between 2004 and 2018. We found that the NIJ originates northeast of Iceland and that its volume transport increases toward Denmark Strait. The bulk of the volume transport is relatively uniform in temperature and salinity; we referred to this small area in temperature-salinity space as the transport mode. The properties of the transport mode are not significantly modified between the transects. By contrast, the volume transport of the NIJ varies considerably between and within the surveys. We investigated the causes of this variability and found neither a clear seasonal signal nor a consistent link to atmospheric wind forcing. Instead, we demonstrated that the NIJ is likely susceptible to barotropic and/or baroclinic instability. In roughly half of the velocity sections, we identified two cores of the current: One was centred near the 600 m isobath, while the other one was found near the 800 m isobath. The total transport of water in the NIJ that can contribute to the overflow at Denmark Strait and exit into the deep North Atlantic exceeds previous estimates from a year-long mooring array and hydrographic/velocity surveys closer to the strait. Those earlier measurements were obtained in a region where the NIJ merges with a branch of the East Greenland Current, which complicated the estimate of the pure NIJ contribution. Our results imply that the NIJ supplies a more substantial portion of dense overflow waters to the lower limb of the AMOC than previously envisaged.

Paper II: The Iceland-Faroe Slope Jet: A conduit for dense water toward the Faroe Bank Channel overflow

Semper, S., R. S. Pickart, K. Våge, K. M. H. Larsen, H. Hátún, and B. Hansen (accepted), Nature Communications

In Paper II we demonstrated the existence of a previously unrecognised deep pathway transporting dense water toward the Faroe Bank Channel overflow. This current,

which we named the Iceland-Faroe Slope Jet (IFSJ), follows the northern slope of the Greenland-Scotland Ridge between northeast Iceland and the Faroe Islands. A high-resolution hydrographic/velocity shipboard survey in autumn 2011 formed the basis for the analysis, which was substantiated by historical hydrographic data and long-term records of current velocities north of the Faroe Islands. We found that the IFSJ is bottom-intensified and consists of two cores centred near the 750 and 1100 m isobaths. The bulk of its volume transport is confined to a small area in temperature-salinity space, and the properties of this transport mode are very similar to the properties of the NIJ. This suggests that the NIJ flowing westward toward the Denmark Strait overflow and the IFSJ flowing eastward toward the Faroe Bank Channel overflow have a common source, which is likely located in the Greenland Sea. We estimated that the volume transport of the IFSJ accounts for approximately half of the total overflow transport through the Faroe Bank Channel. As such, the IFSJ is a significant component of the overturning circulation in the Nordic Seas and a major pathway of dense water supplying the lower limb of the AMOC.

Paper III: The evolution and transformation of the North Icelandic Irminger Current along the north Iceland shelf

Semper, S., K. Våge, R. S. Pickart, S. Jónsson, and H. Valdimarsson (manuscript in preparation)

In Paper III we quantified the evolution of the North Icelandic Irminger Current (NIIC) using eight cross-slope transects from a high-resolution hydrographic/velocity survey extending all the way to the coast, in addition to satellite and surface drifter data as well as historical hydrographic measurements. The NIIC generally follows the shelf break north of Iceland, and the current's hydrographic properties are modified along its entire pathway. Progressing eastward, the core of the current cools and freshens considerably, mainly due to mixing with cold, fresh offshore waters. The NIIC's volume transport decreases significantly northeast of Iceland, where lenses of warm, saline water detach from the current and divert heat and salt into the Iceland Sea. This region of steep bathymetry is recognised from satellite data as a local maximum in eddy kinetic energy and enhanced variability in sea surface temperature. As the NIJ emerges in the same region, the instability and disintegration of the NIIC suggest that there may be a dynamical link to the formation of the NIJ. Furthermore, we demonstrated that while overflow water is present year-round on the north Iceland shelf, most of this water is not formed locally. Water mass transformation on the shelf is limited and may only on rare occasions contribute to the lighter, shallower portion of the NIJ.

Chapter 5

Scientific papers

Paper I

The emergence of the North Icelandic Jet and its evolution from northeast Iceland to Denmark Strait

S. Semper, K. Våge, R. S. Pickart, H. Valdimarsson, D. J. Torres, and S. Jónsson
Journal of Physical Oceanography, **49/10** (2019)

The Emergence of the North Icelandic Jet and Its Evolution from Northeast Iceland to Denmark Strait

STEFANIE SEMPER AND KJETIL VÅGE

Geophysical Institute, University of Bergen, and Bjerknes Centre for Climate Research, Bergen, Norway

ROBERT S. PICKART

Woods Hole Oceanographic Institution, Woods Hole, Massachusetts

HÉÐINN VALDIMARSSON

Marine and Freshwater Research Institute, Reykjavík, Iceland

DANIEL J. TORRES

Woods Hole Oceanographic Institution, Woods Hole, Massachusetts

STEINGRÍMUR JÓNSSON

Marine and Freshwater Research Institute, Reykjavík, and University of Akureyri, Akureyri, Iceland

(Manuscript received 9 April 2019, in final form 12 July 2019)


ABSTRACT

The North Icelandic Jet (NIJ) is an important source of dense water to the overflow plume passing through Denmark Strait. The properties, structure, and transport of the NIJ are investigated for the first time along its entire pathway following the continental slope north of Iceland, using 13 hydrographic/velocity surveys of high spatial resolution conducted between 2004 and 2018. The comprehensive dataset reveals that the current originates northeast of Iceland and increases in volume transport by roughly 0.4 Sv (1 Sv = $10^6 \text{ m}^3 \text{ s}^{-1}$) per 100 km until 300 km upstream of Denmark Strait, at which point the highest transport is reached. The bulk of the NIJ transport is confined to a small area in Θ - S space centered near $-0.29^\circ \pm 0.16^\circ \text{C}$ in Conservative Temperature and $35.075 \pm 0.006 \text{ g kg}^{-1}$ in Absolute Salinity. While the hydrographic properties of this transport mode are not significantly modified along the NIJ's pathway, the transport estimates vary considerably between and within the surveys. Neither a clear seasonal signal nor a consistent link to atmospheric forcing was found, but barotropic and/or baroclinic instability is likely active in the current. The NIJ displays a double-core structure in roughly 50% of the occupations, with the two cores centered at the 600- and 800-m isobaths, respectively. The transport of overflow water 300 km upstream of Denmark Strait exceeds 1.8 ± 0.3 Sv, which is substantially larger than estimates from a year-long mooring array and hydrographic/velocity surveys closer to the strait, where the NIJ merges with the separated East Greenland Current. This implies a more substantial contribution of the NIJ to the Denmark Strait overflow plume than previously envisaged.

1. Introduction

Plumes of cold, dense overflow water spill across gaps in the Greenland–Scotland Ridge from the Nordic Seas to the North Atlantic. They form the lower limb

of the Atlantic Meridional Overturning Circulation (AMOC), which is of key importance for the poleward transport of heat in the Atlantic Ocean. Approximately half of the overflow crossing the Greenland–Scotland Ridge passes through Denmark Strait and supplies the densest water to the Deep Western Boundary Current

 Denotes content that is immediately available upon publication as open access.

Corresponding author: Stefanie Semper, stefanie.semp@uib.no

DOI: 10.1175/JPO-D-19-0088.1

© 2019 American Meteorological Society



This article is licensed under a [Creative Commons Attribution 4.0 license](http://creativecommons.org/licenses/by/4.0/) (<http://creativecommons.org/licenses/by/4.0/>).

(Jochumsen et al. 2017; Østerhus et al. 2019). As such, determining the formation processes and pathways of the Denmark Strait Overflow Water (DSOW) is necessary to further our understanding of the overturning in the Nordic Seas, and hence the AMOC.

Cooper (1955) was the first to recognize the climatic importance of the dense overflow through Denmark Strait. Subsequent studies suggested that DSOW can be formed in the interior basins of the Iceland and Greenland Seas, where winter cooling leads to open-ocean convection to intermediate depths (Swift et al. 1980; Swift and Aagaard 1981; Strass et al. 1993). The idea of open-ocean convection forming overflow water in the interior basin of the Iceland Sea was later dismissed in part since there was no known direct pathway from the basin to Denmark Strait. Mauritzen (1996) proposed instead that warm, saline Atlantic Water was gradually transformed into DSOW within the boundary current system of the Nordic Seas and the Arctic Ocean. This scheme implies that the East Greenland Current (EGC) advects most of the DSOW into Denmark Strait, whereas the interior basins of the Greenland and Iceland Seas contribute only to a limited extent. Studies based on quasi-synoptic measurements (Rudels et al. 2002), historical data (Eldevik et al. 2009), chemical tracers (Tanhua et al. 2005), and high-resolution numerical simulations (Köhl et al. 2007) corroborated the notion that the EGC is the main source of overflow water to Denmark Strait.

The transport of DSOW through the 650-m-deep passage in Denmark Strait is estimated to be 3.2–3.5 Sv ($1 \text{ Sv} \equiv 10^6 \text{ m}^3 \text{ s}^{-1}$; Harden et al. 2016; Jochumsen et al. 2017). It is relatively constant on decadal time scales and does not exhibit a dominant seasonal cycle (Jochumsen et al. 2017). By contrast, the overflow varies substantially on short time scales (e.g., Harden et al. 2016; Almansí et al. 2017). In particular, different mesoscale processes have been identified using in situ data and numerical models. Large lenses of weakly stratified water called boluses pass through the deepest part of the sill every few days (Mastropole et al. 2017; Almansí et al. 2017). Interspersed with these are intermittent periods of enhanced flow characterized by a very thin overflow layer, referred to as pulses (von Appen et al. 2017). Occasionally the current at the sill reverses and warm water flows northward through the strait. Spall et al. (2019) argued that all of these high-frequency processes are associated with baroclinic instability of the hydrographic front in the strait.

There are two primary water masses comprising the DSOW. The water noted above, transported by the rim current in the Nordic Seas, is referred to as Atlantic-origin water. This is because there is a direct

advective link between this relatively warm and saline water and the subpolar North Atlantic south of the Greenland–Scotland Ridge. The second type of overflow water mass is referred to as Arctic-origin water. This water has been transformed in the interior basins of the Nordic Seas via convective overturning, and, as such, it is colder and fresher than Atlantic-origin water. While other water masses are contained within the overflow water mix (e.g., Jeansson et al. 2008), the relative percentages of these constituents appear to be small (Mastropole et al. 2017). Based on previous studies (e.g., Swift and Aagaard 1981; Våge et al. 2013), overflow water colder than 0°C is referred to as Arctic-origin water, while that warmer than 0°C is considered Atlantic-origin water.

These two water masses are transported into Denmark Strait by a system of currents (Fig. 1). The EGC is the main source of Atlantic-origin water. It accounts for approximately two-thirds of the total volume transport (Harden et al. 2016). The current bifurcates north of Blossville Basin and continues toward Denmark Strait as the shelfbreak and separated branches of the EGC (Våge et al. 2013). The former flows along the Greenland shelf break, whereas the latter is located farther offshore, near the base of the Iceland slope (Håvik et al. 2017a).

The other current advecting overflow water into Denmark Strait is the North Icelandic Jet (NIJ). The NIJ transports the coldest and densest portion of DSOW along the continental slope north of Iceland (Våge et al. 2011; Harden et al. 2016). The narrow (15–20 km) current is centered near the 650-m isobath and has a velocity maximum at middepth (Jónsson and Valdimarsson 2004; Våge et al. 2011). The final current in Denmark Strait is the North Icelandic Irminger Current (NIIC), which transports warm and saline Atlantic water northward into the Iceland Sea (Fig. 1). North of Iceland this surface-intensified current shares a common front with the NIJ when the bathymetry brings the currents into close proximity (Pickart et al. 2017).

The discovery of the NIJ by Jónsson (1999) and Jónsson and Valdimarsson (2004) has led to a renewed focus on the Iceland Sea as source for DSOW. Since then, observational, theoretical, and modeling studies have been carried out to enhance our understanding of the NIJ and its role in the Iceland Sea circulation. Using data from multiple shipboard surveys, Våge et al. (2011, 2013) demonstrated that the current is a distinct source of dense water to the Denmark Strait overflow plume. This was further verified by Harden et al. (2016) using measurements from a year-long mooring array approximately 200 km north of the sill.

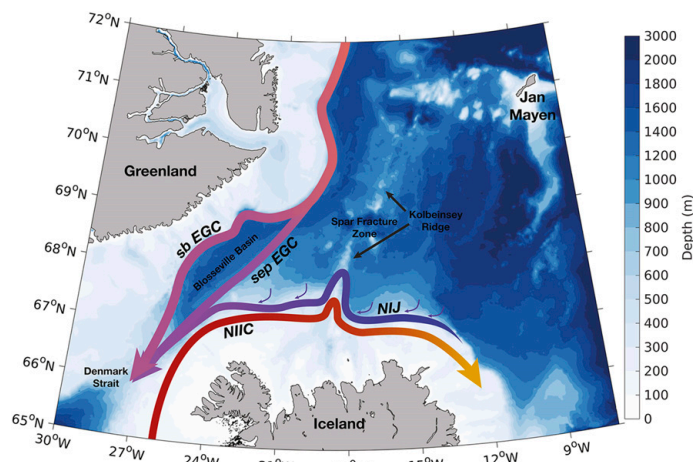


FIG. 1. Schematic circulation in the vicinity of Denmark Strait. The acronyms are: NIIC = North Icelandic Irminger Current, NIJ = North Icelandic Jet, sb EGC = shelfbreak East Greenland Current, sep EGC = separated East Greenland Current. The colored shading is the bathymetry from ETOPO1 (Amante and Eakins 2009).

They estimated that the NIJ contributes roughly one-third of the total DSOV volume transport, and that it merges with the separated EGC north of Denmark Strait. Various modeling studies also show the existence of the NIJ, both in simplified configurations (e.g., Våge et al. 2011; Yang and Pratt 2014), and in more complex general circulation models (e.g., Behrens et al. 2017; Ypma et al. 2019).

The seasonal variability in the NIJ appears to be small. No seasonal cycle is apparent in the velocity time series from three years of moored current meters on the Iceland slope upstream of Denmark Strait (Jónsson 1999). Harden et al. (2016) noted only a slight reduction in transport of the NIJ during winter and spring from their year-long moored records at the same location. Behrens et al. (2017) also found little variability in the volume transport of the current on seasonal to interannual time scales in their model study, while Huang et al. (2019) determined that month-to-month variation of the NIJ strength is significantly correlated with air–sea buoyancy forcing north of Iceland. They explained this connection via the mechanism presented by Spall et al. (2017), in which convection on the continental slope of an island leads to cyclonic flow around the island. On shorter time scales (days to a week), the flow on the Iceland slope north of the sill is very energetic. Harden and Pickart (2018) argued that this is the signature of topographic Rossby waves forced by the meandering of the separated EGC farther

offshore. Huang et al. (2019) showed that there is a strong conversion from mean potential energy to eddy energy at the same location, implying that the NIJ is baroclinically unstable as well.

Recently, de Jong et al. (2018) questioned the existence of the NIJ east of the Kolbeinsey Ridge, an extension of the mid-Atlantic Ridge north of Iceland (Fig. 1). They used RAFOS floats to investigate the subsurface circulation in the Iceland Sea, but did not find a connection between the flow east and west of the ridge. However, many of the floats deployed by de Jong et al. (2018) grounded on the continental slope north of Iceland. Substantial vertical velocities indicate the presence of a bottom Ekman layer, presumably caused by the NIJ, which has also been related to the rising of isopycnals due to cold, dense water banking up on the slope (Jónsson and Valdimarsson 2004). This was possibly the reason for the grounding of the floats.

It has been hypothesized that the NIJ is the lower limb of a local overturning loop north of Iceland that involves water mass transformation in the Iceland Sea. According to the idealized simulation of Våge et al. (2011), Atlantic Water in the NIIC is fluxed into the Iceland Sea by eddies, and the water is subsequently transformed due to air–sea heat loss. The resulting dense water progresses back toward the boundary and sinks, feeding the NIJ. Lagrangian trajectories from a high-resolution numerical model corroborate the importance of water mass transformation

TABLE 1. The scientific cruises, survey times, and occupied transects analyzed in this study. The transects are listed from west to east (Fig. 2). The acronyms are: KG = Kögur, HB = Hornbanki, SI = Siglunes, KR = Kolbeinsey Ridge, SL = Slétta, LN = Langanes Northeast, and LE = Langanes East.

Ship	Month	Year	KG	HB	SI	KR	SL	LN	LE
RRS <i>James Clark Ross</i>	August	2004	x						
R/V <i>Knorr</i>	October	2008	x	x		x			
R/V <i>Bjarni Sæmundsson</i>	August	2009	x	x	x		x	x	
R/V <i>Bjarni Sæmundsson</i>	February	2011	x	x	x		x	x	x
R/V <i>Knorr</i>	September	2011	x	x		x	x	x	
R/V <i>Bjarni Sæmundsson</i>	February	2012	x	x	x		x	x	x
RRS <i>James Clark Ross</i>	August	2012	x	x					
R/V <i>Bjarni Sæmundsson</i>	February	2013	x	x	x		x	x	x
R/V <i>Bjarni Sæmundsson</i>	August	2015	x	x		x	x	x	x
R/V <i>Hákon Mosby</i>	August	2016					x	x	
R/V <i>Bjarni Sæmundsson</i>	August	2017	x	x	x		x	x	x
NRV <i>Alliance</i>	February	2018				x			
R/V <i>Kristine Bonnevie</i>	June	2018				x	x	x	

in the Iceland Sea and the boundary current system north of Iceland for the formation of the NIJ (Behrens et al. 2017). However, this hypothesized local overturning loop has not been verified by observations, and details regarding the origin and underlying dynamics of the NIJ remain unclear.

One open question regards the supply of dense water to the NIJ. Water transformed in the Iceland Sea regularly exceeds the minimum potential density of DSOW (Våge et al. 2015), which is $\sigma_\theta = 27.8 \text{ kg m}^{-3}$ (Dickson and Brown 1994). The deepest and densest mixed layers have been found in the northwestern Iceland Sea, where enhanced heat loss offshore of the ice edge can intensify convection (Våge et al. 2015, 2018). However, Våge et al. (2015) and Pickart et al. (2017) argued that water mass transformation in the Iceland Sea may not be sufficient to account for the densest portion of the NIJ ($\sigma_\theta > 28.03 \text{ kg m}^{-3}$). They suggested instead that this portion may originate from the Greenland Sea, where sufficiently dense waters are regularly formed (e.g., Strass et al. 1993; Brakstad et al. 2019). While a tracer release study indicated export of dense water from the Greenland Sea to the Iceland Sea within 1.5 years (Messias et al. 2008), the exact time scales and pathways of this possible source for water in the NIJ remain unknown.

In this study we use an extensive collection of shipboard data, obtained during multiple cruises over multiple years, to advance our understanding of the NIJ. We compile hydrographic/velocity sections of high spatial resolution of the NIJ at seven different transects across the continental slope north of Iceland. In doing so, we determine the origin of the current and confirm its existence as an independent, major source of dense water to the Denmark Strait overflow. We provide robust estimates of the volume transport, and characterize

the current's properties, thus quantifying the spatial evolution of the hydrography and velocity of the NIJ for the first time along its entire pathway.

2. Data and methods

a. Shipboard measurements

The high-resolution hydrographic and velocity measurements analyzed in this study were collected during 13 shipboard surveys between 2004 and 2018, four of them during winter (Table 1). The surveys included seven transects across the northern slope of Iceland (Fig. 2). Six of the transects are repeated monitoring sections maintained by the Marine and Freshwater Research Institute of Iceland (MFRI), with extra stations added to better resolve the narrow NIJ. The typical station spacing of approximately 5 km over the slope is comparable to the Rossby radius of deformation in the Iceland Sea (4–5 km; Nurser and Bacon 2014). In the paper we refer to the individual transects by their MFRI section names (Table 1 and Fig. 2). For three of the surveys an alternative transect situated between the Kolbeinsey Ridge and the Slétta transect was sampled instead. We projected these stations onto the original bathymetry of the Slétta transect when constructing mean sections, but retained the bathymetry at the sampled location for transport calculations.

Some of the sections in our collection have been used in previous studies. Eight of the occupations at the Kögur transect were used by Pickart et al. (2017) to investigate the relationship between the NIIC and the NIJ. The mean properties at the Hornbanki transect provided the basis for the model validation in the study of Zhao et al. (2018). In addition, Våge et al. (2011), Våge et al. (2013), and Pickart et al. (2017)

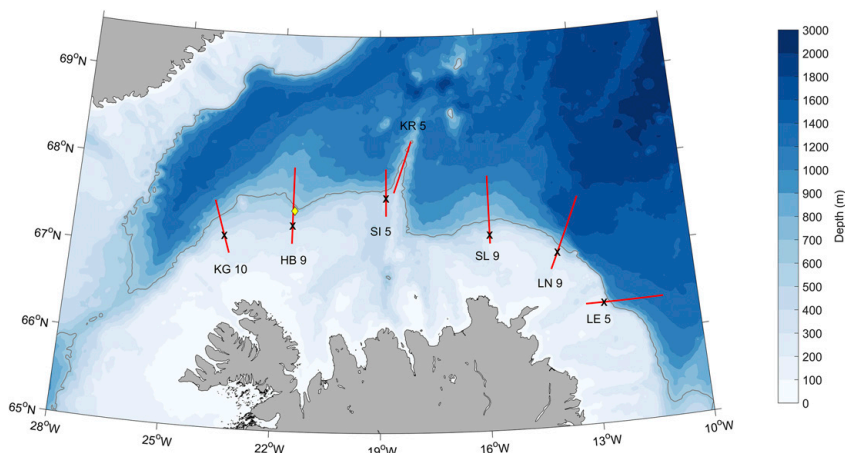


FIG. 2. Shipboard transects used in the study (red lines). The location of the shelf break at each line is indicated by the black crosses. The acronyms and numbers denote the transect names (KG = Kögur, HB = Hornbanki, SI = Siglunes, KR = Kolbeinsey Ridge, SL = Slétta, LN = Langanes Northeast, LE = Langanes East) and the number of occupations for each transect, respectively. The location of the mooring at the Hornbanki section is indicated by the yellow diamond. The bathymetry is shaded, and the 650-m isobath is highlighted by the gray contour.

included individual occupations from various transects in their studies.

The hydrographic data on all of the cruises were obtained using a Sea-Bird 911+ conductivity–temperature–depth (CTD) instrument. The CTD was mounted on a rosette with Niskin bottles to collect water samples, which were used to calibrate the conductivity sensor. The resulting accuracy of the CTD measurements is 0.3 dbar for pressure, 0.001°C for temperature, and 0.002 g kg⁻¹ for salinity (Våge et al. 2011). Velocities were measured using acoustic Doppler current profiler (ADCP) instruments. On three of the cruises (RRS *James Clark Ross* 2004, R/V *Knorr* 2008, NRV *Alliance* 2018), a vessel-mounted ADCP (VMADCP) was used, while an upward- and downward-facing lowered ADCP (LADCP) system mounted on the rosette was utilized on the remaining surveys. The VMADCP data on the R/V *Knorr* 2008 and NRV *Alliance* 2018 cruises were acquired using the University of Hawaii Data Acquisition System (UHDAS) and the VMDAS collection software (Teledyne RDInstruments), respectively. Subsequently, these data were processed using the Common Ocean Data Access System (CODAS; Firing and Hummon 2010). On the RRS *James Clark Ross* 2004 cruise, VMADCP data were collected and processed using a custom data acquisition system unique to the ship (Pstar system). The LADCP data were processed using the LADCP Processing Software Package from

the Lamont–Doherty Earth Observatory (Thurnherr 2010, 2018). Following the processing, the barotropic tides were removed from all of the velocity datasets by applying an updated version of the regional tidal model of Egbert and Erofeeva (2002), which has a resolution of 1/60°.

Using Laplacian-spline interpolation (Pickart and Smethie 1998), we constructed 2 km × 10 m gridded fields of Conservative Temperature and potential density anomaly referenced to the sea surface, as well as Absolute Salinity (hereafter referred to as temperature, density, and salinity, respectively). We followed the TEOS-10 standard (IOC et al. 2010), which differs by on average 0.167 for Absolute Salinity compared to practical salinity for the hydrographic properties of the NIJ. The temperature difference is smaller than the accuracy of the measurements, and the potential density in TEOS-10 is $O(0.001)$ kg m⁻³ greater than in ITS-90. Typical CTD stations indicating the station spacing in the mean sections were identified from the mean distances between the stations. Because the sections were truncated in order to display the same horizontal scale, there is not always a marker at the end of the sections; we have not extrapolated the data for more than two grid points.

We deviated from the normal interpolation routine for the two following situations. First, stations that were separated by more than 11 km (usually located

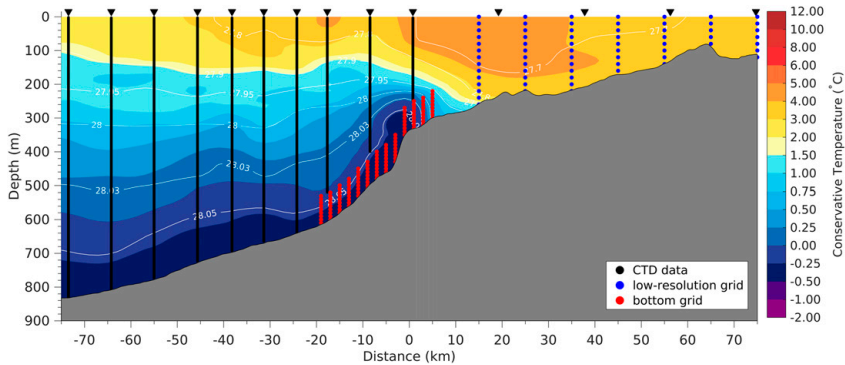


FIG. 3. Example of an occupation (Hornbanki, February 2013) with dense water residing at the shelf break. The CTD stations are indicated by black triangles. The stations on the shelf are separated by more than 11 km, so there the low-resolution grid was applied first (resulting in the blue data points). On the slope, the bottom grid was used (red dots). The low-resolution grid and bottom grid data were then combined with the remaining high-resolution CTD data (black dots), resulting in the final gridded temperature (color) and density (contours) sections. The cold, dense bottom layer of water along the slope is maintained using this multistep gridding routine.

on the shelf) were interpolated onto a low-resolution grid of $10\text{ km} \times 20\text{ m}$. This grid and the remaining, closer-spaced station data were then reinterpolated onto the final, high-resolution grid. Second, we employed a combined interpolation approach for occupations where very dense water ($\sigma_\theta \geq 28.03\text{ kg m}^{-3}$) was observed at the shelf break, in order to conserve the structure of the dense water banked up on the slope. In those sections, we interpolated the data first with respect to depth (depth grid, following the standard interpolation routine) and then with respect to height above the bottom (bottom grid). The bottom grid was used up to 100 m above the bottom at the steepest part of the slope where the dense water was present, while the depth grid was used for the remainder of the section. At the boundaries of the two grids, interpolation was used to ensure a smooth transition. An example in which both of these additional interpolation routines were applied is shown in Fig. 3.

Sections of absolute geostrophic velocity, normal to each transect, were calculated as follows. First, we constructed $2\text{ km} \times 10\text{ m}$ gridded sections of the cross-track ADCP velocities. Next, we computed the relative geostrophic velocity at each section using the hydrographic fields. At each grid point of the section, the depth-averaged relative geostrophic velocity was then matched to the corresponding depth-averaged ADCP velocity. The top and bottom 50 m were excluded for grid points with bottom depths greater than 200 m, in order to avoid surface and bottom boundary layers. The along-stream direction x is taken to be positive toward Denmark Strait, where distances between transects

were calculated following the 650-m isobath (Fig. 2). For each transect the origin (distance $y = 0\text{ km}$) was placed at the shelf break (except for the Kolbeinsey Ridge transect where the latitude of the shelf break at the nearby Siglunes transect was chosen as zero distance). Positive velocities are directed toward Denmark Strait.

The absolutely referenced geostrophic velocity sections were used to estimate the volume transports of the NIJ. The error associated with the volume transport is proportional to the area of the NIJ and estimated from a combination of instrument error and inaccuracies in the tidal model. Våge et al. (2011) estimated the combined uncertainty associated with the LADCP/VMADCP systems and the processing routine to be 3 cm s^{-1} , while they assessed the uncertainty of the tidal model to be 2 cm s^{-1} northwest of Iceland because of inaccuracies in bathymetry and relatively strong tidal currents. Although the tidal model performs slightly better northeast of Iceland, we conservatively assume the same error as for the western transects. An additional source of error arises from the transport calculation at the Kögur section (Fig. 2), where the NIJ at times is difficult to distinguish from the separated EGC (Harden et al. 2016). For each of these occupations, we distinguish the currents based on the differently sloping isopycnals and the subsurface salinity maximum of the separated EGC, which is not present in the NIJ (Harden et al. 2016). The differences between this “best-estimate” boundary, and a maximum and a minimum limit, are included in the total error for these occupations. Finally, we also increase the uncertainty of the transport for occupations where the current is not fully

covered by the observations. We then estimate the missing transport and include both this additional transport and its uncertainty estimated from the instrument and tidal errors to the uncertainty of the transport of the entire occupation.

b. Moored measurements

We use data from a current meter mooring deployed from 23 August 2005 to 10 August 2006, situated 19 km north of the shelf break at the Hornbanki transect ($67^{\circ}30.4516'N$ and $21^{\circ}32.1410'W$, Fig. 2). The instrument was an Aanderaa RCM-7, sampling hourly, which was placed at 360-m depth on the 620-m isobath. It thus provided a year-long time series of temperature, pressure, and velocity in the center of the NIJ. The velocity data were de-tided using the T_TIDE package (Pawlowicz et al. 2002) and rotated into the along- and across-stream directions associated with the Hornbanki transect. Following our convention above, positive along-stream velocities u are directed toward Denmark Strait.

c. Atmospheric data

To assess the wind field during the period of the mooring deployment, and its possible influence on the NIJ, we use the ERA-Interim reanalysis data from the European Centre for Medium-Range Weather Forecast (ECMWF; Dee et al. 2011). This weather prediction model, with an effective horizontal resolution of 80 km, assimilates meteorological data to approximate the atmospheric state every six hours. ERA-Interim reanalysis data have been shown to be accurate in our study region (Harden et al. 2011). Here we use the 6-hourly mean sea level pressure and 10-m wind field in the region across 0° – $45^{\circ}W$ and 55° – $75^{\circ}N$ for the period of the mooring deployment. We also consider the data from the grid point closest to the mooring as well as one grid point directly north of Denmark Strait (at the same latitude farther west).

3. Mean hydrography and velocity

The mean absolute geostrophic velocity sections for each transect (Fig. 4) offer the first robust view of the NIJ along the entire continental slope north of Iceland. Using data from two of the 13 surveys considered here, Våge et al. (2011) noted that the NIJ was weak at their northeasternmost transect (the Langanes Northeast section). This was consistent with the weakened NIJ in their idealized model in this part of the domain. The emergence and strengthening of the NIJ toward Denmark Strait occurring simultaneously with the disintegration of the NIIC toward northeast Iceland was representative of the model's

Iceland Sea overturning loop. Our data allow us to quantify the presence of the NIJ between Denmark Strait and northeast Iceland.

Starting at the easternmost section, Langanes East, a weak flow directed toward Denmark Strait is present near the shelf break in two of the five occupations. In the mean, however, the NIJ is not present at this transect (Fig. 4a). At the Langanes Northeast transect, 94 km farther downstream, velocities toward Denmark Strait were observed in each of the occupations (Fig. 4b). At times two cores of the current were present, although the flow was generally quite weak ($<5 \text{ cm s}^{-1}$ in the mean). Our data thus corroborate the notion by Våge et al. (2011) that the NIJ emerges somewhere between these two transects on the northeast slope of Iceland. At the Slétta transect, 94 km farther downstream, the existence of several cores becomes evident in the mean, and the current velocities are greater (Fig. 4c). The flow becomes even stronger and broadens where it crosses the Kolbeinsey Ridge (Fig. 4d). At the Siglunes transect, immediately downstream of the Kolbeinsey Ridge, the typical structure of the NIJ is more pronounced. In particular, the deep isopycnals slope upward and the shallow isopycnals slope downward toward the shelf break, leading to the characteristic middepth intensification of the current (Fig. 4e). Here only one core of the NIJ was observed in each occupation. Farther downstream at the Hornbanki transect, the NIJ exhibits again two cores in the mean (Fig. 4f). The core near the shelf break is strongest, with velocities approaching 15 cm s^{-1} . Between the two cores, the flow is in the opposite direction.

The last section presented here is the Kögur transect, where the NIJ at times merges with the surface-intensified separated EGC (Harden et al. 2016). Some of the EGC is visible in the westernmost part of the mean section (Fig. 4g). Using two years of mooring data from the Kögur transect, Huang et al. (2019) determined that there were three basic configurations of the flow on the Iceland slope: a strong separated EGC on the midslope, distinct from a weak NIJ farther upslope; a scenario where the two currents are merged; and a case where a strong NIJ is located near the 650-m isobath, its mean position in the moored time series, with a very weak signature of the separated EGC farther offshore. At times this latter scenario can persist close to Denmark Strait (R. Pickart 2019, unpublished data). At the sill, however, the separated EGC and NIJ appear to be fully merged, with the cold Arctic-origin water of the NIJ occupying the deepest part of the sill (Mastropole et al. 2017).

In all of the mean sections except the Kolbeinsey Ridge transect (which is located farther offshore than the others, Fig. 2), the surface-intensified NIIC is present

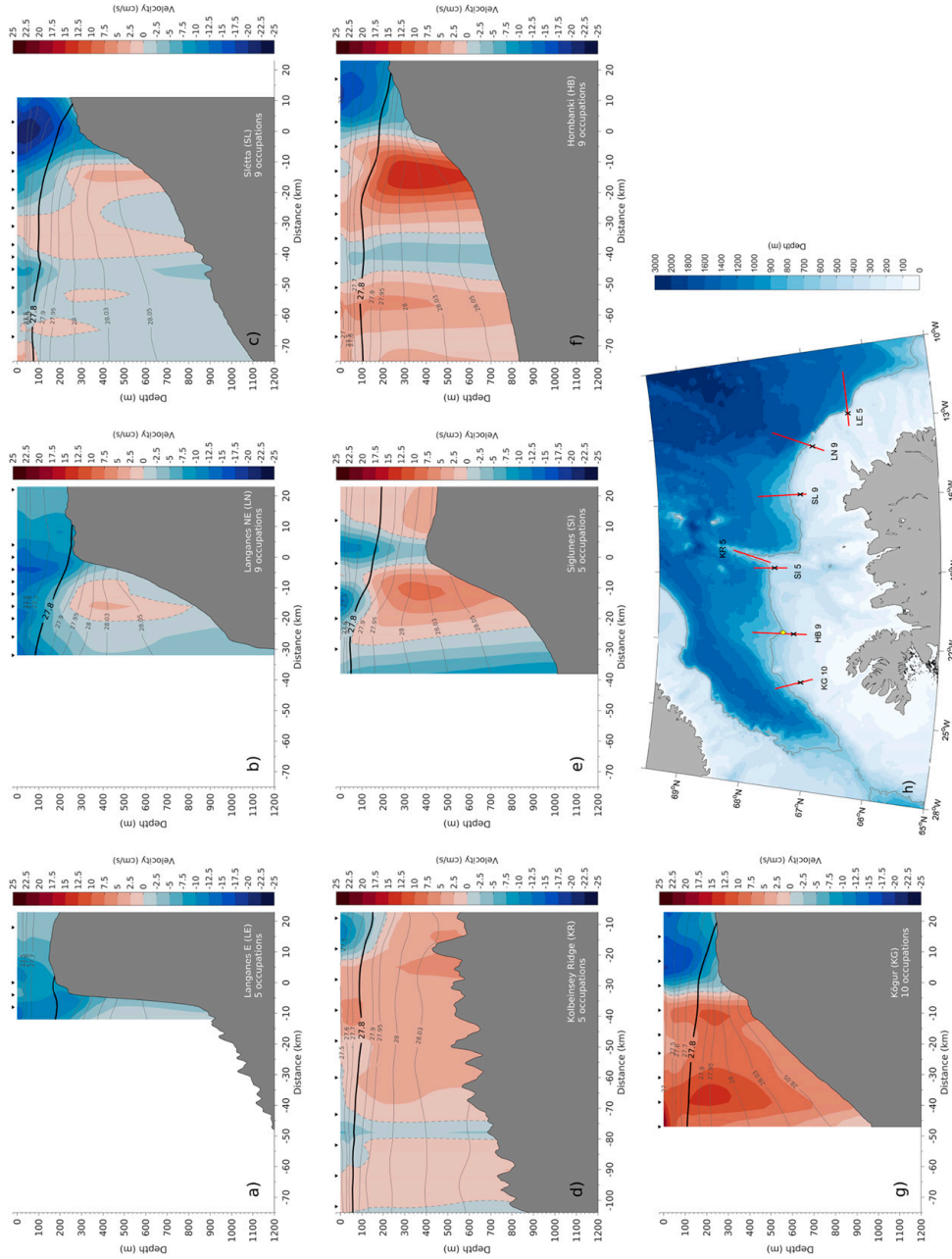


FIG. 4. (a)–(g) Mean absolute geostrophic velocity for each transect, overlain by density contours. The upper limit of overflow water, defined by $\sigma_{\rho} = 27.8 \text{ kg m}^{-3}$, is highlighted by the thick black line, while the zero velocity contour is marked by the dashed line. The black triangles indicate typical locations of CTD stations. Positive velocities are directed toward Denmark Strait. The eastermost and westermost transects are shown in (a) and (g), respectively. (h) A map showing the locations of all transects.

inshore of the NIJ flowing in the opposite direction. Notably, this is in contrast to the notion put forth by Våge et al. (2011) in which the NIIC disintegrates in concert with the NIJ progressing clockwise around the island. While we are unable to fully assess the NIIC transport with our data, since some of the sections do not capture the shoreward end of the current, we note that the mean transport of the core of the NIIC at the Langanes Northeast section is 0.85 Sv. This is half of the 1.7 Sv of NIIC transport at the Kögur transect estimated by Pickart et al. (2017). Hence, at the location where the NIJ first emerges on the northeast Iceland slope, the NIIC is still strong. Recently, Ypma et al. (2019) also called into question the direct connection between the NIIC and the NIJ via the local Iceland Sea overturning loop. Although substantial water mass transformation took place north of Iceland in their numerical simulations, the contribution of the NIIC to the DSOW was small.

The front separating the NIJ and NIIC is evident from the mean hydrographic sections (Figs. 5 and 6). In particular, the saline water of the NIIC is present inshore of the front at each site except for the Kolbeinsey Ridge section (Fig. 6). We note that at some of the transects, particularly the Kögur and Hornbanki sections, a layer of warm water extends well offshore of the shelf break (Fig. 5). Pickart et al. (2017) discussed this feature and demonstrated that, at times, the NIJ was located adjacent to the temperature front at the seaward edge of this layer, instead of the NIIC front. This is seen to be the case for the offshore NIJ core at the mean Kögur section. It is also occasionally true for individual realizations of the offshore core at the different transects. In Figs. 4–6 we have highlighted the 27.8 kg m^{-3} isopycnal, which slopes downward toward the shelf break and grounds on the outer shelf at most of the transects. This implies that the bulk of the overflow water is found seaward of the shelf break.

4. Double-core structure of the NIJ

The double-core structure of the NIJ, evident from the mean sections of absolute geostrophic velocity presented above, was previously noted by Pickart et al. (2017). They identified a second core of the NIJ in all of their winter occupations at the Kögur transect. When this offshore core was present, it was larger and stronger than the inshore core near the shelf break. We find that the double-core structure is not limited to the Kögur transect. The core locations identified from the individual realizations of the Hornbanki and Sléttá sections, west and east of the Kolbeinsey Ridge, respectively, are shown in Fig. 7. Any outer cores that were not entirely bracketed by the observations are not included. In all nine occupations of the Hornbanki transect, the inner core was

situated near the shelf break at the 600-m isobath at distance $y = -20 \text{ km}$. The outer core was present in six of the nine occupations. Its position varied slightly more than that of the inner core, and was found at the 800-m isobath in five of these occupations (Fig. 7).

At the Sléttá transect, east of the Kolbeinsey Ridge, the inner and outer cores were again centered at the 600- and 800-m isobaths, respectively. However, there was more cross-stream variation in the positions of both cores at this site. This could be due to the fact that the continental slope is steeper east of the Kolbeinsey Ridge, which results in a narrower NIJ. The distance between the inner and outer cores is approximately 17 km here compared to approximately 43 km at the transect west of the Kolbeinsey Ridge. Farther downstream, at the Kögur transect near Denmark Strait, the inner core appeared to be diverted higher onto the continental slope (near 400 m, Fig. 4g). We note, however, that this is likely not always the case. As discussed above, using the Kögur mooring array data, Huang et al. (2019) demonstrated that when the separated EGC is strong, the NIJ tends to be located on the upper continental slope. By contrast, when the separated EGC is weak (or absent), the NIJ is located near the 600-m isobath. We do not have enough shipboard realizations to investigate this definitively.

The double-core structure of the NIJ can also be identified from the mean current vectors computed using the repeat LADCP/VMADCP data (Fig. 8, where the currents are averaged between 100 m and the bottom). At both the Hornbanki and the Sléttá transects, the vectors were generally directed toward the west following the bathymetry with cores near the 600- and 800-m isobaths. The mean current vector at 360-m depth from the year-long mooring deployment at the Hornbanki transect west of the Kolbeinsey Ridge agrees well with the depth-averaged ADCP current vectors in magnitude and direction. Hence, the average of our nine synoptic shipboard surveys appears to be representative of the mean conditions.

The double-core structure of the NIJ appears to be a frequent feature of the current, with a second core present in roughly 50% of all occupations. The depth of the velocity maximum of the outer core is generally shallower in the water column (ranging from 200 to 400 m) compared to that of the inner core (ranging from 200 to 600 m). The temperature and salinity properties of the cores varied little within each occupation and did not show a systematic difference between the inner and outer cores. While Pickart et al. (2017) observed the second NIJ core only in the wintertime occupations of the Kögur transect, where it was stronger than the inner core, we did not identify any consistent seasonal variability in our more extensive dataset. At present it is unknown why the NIJ is

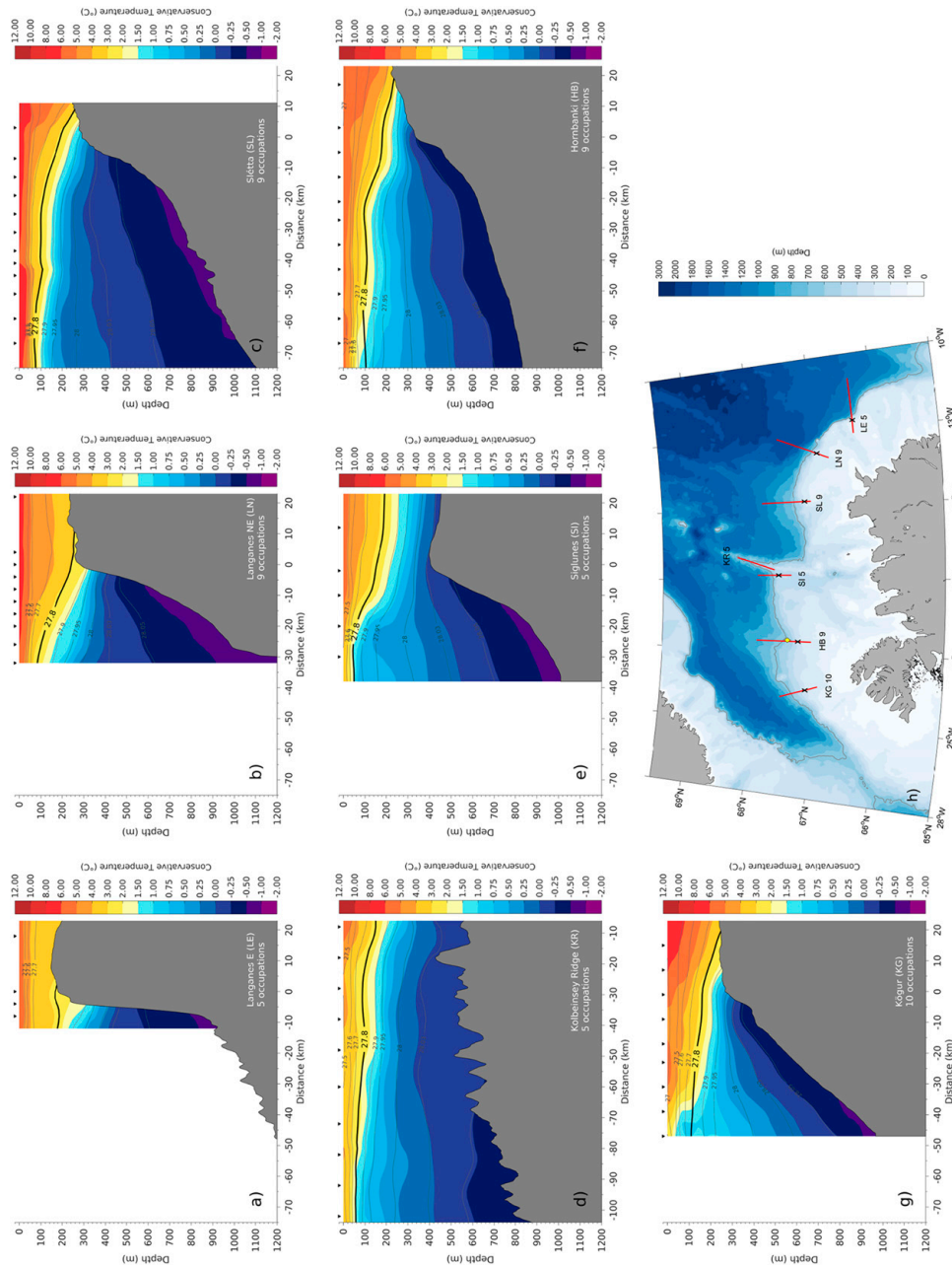


FIG. 5. Mean temperature for each transect, overlain by density contours. The upper limit of overflow water, defined by $\sigma_{\theta} \approx 27.8 \text{ kg m}^{-3}$, is marked by the thick black line. The black triangles indicate typical locations of CTD stations.

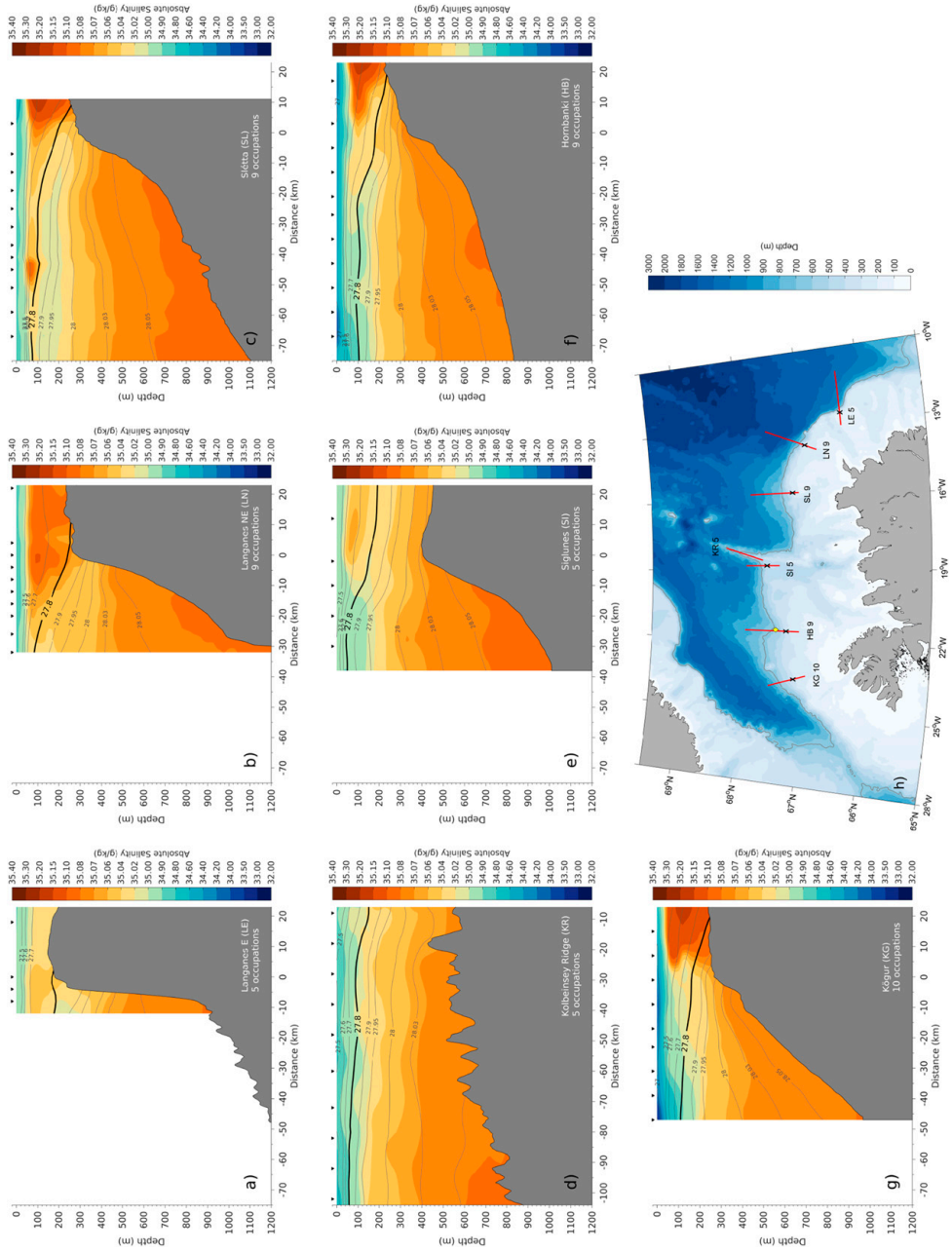


Fig. 6. Mean salinity for each transect, overlain by density contours. The upper limit of overflow water, defined by $\sigma_{\theta} \approx 27.8 \text{ kg m}^{-3}$, is marked by the thick black line. The black triangles indicate typical locations of CTD stations.

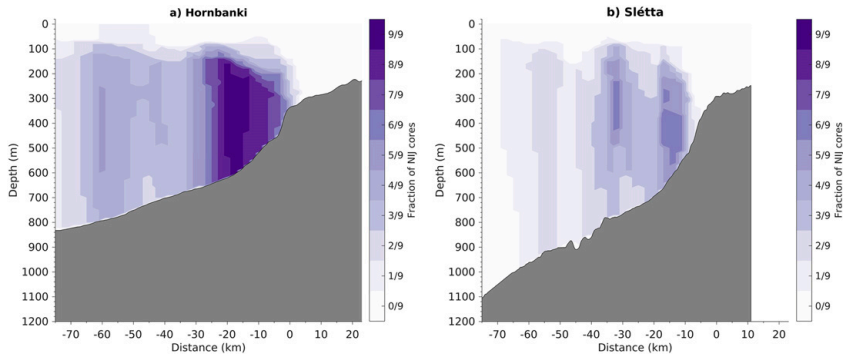


FIG. 7. Overlay of the locations of fully resolved NIJ cores at (a) Hornbanki (west of the Kolbeinsey Ridge) and (b) Slétta (east of the Kolbeinsey Ridge). The color indicates the number of realizations.

filamented in this fashion; we provide some thoughts concerning this in section 7.

5. Along-stream evolution

a. Hydrographic properties

For each of the six transects where the NIJ was present in the mean (which excludes Langanes East), we constructed a volume transport Θ - S diagram, which shows the mean volume transport over all occupations of the transect as a function of temperature and salinity. The resulting diagrams for the Slétta and Hornbanki transects are shown in Fig. 9. This revealed that only a very small portion of the water transported by the NIJ is not overflow water. At the Slétta transect, east of the Kolbeinsey Ridge, water lighter than 27.8 kg m^{-3} was very warm (up to 4°C) and saline (Fig. 9b). While the same was true at the Hornbanki transect west of the Kolbeinsey Ridge, there was also cold, fresh water near the surface (Fig. 9a). The total transport was larger at Hornbanki than Slétta, but at both transects the bulk of the transport was limited to a small area in Θ - S space.

For each of the volume transport Θ - S diagrams, we defined the locus of the 10 Θ - S classes containing the highest transport as the transport mode of the given section. (The exact number of Θ - S classes and their extents do not affect the results substantially; we chose divisions of 0.1°C in temperature and 0.005 g kg^{-1} in salinity). Considering all six transects, the transport mode is centered near $-0.29^\circ \pm 0.16^\circ\text{C}$ in temperature and $35.075 \pm 0.006 \text{ g kg}^{-1}$ in salinity, corresponding to a density of $\sigma_\theta = 28.05 \text{ kg m}^{-3}$. This demonstrates that the main source waters of the NIJ must be very dense. The cold temperature ($<0^\circ\text{C}$) classifies the mode as Arctic-origin water. This agrees

well with the Kögur mooring time series analyzed by Harden et al. (2016), who found that the NIJ transports water of Arctic origin at depth. By comparison, the EGC carries mostly warmer and lighter water of Atlantic origin (e.g., Håvik et al. 2017a). At Denmark Strait, Arctic-origin water is found in the deepest part of the passage, below water of Atlantic origin (Mastropole et al. 2017).

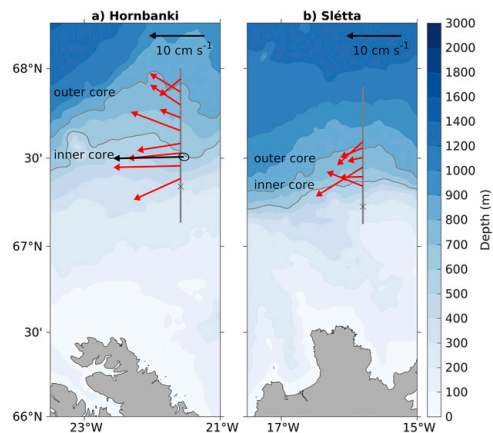


FIG. 8. Mean current vectors (red) for the nine occupations of (a) Hornbanki (west of the Kolbeinsey Ridge) and (b) Slétta (east of the Kolbeinsey Ridge) at the typical stations indicated in Fig. 4. The vectors are averaged between the bottom and 100-m depth, which coincides approximately with the depth of the 27.8 kg m^{-3} isopycnal (Fig. 4). The mean current vector from the year-long mooring record at Hornbanki and its standard error ellipse are shown in black. Black crosses indicate the location of the shelf break. Background colors show bathymetry, and the 600- and 800-m isobaths are highlighted.

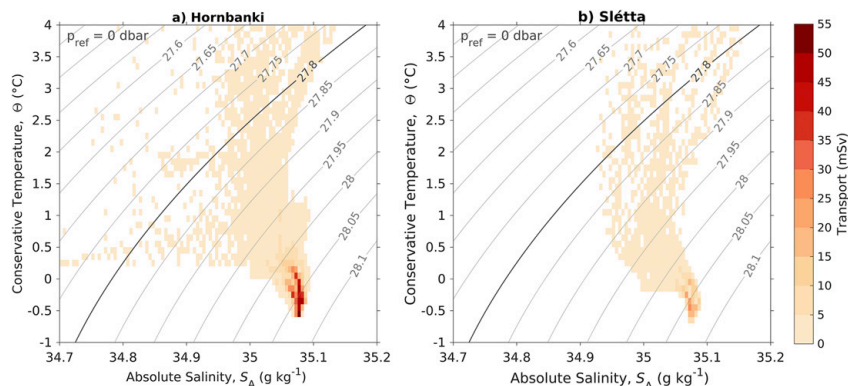


FIG. 9. Mean volume transport of the NIJ as function of temperature and salinity combined from all occupations at the (a) Hornbanki and (b) Slétta transects, west and east of the Kolbeinsey Ridge, respectively. The gray contours represent density, and the 27.8 kg m^{-3} isopycnal is highlighted.

To quantify the evolution of temperature and salinity along the length of the NIJ, we considered the variation of the 10 highest transport Θ - S classes at each site (Fig. 10). This shows how the hydrographic properties of the bulk of the overflow water are modified toward Denmark Strait. There is no significant linear trend of the median values of the 10 classes (red bars in Fig. 10) at the 95% confidence level according to the Student's t test, for either temperature or salinity. Since any such

trends are based on six values only, we used the bootstrap method to estimate the reliability of these trends. The bootstrap method is based on random sampling with replacement from the dataset and is not constrained by assumptions about the underlying probability distribution (e.g., Emery and Thomson 2014). From 1000 sample combinations chosen randomly from the pool of Θ - S classes at each transect, there is no true positive or negative trend in the hydrographic

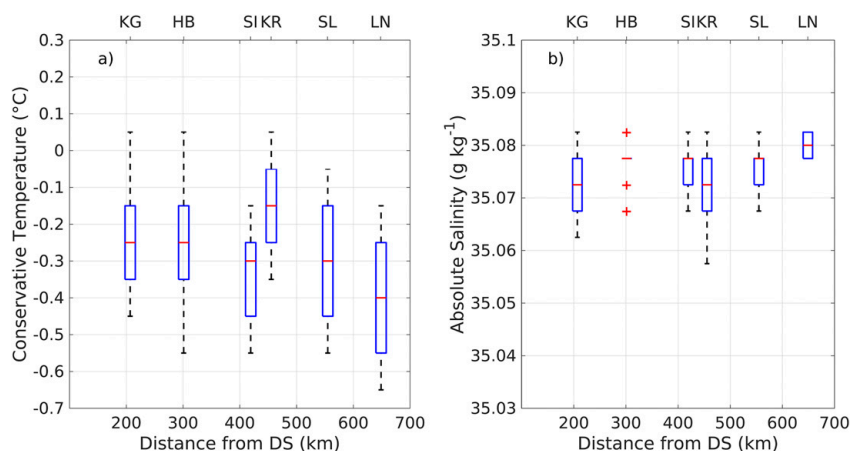


FIG. 10. Along-stream evolution of (a) temperature and (b) salinity for the 10 main transport classes of the NIJ (see text). The 25th and 75th percentiles for each transect are indicated by the blue boxes, and the median value is marked by the red dash. The black dashed lines show the range of values not considered to be outliers, while the red crosses indicate the outliers. The y axis is chosen such that the maximum range corresponds to a change in density of 0.05 kg m^{-3} with constant salinity and temperature for (a) and (b), respectively. The acronyms are: KG = Kögur, HB = Hornbanki, SI = Siglunes, KR = Kolbeinsey Ridge, SL = Slétta, and LN = Langanes Northeast.

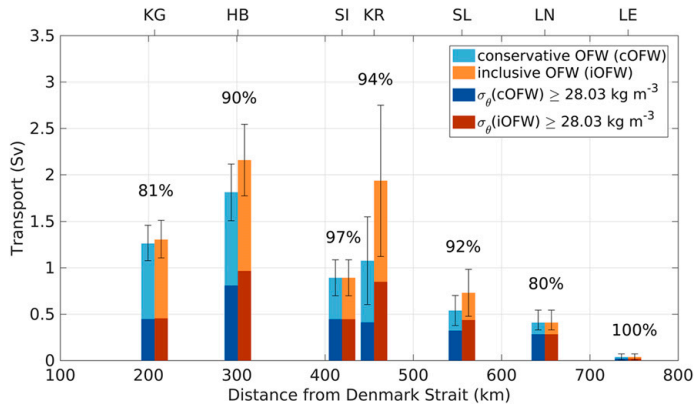


FIG. 11. Mean volume transport of overflow water (OFW) in the NIJ at the different transects, computed as the mean of the individual occupations. For the conservative estimate (cOFW, blue colors), the outer cores that were not fully resolved are ignored. For the inclusive estimate (iOFW, orange colors) the partially resolved outer cores were extrapolated (see text). Also shown is the portion of overflow water denser than $\sigma_\rho = 28.03 \text{ kg m}^{-3}$. The percentage indicates the fraction of overflow water to total transport at each transect. The acronyms are: KG = Kögur, HB = Hornbanki, SI = Siglunes, KR = Kolbeinsey Ridge, SL = Slétta, LN = Langanes Northeast, and LE = Langanes East.

properties at the 95% confidence level. We therefore conclude that the temperature, salinity, and density of the dominant transport mode of the NIJ are not significantly modified from northeast Iceland to Denmark Strait.

Interestingly, the temperature does exhibit a significant warming trend of approximately 0.1°C per 100 km toward Denmark Strait when considering the evolution of the mean temperature for the entire current (not shown). This implies that some portion of the NIJ warms along its path, possibly due to entrainment of ambient waters which are warmer northwest than northeast of Iceland. However, as demonstrated above, the entrainment does not significantly affect the properties of the dense transport mode.

b. Volume transport

While the temperature and salinity of the transport mode do not change significantly toward Denmark Strait, the mean velocity sections of Fig. 4 presented earlier indicate that the volume transport does; recall that the NIJ originates between the Langanes East and Langanes Northeast transects. We now present estimates of the overflow water transport at the different transects, computed as the mean of the individual occupations.

For each transect we provide two estimates. The first is based on a conservative approach where we disregarded all outer cores that were not fully resolved. This estimate

does not include all of the NIJ and provides a lower transport limit. For the second estimate, we doubled the transport of any outer core that was not fully resolved, with the idea being that the ship sampled roughly half of the core. This value, which we refer to as the inclusive estimate, is more realistic because we know that the full extent of the current was not sampled. In cases when we doubled an outer core that was not fully resolved, a larger uncertainty was assigned (section 2a). The two transport estimates are identical for the three transects where the NIJ was completely resolved.

The volume transport of overflow water increases by on average approximately 0.4 Sv per 100 km considering the six transects from Langanes East, northeast of Iceland, to Hornbanki, roughly 300 km upstream of Denmark Strait (Fig. 11). This trend is significant at the 95% confidence level according to the Student's t test. We have included the easternmost transect in Fig. 11, even though there is no flow in the mean section (Fig. 4). Our results emphasize that the NIJ emerges in the region northeast of Iceland. Furthermore, overflow water is by far the dominant constituent of the NIJ: the fraction of overflow water to the total transport is on average 90% for the collection of transects (Fig. 11).

The contribution to the transport from water deeper than 650 m, the approximate depth of the Denmark Strait sill, is comparably small. This portion accounts on average for only 10% of the transport of overflow

water. To contribute to the overflow, this water needs to be brought to shallower depths. Harden et al. (2016) showed that there is significant aspiration in Denmark Strait, which is why the deepest portion is included in our transport estimates. However, since the transport associated with this deepest portion is small, we can still compare the transport estimates to previous estimates by Våge et al. (2011) and Våge et al. (2013) who neglected this deep part of the NIJ.

While the transport increases overall toward Denmark Strait, the value decreases between the last two transects (Hornbanki to Kögur, Fig. 11). Observations (Harden et al. 2016) and numerical models (Behrens et al. 2017) show that the NIJ merges with the separated EGC between Hornbanki and Denmark Strait. Some of the water that is transported by the NIJ at Hornbanki may therefore be entrained into the separated EGC farther downstream, and thus is not accounted for in our transport estimates at Kögur. Our estimates for the Kögur transect are 1.3 ± 0.2 Sv, which agrees well with the 1.4 ± 0.3 and 1.23 ± 0.32 Sv estimated by Våge et al. (2013) and Pickart et al. (2017), respectively, both of whom took similar approaches for determining the transport using different subsets of the data analyzed here.

Notably, the transport estimates using our synoptic realizations of the Kögur transect are larger than the transport of the NIJ estimated by Harden et al. (2016) using data from the mooring array at that location (1.00 ± 0.17 Sv). One possible reason for this discrepancy is that we are presenting only 10 occupations, while the mooring data provided three realizations per day over a year-long period. Another possible reason for the discrepancy is that Harden et al. (2016) calculated net transport between the separated EGC and the Iceland shelf break, while we included only equatorward flow in our transport estimate. As such, these estimates are not directly comparable, and higher transports are expected from our approach. Furthermore, it was often difficult for Harden et al. (2016) to distinguish between the separated EGC and the NIJ. They developed an objective technique for determining the boundaries of these two currents and split the transport in the transition region evenly between them, but there was inherent uncertainty in such a division.

To shed light on this, we examined the gridded velocity sections from the mooring array and assigned a boundary between the separated EGC and the NIJ at each time step guided by the automatically determined separation lines from Harden et al. (2016), but also taking into account the differently sloping isopycnals of the two currents. In approximately 20% of the sections the separated EGC and the NIJ were

clearly distinct, while in the remaining realizations the currents were partially or fully merged. The transport of the NIJ estimated for the entire time series based on our boundary and considering equatorward flow only is 1.4 ± 0.1 Sv, which is in close agreement with our transport from the 10 hydrographic/velocity sections (1.3 ± 0.2 Sv). Considering only the subset of sections where the separated EGC and the NIJ were clearly distinct, the NIJ is recognizable as a middepth-intensified current. In approximately 40% of these sections it exhibited a double-core structure. Furthermore, the bulk of the transport had properties similar to the previously identified transport mode. This strongly suggests that our 10 hydrographic/velocity sections are representative of the mean conditions.

The transport of the NIJ for the subset of Kögur mooring sections where the current was distinct was 1.7 ± 0.2 Sv. This is close to our estimate from the Hornbanki transect where the NIJ has not yet started to merge with the EGC. There the transport is 1.8 ± 0.3 Sv for the conservative estimate and 2.2 ± 0.4 Sv for the inclusive estimate. All things considered, this suggests that the value of Harden et al. (2016) may be an underestimate. In particular, when the NIJ and the EGC are apart, the NIJ has a larger transport. On the other hand, when the currents are merged, some of the water transported by the NIJ may be assigned to the EGC, which would tend to reduce the estimated contribution of the NIJ at the Kögur transect. Our results thus imply a potentially greater role of the NIJ in supplying overflow water to Denmark Strait.

We also present the portion of overflow water transport denser than $\sigma_\theta = 28.03 \text{ kg m}^{-3}$ in Fig. 11. This value represents the bounding isopycnal of the NIJ transport mode discussed in the previous section (Fig. 9). As noted in Våge et al. (2013), water this dense is not found in either the shelfbreak EGC or the separated EGC above sill depth. Furthermore, most boluses passing through Denmark Strait contain water near this density (Mastropole et al. 2017). Våge et al. (2011) computed a transport of 0.6 ± 0.2 Sv of this dense water in Denmark Strait, which is comparable to our value of approximately 0.5 ± 0.1 Sv for the inclusive estimate at the Kögur transect (Fig. 11).

In general, the transport of water denser than $\sigma_\theta = 28.03 \text{ kg m}^{-3}$ increases toward Denmark Strait and accounts for on average 50% of the entire overflow transport (Fig. 11). This implies that the NIJ is supplied with dense water along its entire pathway. The model simulation of Våge et al. (2011) suggested that roughly two-thirds of the NIJ is supplied by sinking of dense water along the northern boundary of Iceland, while the remaining third is due to lateral entrainment.

Alternatively, there could be direct advective sources feeding the NIJ. One possible such source is a southward flow of overflow water that emanates north of the Spar Fracture Zone (Fig. 1) and follows the western side of the Kolbeinsey Ridge. The existence of such a flow has been suggested from RAFOS float tracks (de Jong et al. 2018) and numerical simulations (Behrens et al. 2017). Observations from a year-long mooring deployment close to the Kolbeinsey Ridge also indicated generally southward flow in 2007/08 (Jónsson and Valdimarsson 2012a). However, the mooring was situated near the 1000-m isobath south of the Spar Fracture Zone and hence it may have recorded parts of the NIJ crossing the ridge from the east and not a distinct flow originating from north of the Spar Fracture Zone. From our sections, we can neither confirm nor reject the existence of a southward flow west of the Kolbeinsey Ridge that supplies the NIJ. However, if there is such a current, it would only contribute a minor amount of water to the NIJ, as there is little change in transport between the Kolbeinsey Ridge and Hornbanki transects (Fig. 11).

The origin of the water constituting the densest portion of the NIJ is under debate. Using historical CTD data, Våge et al. (2015) showed that wintertime mixed-layer densities in the Iceland Sea only occasionally exceed $\sigma_\theta = 28.03 \text{ kg m}^{-3}$. This mainly occurs in the northwestern part of the Iceland Sea. (It is worth noting that the data coverage in winter is generally sparse.) In this region, heat loss offshore of the ice edge can intensify convection (Våge et al. 2015), which is facilitated by the removal of fresh surface waters before the onset of winter by northerly winds (Våge et al. 2018). Based on a freshwater budget of the region, Pickart et al. (2017) argued that convection in the northwestern Iceland Sea cannot account for more than half of the water in the NIJ. While water with properties of the densest portion of the NIJ is present throughout the Iceland Sea at greater depths, significant transformation must occur elsewhere.

The Greenland Sea has been suggested as a possible source for the densest portion of the NIJ (Våge et al. 2015; Pickart et al. 2017), where much denser and deeper mixed layers are common (e.g., Strass et al. 1993; Brakstad et al. 2019). For the Greenland Sea gyre, Brakstad et al. (2019) estimated the annual production of waters exceeding $\sigma_\theta = 28.05 \text{ kg m}^{-3}$ to be at least $0.6 \pm 0.5 \text{ Sv}$ for recent winters. This is roughly the same as the amount of water denser than $\sigma_\theta = 28.03 \text{ kg m}^{-3}$ transported by the NIJ, and thus adds credence to the notion that the densest water in the NIJ stems from the Greenland Sea. A tracer release study indicates that rapid export of dense water from the Greenland Sea to the Iceland Sea is

possible (Messias et al. 2008), but the exact pathways have not yet been identified.

While the RAFOS floats of de Jong et al. (2018) did not provide any evidence of the NIJ crossing the Kolbeinsey Ridge, we observed clear westward flow across the ridge on all of the occupations of this transect (Fig. 4d). This provides compelling evidence that the NIJ successfully negotiates the ridge as it flows westward. We note, however, that the transport of the current at the Siglunes transect, immediately downstream of the Kolbeinsey Ridge, appears to be anomalously small (i.e., it does not follow the general trend of increasing transport, Fig. 11). This motivates us to investigate the behavior of the NIJ around this sharp ridge using a scaling analysis.

Marshall and Tansley (2001) derived a condition for the separation of a boundary current from the continental slope which has been applied to different cases, including the middepth-intensified flow of Levantine Intermediate Water around Sardinia in the Mediterranean Sea (Bosse et al. 2015) and the flow of Canadian Basin Deep Water around the Morris Jesup Rise in the Arctic Ocean (Björk et al. 2010). Marshall and Tansley (2001) integrated the potential vorticity over an area encompassing the slope and the boundary current and found that the condition for the separation of the boundary current is comprised of three terms related to the planetary β effect, vortex stretching of the boundary current when crossing isobaths, and the curvature of the coastline or bathymetry. In our case, the β term is small compared to the vortex stretching term and can be neglected. The condition for separation of the current then scales as

$$r < \left(\frac{U}{f\sqrt{H/H}} \right)^{1/2}, \quad (1)$$

where r is the radius of curvature, U is the speed of the boundary current, f is the Coriolis parameter, and H is the depth. The radius of curvature where the NIJ crosses the Kolbeinsey Ridge is $r \approx 4\text{--}8 \text{ km}$, while the depth is $H \approx 600\text{--}800 \text{ m}$. Using the average speed of $U = 4.6 \text{ cm s}^{-1}$ as well as the minimum and maximum speeds ($\pm 2 \text{ cm s}^{-1}$) of the NIJ at the Kolbeinsey Ridge gives a critical r of $5\text{--}9 \text{ km}$, which is very similar to the measured radius of curvature. This result suggests that the entire NIJ cannot remain intact when turning south after crossing the ridge, and that only some part of the current is able to make the sharp turn to the Siglunes transect only 36 km downstream where the transport is lower (Fig. 11). We note that only a single current core has been observed at this transect (Fig. 4e), while the ADCP velocities farther offshore exhibit a southward component (not shown). Such a southward flow

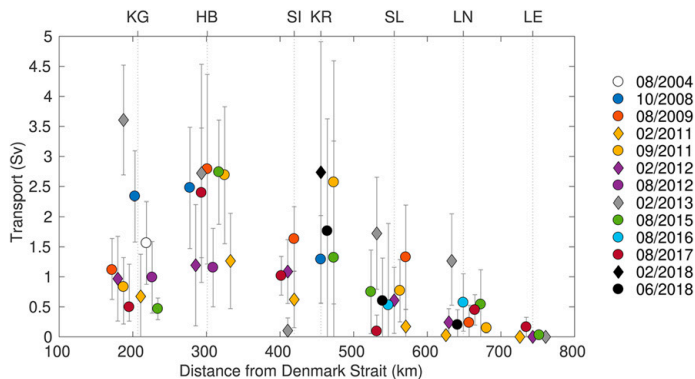


FIG. 12. Volume transport of overflow water in the NIJ and its uncertainty for all occupations and transects. Outer cores which were not fully resolved by the observations were doubled (see text). The survey years are color-coded, and winter occupations are marked by diamonds. For better legibility, estimates for the same transect are plotted adjacent to each other. The acronyms are: KG = Kögur, HB = Hornbanki, SI = Siglunes, KR = Kolbeinsey Ridge, SL = Slétta, LN = Langanes Northeast, and LE = Langanes East.

at the offshore end of the Siglunes transect, which has a north–south orientation, would not be accounted for since the absolute geostrophic velocity fields that the transports are calculated from are normal to the section. As noted above, a southward flow was also observed at a mooring located at the 1000-m isobath on the western side of the Kolbeinsey Ridge (Jónsson and Valdimarsson 2012a). It is possible that this flow is the separated part of the NIJ forced into deeper water due to the curvature of the ridge. The importance of the sharp curvature of the Kolbeinsey Ridge is also apparent from the flow pattern across the ridge (Fig. 4d). After following the bathymetry northward along the slope, the NIJ broadens when crossing the ridge and the double-core structure becomes less defined, likely due to the curvature effect. The separation of the current after crossing the ridge might reestablish the double-core structure of the NIJ and thus could explain the existence of the offshore core at the Hornbanki section, which was observed in six of the nine occupations (section 4).

Another aspect of the NIJ negotiating the Kolbeinsey Ridge pertains to flow observed on the shelf. As mentioned in section 2a, there was a transect situated just east of the ridge (14 km west of the Slétta transect). The continental shelf at this transect, and at the Siglunes transect, is deeper than 300 m—the only two survey lines where this is true. Recall that the maximum velocity of the NIJ is situated vertically in the water column near this depth. It is thus possible that some portion of the NIJ takes a direct route along the shelf instead of flowing

around the Kolbeinsey Ridge. Unfortunately, the occupations of these two transects do not coincide in time, so we cannot make inferences about the continuity of this flow. Further work is required to understand precisely how the NIJ progresses past the Kolbeinsey Ridge, although our data indicate that the current clearly transports overflow water from the east side of the ridge to the west side of the ridge.

6. Variability

The volume transport of the NIJ varies substantially both within and between the surveys. This is seen by plotting the individual transport values for all of the occupations following the inclusive approach (Fig. 12). The large scatter motivates us to explore possible forcing mechanisms that could influence the current's transport over different time scales.

a. Seasonal variability

While our dataset consists predominantly of summer occupations (Table 1), there is nonetheless no apparent difference in NIJ transport between summer and winter (Fig. 12). Both large and small transports occur in winter relative to the mean at most transects. This lack of seasonality agrees with transport time series from moorings as well as numerical simulations. Harden et al. (2016) reported a slight reduction in the NIJ transport in winter and spring from the 1-yr mooring array at Kögur, while Huang et al. (2019) found no consistent seasonal cycle from a 2-yr mooring deployed

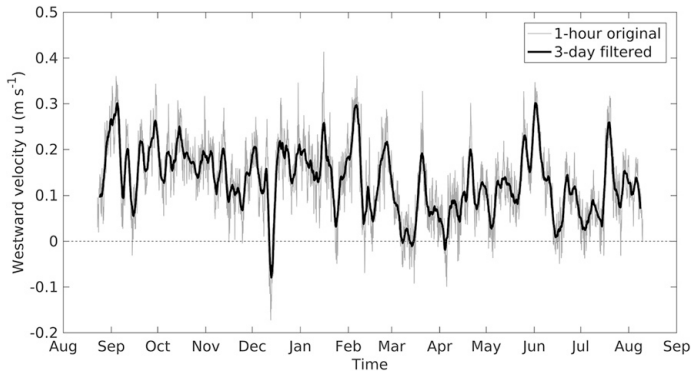


FIG. 13. Time series of de-tided velocity in the NIJ for the period of the mooring deployment (August 2005–August 2006) at the Hornbanki transect west of the Kolbeinsey Ridge (see Fig. 2 for the location of the mooring). The hourly and 3-day filtered time series are shown by the thin gray and thick black line, respectively.

in the NIJ at the same location. This agrees with velocity time series from three years of moored current meters on the Iceland slope of the Kögur transect (Jónsson 1999). Similarly, the transport of the NIJ did not have a seasonal cycle in the high-resolution numerical simulations of Behrens et al. (2017). Seasonal variability appears to be negligible farther upstream at the Hornbanki transect as well, and farther downstream at Denmark Strait. Neither the velocity time series in the core of the NIJ from the Hornbanki mooring (Fig. 13), nor long-term observations of the overflow plume (Jochumsen et al. 2017), reveal a seasonal cycle.

Regarding the hydrographic properties of the NIJ, we cannot identify distinct seasonal differences at any transect when comparing summer and winter subsets of Figs. 5 and 6 (not shown). The lack of a seasonal cycle is also reflected in the quantitative analysis of the individual cores of the NIJ (section 4). This corroborates the results of Mastropole et al. (2017) who found neither a seasonal cycle in the Arctic-origin water at Denmark Strait nor a seasonality in the occurrence of the boluses of Arctic-origin water passing through the strait. Our hydrographic sections reveal a seasonal change only near the surface, within the NIIC. As previously pointed out by Pickart et al. (2017), the water on the shelf is warmer, saltier, and more strongly stratified in summer than in winter. The NIIC varies seasonally in transport also, exhibiting a transport maximum in summer and a minimum in late spring, as other observations (Jónsson and Valdimarsson 2012b) and numerical simulations (Zhao et al. 2018) show. The seasonality in the NIIC is a result of changes in the atmospheric forcing (Logemann and Harms 2006; Zhao et al. 2018), which leads us

to investigate if atmospheric forcing may play a role in the variability of the NIJ on other time scales.

b. Atmospheric forcing

1) MESOSCALE VARIABILITY

Harden et al. (2016) found that, while the transports of the surface-intensified shelfbreak and separated EGC vary in time, the changes largely compensate each other. They argued that this variability is controlled by the across-stream gradient in the local wind through Denmark Strait. Here we investigate the possible effect of the wind on the mesoscale variability in the middepth-intensified NIJ using the moored record in the center of the current at the Hornbanki transect (Fig. 13; section 2b). The westward speed was on average 13 cm s^{-1} , ranging between a maximum of 41 cm s^{-1} in September and a minimum of -17 cm s^{-1} in December. The latter event was unique in that the current reversed its direction for approximately four days.

Using the ERA-Interim reanalysis data (section 2c), we investigate the atmospheric conditions before, during, and after weakening and strengthening events of the NIJ at Hornbanki. The events are defined as times when the velocity from the moored record either exceeded or fell short of a certain threshold (such as a defined velocity, a local maximum, or a gradient). The exact magnitude of this threshold did not affect the results substantially. While a high pressure system south of Iceland induced southerly wind through Denmark Strait against the flow direction of the NIJ during the strong reversal event noted above, similar wind anomalies occurred without weakening the NIJ in a consistent

way. Similarly, we did not detect any relation between strengthening events of the NIJ and the atmospheric conditions. We thus conclude that, despite the coincidence of the extended current reversal and the strong southerly storm, there was no consistent mesoscale response of the NIJ at Hornbanki to atmospheric forcing southwest of Iceland and in Denmark Strait during the period of the mooring deployment.

2) LONG-TERM VARIABILITY

While the compensation in volume transport of the separated and shelfbreak branches of the EGC has only been observed on short time scales (Harden et al. 2016), numerical simulations suggest that the two current branches vary out of phase on seasonal to interannual time scales as well. Behrens et al. (2017) argued that the local wind stress curl pattern substantially affects the EGC, which results in variability in the net volume transport of the combined branches across the Kögur transect on interannual time scales. They did not, however, find a clear response of the NIJ or the NIIC to changes in the wind stress curl. By contrast, in the numerical model used by Zhao et al. (2018), the wind stress southwest of Iceland impacted the transport of Atlantic Water in the NIIC. Furthermore, Pickart et al. (2017) argued that interannual changes in salinity of the NIIC and NIJ are linked through the wind stress curl in the subpolar gyre. Changes in wind stress curl have also been tied to varying sources of dense water advected into Denmark Strait. In the model study of Köhl (2010), strong positive wind stress curl around Iceland caused the EGC to be the main source of overflow water to Denmark Strait, whereas the Iceland Sea was the dominant source when the wind stress curl was weakly positive. De Jong et al. (2018) suggested that the strong wind stress curl during their RAFOS float deployment period may have been the reason why the NIJ appeared weak or absent in the float trajectories.

To investigate the effect of wind on interannual time scales, we identified surveys with consistently strong or weak NIJ transport and assessed the corresponding wind stress curl fields around Iceland, following the approach of de Jong et al. (2018, see their Fig. 9). In particular, we determined the occupations with above-median and below-median transports for each survey. (The median transport was used at each transect to account for the general increase in transport toward Denmark Strait.) Only one survey could be considered to have an overall weak NIJ (February 2011, where all five transects had transports below the median). Conversely, only two surveys had a relatively strong NIJ (February 2013 and August 2009, where four of five transects had

transports above the median). All three surveys were conducted during periods of wind stress curl near its climatological mean value according to the atmospheric time series of de Jong et al. (2018), so we do not see a difference in wind stress curl between surveys with a weak and a strong NIJ, and, most often, there was no overall weak or strong NIJ. As such, our observations clearly do not support the hypothesis that the wind stress curl controls the strength of the NIJ on interannual time scales.

c. Internal variability

It has long been known that the overflow at Denmark Strait is highly variable on periods of a few days to a week (Aagaard and Malmberg 1978; Ross 1978; Macrander et al. 2007; Jochumsen et al. 2017; von Appen et al. 2017). Different configurations of the overflow have been identified, including the large boluses mentioned above, as well as another common scenario where the overflow layer thins and accelerates (referred to as pulses; von Appen et al. 2017). It has been argued that the dominant driver of this high-frequency variability is baroclinic instability (Smith 1976; Spall et al. 2019). Upstream of the sill, Håvik et al. (2017b) showed that the EGC is subject to baroclinic instability in winter, and suggested that this may be a source of the high-frequency variability in Denmark Strait. Regarding the NIJ, Harden and Pickart (2018) demonstrated that energetic topographic Rossby waves, with a dominant period of 3.6 days, are present at the Kögur site. They argued that the source of the waves is the meandering separated EGC seaward of the NIJ. Huang et al. (2019) calculated a significant conversion of potential energy from the mean to the eddies at the same site, indicative of baroclinic instability. Using our shipboard data, we now consider internal variability of the NIJ.

1) BAROTROPIC INSTABILITY

Barotropic instability is generally caused by strong horizontal velocity gradients, although it can be suppressed by steep bathymetry (von Appen et al. 2016). Eddies resulting from these instabilities extract kinetic energy from the mean flow and transport momentum down the lateral velocity gradient (Spall et al. 2008). A necessary criterion for barotropic instability to occur is that $\beta - (\partial^2 u / \partial y^2)$ changes sign somewhere in the domain (e.g., Cushman-Roisin and Beckers 2011). The topographic β effect is represented by $\beta = -(fH)(\partial H / \partial y)$, where f denotes the Coriolis parameter and H depth. The bathymetric slopes in our study area yield relatively large values of $\beta = O(10^{-8})$. We compared this to $u_{yy} = \partial^2 u / \partial y^2$ for each current core. For example, at the Hornbanki transect west of the Kolbeinsey Ridge, the along-stream

velocity u is on average 16 cm s^{-1} with current widths of order 16 km. This means that u_{yy} is of the same order of magnitude as β . The same result holds for the majority of the transects. Therefore, the necessary—but not sufficient—condition for barotropic instability is fulfilled for the NIJ.

2) BAROCLINIC INSTABILITY

Baroclinic instability is generally facilitated by strong vertical shear of the horizontal velocity, whereas it can be suppressed by a strong stratification (von Appen et al. 2016). Resulting eddies extract the available potential energy from the mean field and transport this energy down the mean lateral density gradient (Spall et al. 2008). A necessary condition for baroclinic instability to occur is that the horizontal gradient of the total potential vorticity changes sign with depth (e.g., Spall et al. 2008). The Ertel potential vorticity is the sum of the planetary stretching term, the relative vorticity, and the tilting vorticity (e.g., Pickart et al. 2005; Spall et al. 2008). We find that the stretching term is the dominant contribution to the total potential vorticity. As such, we can simplify the Ertel potential vorticity (PV) to $PV \approx -(\mathcal{f}/\rho_0)(\partial\rho/\partial z)$, where ρ_0 is the background potential density. The vertical sections of PV for the individual occupations of the different transects yield the consistent result that the horizontal gradient of PV reverses sign with depth. Therefore, the necessary criterion for baroclinic instability is also fulfilled for the NIJ.

These results imply that some of the observed variability in structure and transport of the NIJ may be due to internal variability in the form of both barotropic and baroclinic instability. We note that such high-frequency fluctuations could make it more difficult to infer responses of the NIJ to atmospheric forcing; continued measurements of the current will hopefully make this easier. The internal variability in the NIJ requires further investigation and will be the subject of future work.

7. Summary and conclusions

In this study we used high-resolution hydrographic/velocity measurements from 13 surveys along the slope north of Iceland to characterize and quantify the properties and transport of the NIJ for the first time along its entire path. The current emerges northeast of Iceland and crosses the Kolbeinsey Ridge, an extension of the mid-Atlantic Ridge north of Iceland. Near Denmark Strait the NIJ merges with the separated EGC, and from that point onward it cannot be distinguished as a distinct current. Our results demonstrate that the NIJ represents an important contribution to the Denmark Strait overflow.

The current displays a double-core structure that is present both east and west of the Kolbeinsey Ridge at roughly 50% of all occupations. The inner core is generally found at the 600-m isobath, while the outer core is located farther downslope at the 800-m isobath. It is presently unclear whether the outer core is a separate component of the current or if it is related to eddies or wave activity. Harden and Pickart (2018) demonstrated that topographic Rossby waves on the Iceland slope cause high-frequency variability in the NIJ signature at the Kögur site, but whether these or other waves also exist farther upstream remains to be determined. Here we considered the outer core to be an integral part of the current and included it in the transport estimates.

The volume transport of overflow water in the NIJ, which comprises on average 90% of the total transport of the current, increased by approximately 0.4 Sv per 100 km along the current's path until the Hornbanki transect, roughly 300 km upstream of Denmark Strait. This gradual increase is consistent with the model results of Våge et al. (2011) which suggest that the current is fed by sinking of dense water along the entire north slope of Iceland. The water transported by the NIJ is mainly of Arctic origin, with the coldest and densest portion banked up against the continental slope. The bulk of the volume transport is confined to a small area in Θ - S space centered near $-0.29^\circ \pm 0.16^\circ\text{C}$ in temperature and $35.075 \pm 0.006 \text{ g kg}^{-1}$ in salinity, corresponding to a density of $\sigma_\theta = 28.05 \text{ kg m}^{-3}$. The hydrographic properties of this transport mode do not change significantly along the current's path, which indicates that the mode is largely unaffected by entrainment of warmer, ambient waters. This densest portion of the NIJ most likely stems from the Greenland Sea, where sufficiently dense waters are regularly formed (Brakstad et al. 2019). However, the exact pathways between the Greenland and Iceland Seas remain unknown.

Comparing the volume transport of the NIJ to the transport estimated from the year-long mooring array at the Kögur transect ($1.00 \pm 0.17 \text{ Sv}$; Harden et al. 2016), we found a higher mean transport of $1.3 \pm 0.2 \text{ Sv}$ for both the conservative and inclusive estimates. Some of this discrepancy is likely due to the different types of measurements (multiple realizations per day for a year versus our 10 occupations over 13 years) and the different methods of estimating transport (the different approach for assigning current boundaries and the consideration of net flow versus equatorward flow). Extracting periods from the gridded mooring sections when the NIJ is clearly distinct from the EGC, we found a transport of $1.7 \pm 0.2 \text{ Sv}$. This result agrees well with the transport of the NIJ at the Hornbanki transect farther upstream, where it is at least $1.8 \pm 0.3 \text{ Sv}$ and more likely

2.2 ± 0.4 Sv according to the conservative and inclusive estimates, respectively. This suggests that when the currents are distinct at the Kögur transect, the contribution from the NIJ is higher than when the currents have merged and some of the NIJ transport may have been entrained into the separated EGC, appearing to lower the NIJ transport. We therefore argue that the contribution of water from the NIJ to the Denmark Strait overflow is higher than previously envisaged.

The variability in volume transport between and within the surveys was substantial. On short time scales, no direct link between the variability of the NIJ and the local wind could be identified. While a current reversal observed in the moored record at the Hornbanki transect coincided with anomalously strong southerly wind through Denmark Strait, no consistent response to similar atmospheric patterns was found. Similarly, no clear seasonal variability of the NIJ was detected, in agreement with previous observational and modeling results (Harden et al. 2016; Behrens et al. 2017).

On longer time scales, it has been hypothesized that the wind stress curl around Iceland affects the strength of the NIJ (Köhl 2010; de Jong et al. 2018). However, no clear link between the wind stress curl and the strength of the NIJ could be established from our observations. The most likely explanation for the variability in our transport estimates is internal forcing, as the necessary conditions for both barotropic and baroclinic instability are fulfilled in the NIJ.

This study, by characterizing and quantifying the along-stream evolution of the NIJ, provides the basis for future dynamical investigations addressing the formation and variability of the current. Our comprehensive dataset has definitively confirmed that the NIJ emerges northeast of Iceland, is fed by a continuous supply of dense water along the current's entire pathway, and is a main source of DSOW into Denmark Strait. The NIJ thus constitutes a fundamental component of the overturning in the Nordic Seas that needs to be accounted for when considering the response of the AMOC to varying climate forcing.

Acknowledgments. Six different research vessels were involved in the collection of the data used in this study: RRS *James Clark Ross*, R/V *Knorr*, R/V *Bjarni Sæmundsson*, R/V *Håkon Mosby*, NRV *Alliance*, and R/V *Kristine Bonnevie*. We thank the captain and crew of each of these vessels for their hard work as well as the many watch standers who have sailed on the cruises and helped collect the measurements. We also thank Frank Bahr for processing the VMADCP data collected on NRV *Alliance* and Magnús Danielsen for the processing of the hydrographic data collected on R/V *Bjarni Sæmundsson*. We acknowledge Leah

Trafford McRaven for assistance with Fig. 1 and two anonymous reviewers for their helpful comments, which improved the manuscript. Funding for the project was provided by the Bergen Research Foundation Grant BFS2016REK01 (K. Våge and S. Semper), the Norwegian Research Council under Grant Agreement 231647 (K. Våge), and the U.S. National Science Foundation Grants OCE-1259618 and OCE-1756361 (R. S. Pickart and D. J. Torres), as well as OCE-1558742 (R. S. Pickart). The dataset is available on PANGAEA under <https://doi.pangaea.de/10.1594/PANGAEA.903535>.

REFERENCES

- Aagaard, K., and S. A. Malmberg, 1978: Low-frequency Characteristics of the Denmark Strait Overflow. ICES CM 1978/C:47, International Council for the Exploration of the Sea, 22 pp.
- Almansi, M., T. W. N. Haine, R. S. Pickart, M. G. Magaldi, R. Gelderloos, and D. Mastropole, 2017: High-frequency variability in the circulation and hydrography of the Denmark Strait overflow from a high-resolution numerical model. *J. Phys. Oceanogr.*, **47**, 2999–3013, <https://doi.org/10.1175/JPO-D-17-0129.1>.
- Amante, C., and B. W. Eakins, 2009: ETOPO1 1 arc-minute global relief model: Procedures, data sources, and analysis. NOAA Tech. Memo. NESDIS NGDC-24, 25 pp., <https://www.ngdc.noaa.gov/mgg/global/relief/ETOPO1/docs/ETOPO1.pdf>.
- Behrens, E., K. Våge, B. Harden, A. Biastoch, and C. Böning, 2017: Composition and variability of the Denmark Strait Overflow Water in a high-resolution numerical model hindcast simulation. *J. Geophys. Res. Oceans*, **122**, 2830–2846, <https://doi.org/10.1002/2016JC012158>.
- Björk, G., and Coauthors, 2010: Flow of Canadian basin deep water in the Western Eurasian Basin of the Arctic Ocean. *Deep-Sea Res. I*, **57**, 577–586, <https://doi.org/10.1016/j.dsr.2010.01.006>.
- Bosse, A., P. Testor, L. Mortier, L. Prieur, V. Taillandier, F. D'Ortenzio, and L. Coppola, 2015: Spreading of Levantine Intermediate Waters by submesoscale coherent vortices in the northwestern Mediterranean Sea as observed with gliders. *J. Geophys. Res. Oceans*, **120**, 1599–1622, <https://doi.org/10.1002/2014JC010263>.
- Brakstad, A., K. Våge, L. Håvik, and G. W. K. Moore, 2019: Water mass transformation in the Greenland Sea during the period 1986–2016. *J. Phys. Oceanogr.*, **49**, 121–141, <https://doi.org/10.1175/JPO-D-17-0273.1>.
- Cooper, L. H. N., 1955: Deep water movements in the North Atlantic as a link between climatic changes around Iceland and biological productivity of the English Channel and Celtic Sea. *J. Mar. Res.*, **14** (4), 347–362.
- Cushman-Roisin, B., and J.-M. Beckers, 2011: *Physical and Numerical Aspects*. 2nd ed. Introduction to Geophysical Fluid Dynamics, Vol. 101, Academic Press, 845 pp.
- Dee, D. P., and Coauthors, 2011: The ERA-Interim reanalysis: Configuration and performance of the data assimilation system. *Quart. J. Roy. Meteor. Soc.*, **137**, 553–597, <https://doi.org/10.1002/qj.828>.
- de Jong, M. F., H. Sjøland, A. S. Bower, and H. H. Furey, 2018: The subsurface circulation of the Iceland Sea observed with RAFOS floats. *Deep-Sea Res. I*, **141**, 1–10, <https://doi.org/10.1016/j.dsr.2018.07.008>.

- Dickson, R. R., and J. Brown, 1994: The production of North Atlantic Deep Water: Sources, rates, and pathways. *J. Geophys. Res.*, **99**, 12 319–12 341, <https://doi.org/10.1029/94JC00530>.
- Egbert, G. D., and S. Y. Erofeeva, 2002: Efficient inverse modeling of barotropic ocean tides. *J. Atmos. Oceanic Technol.*, **19**, 183–204, [https://doi.org/10.1175/1520-0426\(2002\)019<0183:EIMOBO>2.0.CO;2](https://doi.org/10.1175/1520-0426(2002)019<0183:EIMOBO>2.0.CO;2).
- Eldevik, T., J. E. Ø. Nilsen, D. Iovino, K. Anders Olsson, A. B. Sandø, and H. Drange, 2009: Observed sources and variability of Nordic seas overflow. *Nat. Geosci.*, **2**, 406–410, <https://doi.org/10.1038/ngeco518>.
- Emery, W. J., and R. E. Thomson, 2014: *Data Analysis Methods in Physical Oceanography*. 3rd ed., Elsevier, 728 pp.
- Firing, E., and J. M. Hummon, 2010: Shipboard ADCP measurements. IOCCP Rep. 14, ICPO Publication Series 134, International CLIVAR Project Office, 11 pp., http://www.go-ship.org/Manual/Firing_SADCP.pdf.
- Harden, B. E., and Coauthors, 2016: Upstream sources of the Denmark Strait Overflow: Observations from a high-resolution mooring array. *Deep-Sea Res. I*, **112**, 94–112, <https://doi.org/10.1016/j.dsr.2016.02.007>.
- , and R. S. Pickart, 2018: High-frequency variability in the North Icelandic Jet. *J. Mar. Res.*, **76**, 47–62, <https://doi.org/10.1357/002224018824845910>.
- , I. A. Renfrew, and G. N. Petersen, 2011: A climatology of wintertime barrier winds off southeast Greenland. *J. Climate*, **24**, 4701–4717, <https://doi.org/10.1175/2011JCLI4113.1>.
- Hävik, L., R. S. Pickart, K. Våge, D. J. Torres, A. M. Thurnherr, A. Beszczynska-Möller, W. Walczowski, and W. J. von Appen, 2017a: Evolution of the East Greenland Current from Fram Strait to Denmark Strait: Synoptic measurements from summer 2012. *J. Geophys. Res. Oceans*, **122**, 1974–1999, <https://doi.org/10.1002/2016JC012228>.
- , K. Våge, R. S. Pickart, B. Harden, W. J. von Appen, S. Jónsson, and S. Østerhus, 2017b: Structure and variability of the shelfbreak East Greenland Current north of Denmark Strait. *J. Phys. Oceanogr.*, **47**, 2631–2646, <https://doi.org/10.1175/JPO-D-17-0062.1>.
- Huang, J., R. S. Pickart, H. Valdimarsson, P. Lin, M. A. Spall, and F. Xu, 2019: Structure and variability of the North Icelandic Jet from two years of mooring data. *J. Geophys. Res. Oceans*, **124**, 3987–4002, <https://doi.org/10.1029/2019JC015134>.
- IOC, SCOR, and IAPSO, 2010: The international thermodynamic equation of seawater – 2010: Calculation and use of thermodynamic properties. Intergovernmental Oceanographic Commission, Manuals and Guides 56, UNESCO, 196 pp., http://www.teos-10.org/pubs/TEOS-10_Manual.pdf.
- Jansson, E., S. Jutterström, B. Rudels, L. G. Anderson, K. Anders Olsson, E. P. Jones, W. M. Smethie, and J. H. Swift, 2008: Sources to the East Greenland Current and its contribution to the Denmark Strait Overflow. *Prog. Oceanogr.*, **78**, 12–28, <https://doi.org/10.1016/j.pocean.2007.08.031>.
- Jochumsen, K., M. Moritz, N. Nunes, D. Quadfasel, K. M. Larsen, B. Hansen, H. Valdimarsson, and S. Jónsson, 2017: Revised transport estimates of the Denmark Strait overflow. *J. Geophys. Res. Oceans*, **122**, 3434–3450, <https://doi.org/10.1002/2017JC012803>.
- Jónsson, S., 1999: The circulation in the northern part of the Denmark Strait and its variability. ICES CM 1999/L06, International Council for the Exploration of the Sea, 9 pp., <http://www.ices.dk/sites/pub/CM%20Documents/1999/L06099.pdf>.
- , and H. Valdimarsson, 2004: A new path for the Denmark Strait overflow water from the Iceland Sea to Denmark Strait. *Geophys. Res. Lett.*, **31**, L03305, <https://doi.org/10.1029/2003GL019214>.
- , and —, 2012a: Hydrography and circulation over the southern part of the Kolbeinsey Ridge. *ICES J. Mar. Sci.*, **69**, 1255–1262, <https://doi.org/10.1093/icesjms/fss101>.
- , and —, 2012b: Water mass transport variability to the North Icelandic shelf, 1994–2010. *ICES J. Mar. Sci.*, **69**, 809–815, <https://doi.org/10.1093/icesjms/fss024>.
- Köhl, A., 2010: Variable source regions of Denmark Strait and Faroe Bank Channel overflow waters. *Tellus*, **62A**, 551–568, <https://doi.org/10.1111/j.1600-0870.2010.00454.x>.
- , R. H. Käse, D. Stammer, and N. Serra, 2007: Causes of changes in the Denmark Strait Overflow. *J. Phys. Oceanogr.*, **37**, 1678–1696, <https://doi.org/10.1175/JPO3080.1>.
- Logemann, K., and I. Harms, 2006: High resolution modelling of the North Icelandic Irminger Current (NIIC). *Ocean Sci.*, **2**, 291–304, <https://doi.org/10.5194/os-2-291-2006>.
- Macrander, A., R. H. Käse, U. Send, H. Valdimarsson, and S. Jónsson, 2007: Spatial and temporal structure of the Denmark Strait Overflow revealed by acoustic observations. *Ocean Dyn.*, **57**, 75–89, <https://doi.org/10.1007/s10236-007-0101-x>.
- Marshall, D., and C. E. Tansley, 2001: An implicit formula for boundary current separation. *J. Phys. Oceanogr.*, **31**, 1633–1638, [https://doi.org/10.1175/1520-0485\(2001\)031<1633:AIFBFC>2.0.CO;2](https://doi.org/10.1175/1520-0485(2001)031<1633:AIFBFC>2.0.CO;2).
- Mastropole, D., R. S. Pickart, H. Valdimarsson, K. Våge, K. Jochumsen, and J. B. Girtton, 2017: On the hydrography of Denmark Strait. *J. Geophys. Res. Oceans*, **122**, 306–321, <https://doi.org/10.1002/2016JC012007>.
- Mauritzen, C., 1996: Production of dense overflow waters feeding the North Atlantic across the Greenland-Scotland Ridge. Part 1: Evidence for a revised circulation scheme. *Deep-Sea Res.*, **43**, 769–806, [https://doi.org/10.1016/0967-0637\(96\)00037-4](https://doi.org/10.1016/0967-0637(96)00037-4).
- Messias, M. J., and Coauthors, 2008: The Greenland Sea tracer experiment 1996–2002: Horizontal mixing and transport of Greenland Sea Intermediate Water. *Prog. Oceanogr.*, **78**, 85–105, <https://doi.org/10.1016/j.pocean.2007.06.005>.
- Nurser, A. J. G., and S. Bacon, 2014: The Rossby radius in the Arctic Ocean. *Ocean Sci.*, **10**, 967–975, <https://doi.org/10.5194/os-10-967-2014>.
- Østerhus, S., and Coauthors, 2019: Arctic Mediterranean exchanges: A consistent volume budget and trends in transports from two decades of observations. *Ocean Sci.*, **15**, 379–399, <https://doi.org/10.5194/os-15-379-2019>.
- Pawlowicz, R., B. Beardsley, and S. Lentz, 2002: Classical tidal harmonic analysis including error estimates in MATLAB using T_TIDE. *Comput. Geosci.*, **28**, 929–937, [https://doi.org/10.1016/S0098-3004\(02\)00013-4](https://doi.org/10.1016/S0098-3004(02)00013-4).
- Pickart, R. S., and W. M. Smethie, 1998: Temporal evolution of the Deep Western Boundary Current where it enters the subtropical domain. *Deep-Sea Res. I*, **45**, 1053–1083, [https://doi.org/10.1016/S0967-0637\(97\)00084-8](https://doi.org/10.1016/S0967-0637(97)00084-8).
- , D. J. Torres, and P. S. Fratantoni, 2005: The East Greenland Spill Jet. *J. Phys. Oceanogr.*, **35**, 1037–1053, <https://doi.org/10.1175/JPO2734.1>.
- , and Coauthors, 2017: The North Icelandic Jet and its relationship to the North Icelandic Irminger Current. *J. Mar. Res.*, **75**, 605–639, <https://doi.org/10.1357/002224017822109505>.
- Ross, C. K., 1978: Overflow variability in Denmark Strait. *ICES J. Mar. Sci.*, **21**, 1–9.
- Rudels, B., E. Fahrback, J. Meincke, G. Budéus, and P. Eriksson, 2002: The East Greenland Current and its contribution to the Denmark Strait overflow. *ICES J. Mar. Sci.*, **59**, 1133–1154, <https://doi.org/10.1006/jmsc.2002.1284>.

- Smith, P. C., 1976: Baroclinic instability in the Denmark Strait Overflow. *J. Phys. Oceanogr.*, **6**, 355–371, [https://doi.org/10.1175/1520-0485\(1976\)006<0355:BIITDS>2.0.CO;2](https://doi.org/10.1175/1520-0485(1976)006<0355:BIITDS>2.0.CO;2).
- Spall, M. A., R. S. Pickart, P. S. Fratantoni, and A. J. Plueddemann, 2008: Western Arctic shelfbreak eddies: Formation and transport. *J. Phys. Oceanogr.*, **38**, 1644–1668, <https://doi.org/10.1175/2007JPO3829.1>.
- , J. Pedlosky, and C. Cenedese, 2017: Circulation induced by isolated dense water formation over closed topographic contours. *J. Phys. Oceanogr.*, **47**, 2251–2265, <https://doi.org/10.1175/JPO-D-17-0042.1>.
- , R. S. Pickart, P. Lin, H. Valdimarsson, T. W. N. Haine, and M. Almansi, 2019: Frontogenesis and variability in Denmark Strait and its influence on overflow water. *J. Phys. Oceanogr.*, **49**, 1889–1904, <https://doi.org/10.1175/JPO-D-19-0053.1>.
- Strass, V. H., E. Fahrback, U. Schauer, and L. Sellmann, 1993: Formation of Denmark Strait overflow water by mixing in the East Greenland Current. *J. Geophys. Res.*, **98**, 6907–6919, <https://doi.org/10.1029/92JC02732>.
- Swift, J. H., and K. Aagaard, 1981: Seasonal transitions and water mass formation in the Iceland and Greenland seas. *Deep-Sea Res. I*, **28**, 1107–1129, [https://doi.org/10.1016/0198-0149\(81\)90050-9](https://doi.org/10.1016/0198-0149(81)90050-9).
- , —, and S. A. Malmberg, 1980: The contribution of the Denmark Strait overflow to the deep North Atlantic. *Deep-Sea Res. I*, **27**, 29–42, [https://doi.org/10.1016/0198-0149\(80\)90070-9](https://doi.org/10.1016/0198-0149(80)90070-9).
- Tanhua, T., K. Bulsiewicz, and M. Rhein, 2005: Spreading of overflow water from the Greenland to the Labrador Sea. *Geophys. Res. Lett.*, **32**, L10605, <https://doi.org/10.1029/2005GL022700>.
- Thurnherr, A. M., 2010: A practical assessment of the errors associated with full-depth LADCP profiles obtained using Teledyne RDI Workhorse acoustic Doppler current profilers. *J. Atmos. Oceanic Technol.*, **27**, 1215–1228, <https://doi.org/10.1175/2010JTECHO708.1>.
- , 2018: How to process LADCP data with the LDEO software. User manual, Columbia University, 32 pp., <https://www.ldeo.columbia.edu/~ant/LADCP.html>.
- Våge, K., R. S. Pickart, M. A. Spall, H. Valdimarsson, S. Jónsson, D. J. Torres, S. Østerhus, and T. Eldevik, 2011: Significant role of the North Icelandic Jet in the formation of Denmark Strait overflow water. *Nat. Geosci.*, **4**, 723–727, <https://doi.org/10.1038/ngeo1234>.
- , —, —, G. W. K. Moore, H. Valdimarsson, D. J. Torres, S. Y. Erofeeva, and J. E. Ø. Nilsen, 2013: Revised circulation scheme north of the Denmark Strait. *Deep-Sea Res. I*, **79**, 20–39, <https://doi.org/10.1016/j.dsr.2013.05.007>.
- , G. W. K. Moore, S. Jónsson, and H. Valdimarsson, 2015: Water mass transformation in the Iceland Sea. *Deep-Sea Res. I*, **101**, 98–109, <https://doi.org/10.1016/j.dsr.2015.04.001>.
- , L. Papritz, L. Håvik, M. A. Spall, and G. W. K. Moore, 2018: Ocean convection linked to the recent ice edge retreat along east Greenland. *Nat. Commun.*, **9**, <https://doi.org/10.1038/s41467-018-03468-6>.
- von Appen, W. J., U. Schauer, T. Hattermann, and A. Beszczynska-Möller, 2016: Seasonal cycle of mesoscale instability of the West Spitsbergen Current. *J. Phys. Oceanogr.*, **46**, 1231–1254, <https://doi.org/10.1175/JPO-D-15-0184.1>.
- , D. Mastropole, R. S. Pickart, H. Valdimarsson, S. Jónsson, and J. B. Girton, 2017: On the nature of the mesoscale variability in Denmark Strait. *J. Phys. Oceanogr.*, **47**, 567–582, <https://doi.org/10.1175/JPO-D-16-0127.1>.
- Yang, J., and L. Pratt, 2014: Some dynamical constraints on upstream pathways of the Denmark Strait Overflow. *J. Phys. Oceanogr.*, **44**, 3033–3053, <https://doi.org/10.1175/JPO-D-13-0227.1>.
- Ypma, S. L., N. Brüggemann, S. Georgiou, P. Spence, H. A. Dijkstra, J. D. Pietrzak, and C. A. Katsman, 2019: Pathways and watermass transformation of Atlantic Water entering the Nordic Seas through Denmark Strait in two high resolution ocean models. *Deep-Sea Res. I*, **145**, 59–72, <https://doi.org/10.1016/j.dsr.2019.02.002>.
- Zhao, J., J. Yang, S. Semper, R. S. Pickart, K. Våge, H. Valdimarsson, and S. Jónsson, 2018: A numerical study of interannual variability in the North Icelandic Irminger Current. *J. Geophys. Res. Oceans*, **123**, 8994–9009, <https://doi.org/10.1029/2018JC013800>.

Paper II

The Iceland-Faroe Slope Jet: A conduit for dense water toward the Faroe Bank Channel overflow

S. Semper, R. S. Pickart, K. Våge, K. M. H. Larsen, H. Hátún, and B. Hansen
Nature Communications (accepted)

The Iceland-Faroe Slope Jet: A conduit for dense water toward the Faroe Bank Channel overflow

Stefanie Semper^{*1}, Robert S. Pickart², Kjetil Våge¹, Karin Margretha Húsgarð Larsen³, Hjálmar Hátún³, and Bogi Hansen³

1 – Geophysical Institute, University of Bergen and Bjerknes Centre for Climate Research, Bergen, Norway.

2 – Woods Hole Oceanographic Institution, Woods Hole, Massachusetts, USA.

3 – Faroe Marine Research Institute, Tórshavn, Faroe Islands.

* *Corresponding author address:* Geophysical Institute, University of Bergen and Bjerknes Centre for Climate Research, Allégaten 70, 5007 Bergen, Norway.

E-mail: stefanie.semper@uib.no

Manuscript accepted for publication in *Nature Communications*

Dense water from the Nordic Seas passes through the Faroe Bank Channel and supplies the lower limb of the Atlantic Meridional Overturning Circulation, a critical component of the climate system. Yet, the upstream pathways of this water are not fully known. Here we present evidence of a previously unrecognised deep current following the slope from Iceland toward the Faroe Bank Channel using high-resolution, synoptic shipboard observations and long-term measurements north of the Faroe Islands. The bulk of the volume transport of the current, named the Iceland-Faroe Slope Jet (IFSJ), is relatively uniform in hydrographic properties, very similar to the North Icelandic Jet flowing westward toward Denmark Strait. This suggests a common source for the two major overflows across the Greenland-Scotland Ridge. The IFSJ accounts for approximately half of the total overflow transport through the Faroe Bank Channel, thus constituting a significant component of the overturning circulation in the Nordic Seas.

Introduction

The Nordic Seas, comprising the Norwegian, Greenland, and Iceland Seas, are a critical region at the northern extremity of the Atlantic Meridional Overturning Circulation (AMOC). Warm and saline Atlantic Water flowing northward across the Greenland-Scotland Ridge into the Nordic Seas releases heat to the atmosphere and helps maintain the temperate climate of northwest Europe^{1;2}. Transformation to colder, fresher, and denser water masses occurs both in the interior basins and within the boundary current system around the Nordic Seas³⁻⁵. These dense water masses return southward at depth as overflow plumes through gaps in the ridge (Fig. 1a). The plumes contain water denser than $\sigma_{\Theta} = 27.8 \text{ kg m}^{-3}$, hereafter referred to as overflow water⁶. Overflow water formed in the eastern part of the Nordic Seas is referred to as Atlantic-origin water, while that formed in the interior of the western basins is referred to as Arctic-origin water, which is the densest contributor to the lower limb of the AMOC^{3;7}. Recent studies have focused primarily on Denmark Strait between Greenland and Iceland, which is the second-deepest passage (approximately 650 m) through the ridge and has the largest volume transport of overflow water⁸⁻¹². The Atlantic-origin overflow in Denmark Strait is supplied by two branches of the East Greenland Current^{8;13}, while the Arctic-origin overflow is advected by the North Icelandic Jet (NIJ)^{7;8;14} originating northeast of Iceland^{7;15}.

The densest Arctic-origin overflow water emanating from the Nordic Seas passes through the approximately 850 m deep Faroe Bank Channel (FBC)^{12;16} and is subject to extensive mixing and entrainment south of the Greenland-Scotland Ridge¹⁷⁻¹⁹. The magnitude of the FBC overflow has been monitored continuously since 1995; the most recent estimate of its volume transport is $1.9 \pm 0.3 \text{ Sv}$ ^{12;20} ($1 \text{ Sv} \equiv 10^6 \text{ m}^3 \text{ s}^{-1}$). The bulk of this transport is composed of intermediate and deep water masses^{16;18}. These water masses are most likely ventilated during winter in the Iceland and Greenland Seas, with a contribution from the Arctic Ocean^{17;21}.

Before reaching the FBC sill, the overflow waters pass through the Faroe-Shetland Channel (Fig. 1a). While the hydrographic properties of the water masses in the channel and their interannual variability are well documented^{12;20;22}, the dense-water pathways feeding this passage are as of yet not fully determined. Previous studies suggested that the FBC is fed by water emanating from the interior Norwegian Sea^{17;23}, whereas other data have indicated the presence of a deep flow directed toward the channel along the northern side of the Iceland-Faroe Ridge^{24;25}.

Here we provide direct evidence of a deep current following the northern slope of the Greenland-Scotland Ridge from Iceland toward the Faroe Islands. This is the first concrete documentation of the existence of this bottom-intensified current, which we name the Iceland-Faroe Slope Jet (IFSJ). The IFSJ transports water matching the densest water observed in the FBC and appears to supply approximately half of the total FBC overflow. As such, the IFSJ constitutes a significant component of the overturning in the Nordic Seas and is therefore of key importance to the AMOC^{26;27}. To predict the AMOC's response to a changing climate, it is imperative to identify the origin and pathways of the dense water supplying its lower limb.

Results and Discussion

Pathway and transport of the IFSJ

Using high-resolution hydrographic/velocity measurements from a September 2011 shipboard survey²⁸⁻³¹ (Fig. 1b), we identified a spatially coherent eastward flow between northeast Iceland and the Faroe Islands. Vertical sections of absolutely referenced geostrophic velocity (Fig. 2), which were constructed from the combined shipboard hydrographic and velocity data (see the methods section for details), show that the IFSJ has a consistent hydrographic and kinematic structure. The narrow current is bottom-intensified and comprises two cores of overflow water, which approximately follow the 750 and 1100 m isobaths, respectively. It is composed of cold, dense water that is banked up against the slope (Supplementary Fig. 1, 2). An extensive collection of hydrographic measurements from the Nordic Seas³² confirms the persistent presence of anomalously dense water on the upper slope north of Iceland and the Iceland-Faroe Ridge. This isopycnal structure supports the bottom-intensified IFSJ flowing eastward toward the entrance of the Faroe-Shetland Channel, from where the dense water enters the FBC. It is also consistent with the NIJ flowing westward toward Denmark Strait, which is middepth-intensified as the isopycnal tilt reverses again in the upper 300 m of the water column^{7;15}. East of the Kolbeinsey Ridge, the extension of the mid-Atlantic Ridge north of Iceland, the IFSJ and NIJ are in close proximity (Fig. 1a). While it is well documented that the NIJ emerges northeast of Iceland^{7;15}, the origin of the IFSJ remains unknown. Recent work suggests that both currents are supplied by dense water emanating from the Greenland Sea that subsequently flows southward through the Iceland Sea along

the Kolbeinsey Ridge³². Eastward flow of dense water through the Spar Fracture Zone may also supply the IFSJ (Fig. 1b).

The mean volume transport of overflow water in the IFSJ, estimated from the high-resolution hydrographic/velocity sections, is 1.0 ± 0.1 Sv. The uncertainty reflects instrument and processing errors of the velocity measurements and is taken to be independent for each section (see the methods section for details). The mean transport estimated from the 2011 survey suggests that the IFSJ supplies approximately half of the total overflow through the FBC (1.9 ± 0.3 Sv)^{12;20}. The contribution of the deep core to the total transport of the IFSJ generally exceeds the contribution of the shallow core (Fig. 3a). On two sections (B and C) the deep core was not completely bracketed by the observations, resulting in an underestimated transport of the IFSJ. The increase in transport between sections C and D may additionally be caused by entrainment of ambient water from the Norwegian Basin, while the low transport at section E likely results from a mesoscale feature suppressing the 27.8 kg m^{-3} isopycnal (Fig. 2). The volume transport was conservatively estimated only for depths shallower than 850 m, the approximate depth of the FBC sill. However, water may be lifted from greater depths by aspiration and supply the overflow³³. If the depth restriction is removed, the total contribution of the IFSJ to the FBC overflow, according to the 2011 shipboard survey, could be as high as 1.4 ± 0.2 Sv.

The bulk of the IFSJ's volume transport is confined to a small range in Θ -S space (Fig. 3b). The locus of the Θ -S classes with the highest transport, which we refer to as the transport mode, is centred near -0.52 ± 0.11 °C and 35.075 ± 0.003 g kg⁻¹ in temperature and salinity, respectively (see the methods section for details). While the upper part of the IFSJ becomes warmer and more saline as it progresses eastward, due to mixing with Atlantic Water near the Faroe Islands, the hydrographic properties of the transport mode are not significantly modified along the current's pathway. The density of the transport mode is $\sigma_{\Theta} = 28.06 \text{ kg m}^{-3}$. This is not significantly denser than the transport mode of the NIJ ($\sigma_{\Theta} = 28.05 \text{ kg m}^{-3}$), which has a higher temperature (-0.29 ± 0.16 °C) but the same salinity¹⁵. The similarity of these transport modes suggests that the water masses in the two currents have the same origin. Waters of sufficient density are regularly ventilated in the Greenland Sea during winter³⁴, and the density difference between the mixed layers there and the two transport modes can be as small as 0.005 kg m^{-3} , which corresponds to differences of 0.1 °C or 0.007 g kg^{-1} for temperature or salinity at this density,

respectively³². As such, the Greenland Sea can supply the densest portions of the two major overflows across the Greenland-Scotland Ridge. Changes in dense-water formation in the Greenland Sea, which are expected in a warming climate due to the retreat of sea ice leading to reduced wintertime air-sea heat fluxes in the region³⁵, may thus affect both pathways.

As is the case for the IFSJ, the NIJ is often composed of separate cores¹⁵. In particular, northeast of Iceland the slightly warmer NIJ tends to flow toward Denmark Strait along the 600 and 800 m isobaths, while the slightly colder IFSJ flows toward the FBC approximately along the 750 and 1100 m isobaths. Notably, the 600 and 750 m isobaths are close to the sill depths of Denmark Strait and the FBC, respectively. This implies that hydraulic control occurring at the two passages^{33;36;37} may be influencing the shallow core of each current.

Data from past studies have hinted at a deep flow along the northern side of the Iceland-Faroe Ridge. Four moorings deployed during 1988–1989 along the 1000 m isobath recorded a deep, bottom-intensified current²⁴. This pathway was also identified in a two-layer numerical model with realistic bathymetry³⁸. Deep currents in this region are thus suggested to be strongly guided by the bathymetry, which is further supported by estimates from a simplified dynamical model³⁹. Moreover, a subset of RAFOS floats deployed at 600–800 m depth northeast of Iceland in 2013 and 2014⁴⁰, and near the Faroe Islands in 2004²⁵, drifted southeastward along the slope between Iceland and the Faroe Islands. In the latter case, all but one of the nine floats deployed over isobaths shallower than 1750 m followed the bathymetry southeastward into the Faroe-Shetland Channel, where the floats' trajectories became more chaotic before approaching the Shetland slope and exiting across the sill into the North Atlantic. This behaviour was explained in the context of a large-scale pressure gradient dominating the topographic control and adjusting the potential vorticity of the flow²⁵. An alternate explanation is that the floats underwent turbulent entrainment into the deep Faroe-Shetland Channel Jet, located at the foot of the Shetland slope⁴¹, and were subsequently advected into the FBC.

To investigate whether the water in the IFSJ may follow this pathway and feed the overflow through the FBC, we compared the IFSJ's properties and volume transport to those of the overflow in the -1 – 0 °C temperature class³³, which encompasses the IFSJ transport mode. This indicates that the transport of the IFSJ can account for 92% of the total overflow through the FBC within this temperature class (65% if the IFSJ's transport below sill depth is excluded; Fig. 3c). Despite the slight differ-

ence in salinity, which may be caused by the extensive mixing in the Faroe-Shetland Channel^{18;33}, the hydrographic properties of the IFSJ are in close agreement with the properties of the FBC overflow for this temperature class (Fig. 3d). This corroborates the notion that the IFSJ is a major contributor to the overflow through the FBC. The flow dynamics between section N and the entrainment into the Faroe-Shetland Channel Jet, however, warrant more dedicated scrutiny.

While the shipboard survey constitutes a snapshot of the IFSJ between Iceland and the Faroe Islands during autumn 2011, eight additional surveys were conducted northeast of Iceland between 2011 and 2018 that have previously been used in a study focusing on the NIJ¹⁵. At Slétta and Langanes NE (Fig. 1b) the bottom-intensified IFSJ core at 750m depth was present in seven and four of the nine occupations, respectively. In the September 2011 survey, the transport of the 750 m core at Slétta was slightly larger than the average over all the surveys where the IFSJ was detected, while that at Langanes NE was slightly smaller than the average. (The deep IFSJ cores were not sampled at these transects.) However, there was considerable variability in the strength and the width of the current between the surveys. Similarly, the transport of the NIJ is quite variable, which has been attributed to internal variability rather than large-scale atmospheric conditions¹⁵.

Inferences from shipboard hydrographic time series

To shed more light on the structure of the IFSJ, we analysed a collection of 120 repeat hydrographic transects along section N directly north of the Faroe Islands (Fig. 1), spanning the last 30 years. While the station spacing of 10 nautical miles is too coarse to properly resolve the IFSJ, we considered the isopycnal structure near the upper slope to identify occupations where particularly dense water ($\sigma_{\theta} \geq 28.03 \text{ kg m}^{-3}$) was present at the bottom of station 4 (referred to as the “elevated isopycnal” state, which includes 38/120 surveys). We note that only the most extreme occurrences of dense water banked up on the slope are captured due to the large distance between stations. As such, more moderate banking of dense water cannot be resolved (i.e., the remaining surveys with a “relaxed isopycnal” state show very little isopycnal slope, but this does not imply that the IFSJ was not present). The composite mean of the elevated isopycnal state is shown in Fig. 4.

The surface layer consists of warm, saline water transported by the Faroe Current. Beneath this surface layer, the isopycnal tilt reverses, and cold, dense water is banked up against the slope (Fig. 4a–b). This is characteristic of the IFSJ (Sup-

plementary Fig. 1, 2), and the elevated isopycnal composite section of geostrophic velocity relative to the 28.0 kg m^{-3} isopycnal illustrates the bottom-intensified flow near the slope, directed toward the Faroe-Shetland Channel (Fig. 4c). The deep current is located between stations 4 and 5, which encompass the isobaths of both cores of the IFSJ farther upstream. (The combination of the steep continental slope and coarse resolution along section N makes it impossible to resolve separate IFSJ cores.) As such, the elevated isopycnal state qualitatively resembles the bottom-intensified structure and properties of the IFSJ farther upstream.

In autumn 2011 section N was sampled 18 days before and 46 days after the nearest high-resolution upstream section. The isopycnals were elevated during the former survey, but not during the latter. In general over the 30-year period, the variability is high, and elevated isopycnal sections were identified in most years and every season, but without clear interannual and seasonal signals or long-term persistence indicating influence by large-scale atmospheric patterns.

Vertical structure and variability from moored measurements

To investigate the vertical structure and variability of the IFSJ, we analysed moored records of direct current velocities at section N. From June 2017 to May 2018, two moorings were deployed at depths of 960 m and 1210 m (Fig. 4c). These were shoreward and seaward, respectively, of the deep IFSJ core (1100 m) identified in the high-resolution shipboard data farther upstream. A combined mean along-stream velocity profile constructed from the two moorings reveals bottom-intensified flow directed toward the FBC (Fig. 5a). The structure and magnitude of the flow is consistent with the IFSJ (Fig. 2). The mean velocity in the strongest part of the current (below the dashed line in Fig. 5a) was 6.7 cm s^{-1} (Fig. 1b). This is likely an underestimate due to sidelobe reflections from the bottom (see the methods section for details). Short, intermittent periods of negative (northwestward) velocities (Fig. 5d) may be due to lateral meandering of the deep IFSJ core. The mean hydrographic properties closest to the mooring from section N match those of the IFSJ's transport mode (Fig. 5b–c). Taken together, there is strong evidence of a bottom-intensified current resembling the IFSJ at section N.

The inshore mooring in Fig. 4c is part of a long time series of velocity measurements designed to monitor the Atlantic Water transport in the surface-intensified Faroe Current. However, the mooring's depth range extends sufficiently deep to capture the upper portion of the IFSJ (Fig. 5a). Encouragingly, the measurements from

the overlapping depth range of the inshore and offshore moorings are well correlated ($r=0.63$). Furthermore, the variability in the strongest part of the IFSJ from the offshore mooring (below the dashed line in Fig. 5a) is also well correlated ($r=0.59$) with the uppermost portion of the IFSJ from the inshore mooring (570–675 m). Both correlations are statistically significant at the 99% confidence level (see the methods section for details). As such, measurements from the inshore mooring may be considered a longer-term proxy for the variability in the IFSJ.

We examined a 7-year long subset of the inshore mooring velocity record (2006–2013) when the mooring was deployed at approximately the same bottom depth (956 ± 5 m). There is nothing remarkable about the period of the 2011 survey in terms of magnitude and variability in this record. Comparing the deepest velocities, which extend into the upper portion of the IFSJ, to the elevated and relaxed isopycnal states of the section N occupations, the elevated isopycnals appear to be a sufficient, but not necessary condition for eastward velocities in the upper portion of the IFSJ (not shown). This indicates that the hydrographic occupations of section N are not well suited to infer the strength of the IFSJ.

From the 7-year long mooring record we can determine the dominant variability of the along-stream velocity by computing empirical orthogonal functions (EOFs). The two leading modes explain 68 and 25% of the velocity variance, respectively (Fig. 6). The first EOF represents a barotropic mode, where the Faroe Current and the IFSJ are in phase, while the second EOF is a baroclinic mode in which the strengths of the Faroe Current and IFSJ vary out of phase.

A periodogram of the principal component time series of the first EOF mode exhibits variability on seasonal time scales, while that of the second mode is dominated by variability on a 2–3 week period (not shown). Interestingly, the NIJ has no such seasonal signal^{8;15;42;43}. Since the IFSJ has similar properties, likely the same source waters, and is located even deeper in the water column, a seasonal signal in the IFSJ northeast of Iceland was not expected. While the offshore mooring record from section N is too short to resolve a seasonal cycle, the velocities toward the Faroe-Shetland Channel appear to be enhanced from November to January compared to July and August (Fig. 5d), consistent with the long-term proxy of the IFSJ from the inshore mooring. We note that the energetic Faroe Current, which is in close proximity to the IFSJ near section N, has the same seasonality⁴⁴ (Fig. 6).

Wider implications

In conclusion, we have provided compelling evidence of a current transporting dense water from northeast Iceland toward the FBC overflow, using four independent observational data sets with different spatial and temporal resolutions. The current is named the Iceland-Faroe Slope Jet (IFSJ). While previous studies have hinted at the existence of such a flow, the data employed here are extensive and multi-faceted, including the first high-resolution observations of the IFSJ. The current is bottom-intensified and comprises two cores centred on the 750 and 1100 m isobaths along the Iceland-Faroe Ridge. The bulk of the transport is confined to a small range in temperature-salinity space, centred near -0.52 ± 0.11 °C and 35.075 ± 0.003 g kg⁻¹. This transport mode has a density of $\sigma_{\Theta} = 28.06$ kg m⁻³, consistent with the densest waters in the FBC overflow. Long-term repeat shipboard observations north of the Faroe Islands suggest the presence of the IFSJ through dense water banked up along the slope, thus supporting the results of the high-resolution synoptic survey. Direct current measurements corroborate the existence of the IFSJ, and a long-term velocity record indicates a link between the variability in the surface-intensified Faroe Current and the uppermost part of the IFSJ. Our measurements suggest that the IFSJ transports approximately 1 Sv of overflow water toward the FBC, which can account for half of the total transport through the passage. As such, the current is a major pathway of dense water to the easternmost overflow ventilating the deep North Atlantic.

Recent studies emphasise the importance of dense-water formation in the Nordic Seas in sustaining the lower limb of the AMOC^{26;27}. A basic understanding of the origin and the circulation of this dense water mass is thus required for accurate predictions of the future state of the AMOC. The processes and locations of dense-water formation are changing^{32;35;45;46}, which in turn could affect the composition and the pathways of the dense waters contributing to the overflow across the Greenland-Scotland Ridge. The IFSJ is one of these pathways, and our findings highlight its significance for the overturning circulation and thus the climate system.

Methods

High-resolution hydrographic/velocity survey

The high-resolution hydrographic/velocity survey, which included eight transects north of Iceland (Fig. 1b), was conducted on R/V *Knorr* in September 2011. The

hydrographic data were acquired using a Sea-Bird 911+ conductivity-temperature-depth (CTD) instrument, which was mounted on a rosette with 24 Niskin bottles. Water samples were obtained to calibrate the conductivity sensor, and the final accuracy of the CTD measurements was estimated to be $0.001\text{ }^{\circ}\text{C}$ for temperature, 0.002 g kg^{-1} for salinity, and 0.3 dbar for pressure¹⁵. Velocities were measured using upward and downward-facing lowered acoustic Doppler current profiler (LADCP) instruments. The velocity measurements were processed using the LADCP Processing Software Package from the Lamont-Doherty Earth Observatory^{47;48}. An updated version of a regional inverse tidal model⁴⁹ was used to solve for the eight main tidal constituents; these barotropic tidal currents were then subtracted from the current velocities.

Vertical sections of Conservative Temperature (temperature), Absolute Salinity (salinity), and potential density anomaly (density) were constructed using Laplacian-spline interpolation⁵⁰, with a grid spacing of 2 km in the horizontal and 10 m in the vertical. Absolutely referenced geostrophic velocities normal to each transect were calculated as follows: The cross-track ADCP velocities were interpolated onto the 2 km by 10 m regular grid. At each grid point the reference-level velocity, (i.e., the difference between the depth-averaged ADCP velocity and the depth-averaged relative geostrophic velocity computed from the hydrography) was added to the relative geostrophic velocity. To avoid undue influence from surface and bottom boundary layers, the top and bottom 50 m were excluded from the depth averages. Positive along-stream direction is toward the Faroe-Shetland Channel. The volume transport of the IFSJ was calculated from the absolutely referenced geostrophic velocity fields. We estimated the uncertainty of the transport from instrument and processing errors scaled by the cross-sectional area of the current. The combined error of the LADCP instrument and the processed velocity data was estimated to be 3 cm s^{-1} , while the inaccuracies in the tidal model are 2 cm s^{-1} north of Iceland⁷. The total uncertainty, determined as the root-sum-square of the instrument/processing and tidal model errors, is 3.6 cm s^{-1} . This uncertainty does not reflect the temporal variability at each transect, which cannot be assessed from a single survey. The transport estimate from each section is taken to be independent: On average, the sections were obtained 1.6 days apart, which exceeds the autocorrelation of the velocity time series at the deep, offshore mooring of 1.3 days. Furthermore, it would take more than two weeks for a water parcel to cover the distance of over 100 km between sections at a typical speed of $7.5\text{--}10\text{ cm s}^{-1}$.

The transport mode of the IFSJ was determined following a similar approach as for the NIJ¹⁵: For each transect, the volume transport in each grid cell of both IFSJ cores was binned into temperature and salinity classes of $0.075\text{ }^{\circ}\text{C}$ and 0.003 g kg^{-1} , respectively. (The extent of the classes does not affect the results significantly.) Each Θ -S matrix was normalised by its maximum transport, such that each transect was given equal weight. The transport matrices were then added, and grid cells with transports below the e-folding scale of the maximum transport were ignored. The transport-weighted average of the remaining Θ -S classes determines the locus of the main transport, i.e., the properties of the transport mode.

Monitoring hydrographic stations

The seven hydrographic stations from the standard monitoring section N north of the Faroe Islands along $6.083\text{ }^{\circ}\text{W}$ (Fig. 1b) are spaced 10 nautical miles apart and were typically occupied three to four times per year between 1987 and 2018. The accuracies of the temperature and salinity measurements are better than $0.001\text{ }^{\circ}\text{C}$ and 0.005 g kg^{-1} from 1997 onwards⁴⁴. Laplacian-spline interpolation was used to construct vertical sections of temperature and salinity, with a grid spacing of 5 km by 10 m. The wide station spacing and steep slope between stations 4 and 5 led to a large “bottom triangle”. This was filled using measurements from the bottom of station 4 prior to interpolation, which helped conserve the structure of the dense water banked up on the slope. Gridded sections of relative geostrophic velocities referenced to the 28.0 kg m^{-3} isopycnal were computed from the hydrographic data.

Moored ADCP measurements

We used one year (June 2017 to May 2018) of current measurements from ADCP instruments on section N at $62.95\text{ }^{\circ}\text{N}$ and $62.92\text{ }^{\circ}\text{N}$ (separated by 3.1 km). The moorings were located at bottom depths of 1210 m and 960 m and measured current speed and direction in ranges of approximately 515–1185 m and 125–675 m, respectively. A lowpass filter of 36 hours was applied to the velocity time series, originally recorded every 20 min, before daily averages were computed. The velocities were rotated to align with the direction of the mean flow of the strongest part of the IFSJ below 975 m, which is 105° clockwise from true north.

The velocity measurements of the bottom-mounted ADCP at the offshore mooring are affected by interference from sidelobe reflection. This typically occurs in

the lowest 200–300 m and results in a strong artificial velocity bias toward zero^{51,52}. The following procedure was used to determine the cut-off depth of the contaminated measurements, which were removed prior to further analysis: We selected daily profiles with a bottom-intensified structure characteristic of the IFSJ (66 % of all profiles for a velocity maximum above 4 cm s^{-1} ; the results are not very sensitive to this choice). We then identified the depth of the velocity maximum for each of these profiles (1065 m on average) and the depths where the maximum is reduced to 95 %. The upper value of this range (1036 m) is taken to be the limit of the strongest part of the IFSJ (dashed line in Fig. 5a). The lower value of this range (1096 m) is the cut-off depth, and measurements of all profiles below this threshold were disregarded. The limit is a compromise between removing too many measurements and keeping profiles that underestimate the true velocity at depth due to the sidelobe interference.

The correlations between the strongest part of the IFSJ from the offshore mooring and the uppermost portion of the IFSJ from the inshore mooring ($r = 0.59$) and between the overlapping depth range of the inshore and offshore moorings ($r = 0.63$) are statistically significant at the 99 % confidence level, taking the autocorrelations of the time series into account.

We used a 7-year long record (2006–2013) of the inshore mooring at section N. The mooring at this location has been continuously deployed since 1997. However, the exact location and bottom depth varied over the period; it was on average located at the 925 m isobath⁴⁴. We selected the longest continuous subset with the deepest available measurements that were collected at a consistent bottom depth ($956 \pm 5 \text{ m}$, with velocities measured between 120 and 670 m depth), such that the ADCP bins extending into the upper portion of the IFSJ could be used without interpolation in the vertical. The chosen 7-year record does not differ markedly in terms of interannual variability of the velocity at depth when compared to the full record. As for the single-year deployments, a lowpass filter of 36 hours was applied to the velocity time series, originally recorded every 20 min, before daily averages were computed. To be consistent with the single-year deployments, the velocity was rotated to align with the mean flow of the strongest part of the IFSJ below 975 m from the offshore, deeper mooring, which is 105° clockwise from true north. To determine the dominant variability of the velocity, we computed empirical orthogonal functions (EOFs). Before decomposing the velocity time series into its eigenmodes of variability and the corresponding principal component time series, we

linearly interpolated the gaps of two to four weeks every summer when the mooring was serviced. Different interpolation methods gave quantitatively similar results in the EOF analysis.

Acknowledgements

Support for this work was provided by the Bergen Research Foundation Grant BFS2016REK01 (S.S. and K.V.), the U.S. National Science Foundation Grants OCE-1558742 and OCE-1259618 (R.S.P.), the Danish Ministry of Climate, Energy and Utilities (K.M.H.L., H.H., and B.H.), and the European Union's Horizon 2020 research and innovation programme under grant agreement 727852 (Blue-Action) (K.M.H.L., H.H., and B.H.).

Data availability

The high-resolution hydrographic/velocity data, obtained by the Woods Hole Oceanographic Institution, are available in PANGAEA with the identifiers 10.1594/PANGAEA.919516, 10.1594/PANGAEA.919515, 10.1594/PANGAEA.903535, and 10.1594/PANGAEA.919569²⁸⁻³¹. The hydrographic repeat transects and velocity measurements from the moorings at section N acquired by the Faroe Marine Research Institute are available at www.envofar.fo, except for the data from the offshore, deep mooring, which are available on request from K.M.H.L. (E-mail: karinl@hav.fo). These data are not yet publicly available due to quality problems that do not affect the results presented here.

Code availability

The computer codes used to analyse the data are available on request from the corresponding author.

Author contributions

R.S.P. led the cruise on R/V *Knorr* and supplied the initial idea for this study. S.S., R.S.P., and K.V. analysed the data and wrote the paper. B.H. and K.M.H.L. led most of the R/V *Magnus Heinason* cruises that provided the hydrographic and velocity data at section N. H.H. contributed with ideas for analysis and discussion. All authors interpreted the results and clarified the implications.

Competing interests

The authors declare no competing interests.

References

- [1] Árrthun, M., Kolstad, E. W., Eldevik, T. & Keenlyside, N. S. Time scales and sources of European temperature variability. *Geophys. Res. Lett.* **45**, 3597–3604 (2018).
- [2] Eldevik, T. *et al.* A brief history of climate – the northern seas from the Last Glacial Maximum to global warming. *Quat. Sci. Rev.* **106**, 225–246 (2014).
- [3] Swift, J. H. & Aagaard, K. Seasonal transitions and water mass formation in the Iceland and Greenland Seas. *Deep Sea Res.* **28A**, 1107–1129 (1981).
- [4] Strass, V. H., Fahrbach, E., Schauer, U. & Sellmann, L. Formation of Denmark Strait overflow water by mixing in the East Greenland Current. *J. Geophys. Res.* **98**, 6907–6919 (1993).
- [5] Mauritzen, C. Production of dense overflow waters feeding the North Atlantic across the Greenland-Scotland Ridge. Part 1: Evidence for a revised circulation scheme. *Deep Sea Res. Part I Oceanogr. Res. Pap.* **43**, 769–806 (1996).
- [6] Dickson, R. R. & Brown, J. The production of North Atlantic Deep Water: sources, rates, and pathways. *J. Geophys. Res. Oceans* **99**, 12319–12341 (1994).
- [7] Våge, K. *et al.* Significant role of the North Icelandic Jet in the formation of Denmark Strait overflow water. *Nat. Geosci.* **4**, 723–727 (2011).
- [8] Harden, B. *et al.* Upstream sources of the Denmark Strait Overflow: Observations from a high-resolution mooring array. *Deep Sea Res. Part I Oceanogr. Res. Pap.* **112**, 94–112 (2016).
- [9] Mastropole, D. *et al.* On the hydrography of Denmark Strait. *J. Geophys. Res. Oceans* **122**, 306–321 (2017).
- [10] Spall, M. A. *et al.* Frontogenesis and variability in Denmark Strait and its influence on overflow water. *J. Phys. Oceanogr.* **49**, 1889–1904 (2019).

-
- [11] Moritz, M., Jochumsen, K., North, R. P., Quadfasel, D. & Valdimarsson, H. Mesoscale eddies observed at the Denmark Strait sill. *J. Geophys. Res. Oceans* 7947–7961 (2019).
- [12] Østerhus, S. *et al.* Arctic Mediterranean exchanges: A consistent volume budget and trends in transports from two decades of observations. *Ocean Sci.* **15**, 379–399 (2019).
- [13] Våge, K. *et al.* Revised circulation scheme north of the Denmark Strait. *Deep Sea Res. Part I Oceanogr. Res. Pap.* **79**, 20–39 (2013).
- [14] Jónsson, S. & Valdimarsson, H. A new path for the Denmark Strait overflow water from the Iceland Sea to Denmark Strait. *Geophys. Res. Lett.* **31**, L03305 (2004).
- [15] Semper, S. *et al.* The emergence of the North Icelandic Jet and its evolution from northeast Iceland to Denmark Strait. *J. Phys. Oceanogr.* **49**, 2499–2521 (2019).
- [16] Hansen, B. & Østerhus, S. North Atlantic-Nordic Seas exchanges. *Progr. Oceanogr.* **45**, 109–208 (2000).
- [17] Fogelqvist, E. *et al.* Greenland-Scotland overflow studied by hydro-chemical multivariate analysis. *Deep Sea Res. Part I Oceanogr. Res. Pap.* **50**, 73–102 (2003).
- [18] Mauritzen, C., Price, J., Sanford, T. & Torres, D. Circulation and mixing in the Faroese Channels. *Deep Sea Res. Part I Oceanogr. Res. Pap.* **52**, 883–913 (2005).
- [19] Beaird, N. L., Rhines, P. B. & Eriksen, C. C. Overflow waters at the Iceland-Faroe Ridge observed in multiyear seaglider surveys. *J. Phys. Oceanogr.* **43**, 2334–2351 (2013).
- [20] Hansen, B., Larsen, K. M. H., Hátún, H. & Østerhus, S. A stable Faroe Bank Channel overflow 1995–2015. *Ocean Sci.* **12**, 1205–1220 (2016).
- [21] Jeansson, E., Olsen, A. & Jutterström, S. Arctic Intermediate Water in the Nordic Seas, 1991–2009. *Deep Sea Res. Part I Oceanogr. Res. Pap.* **128**, 82–97 (2017).

- [22] Turrell, W. R., Slessor, G., Adams, R. D., Payne, R. & Gillibrand, P. A. Decadal variability in the composition of Faroe Shetland Channel bottom water. *Deep Sea Res. Part I Oceanogr. Res. Pap.* **46**, 1–25 (1999).
- [23] Eldevik, T. *et al.* Observed sources and variability of Nordic seas overflow. *Nat. Geosci.* **2**, 406–410 (2009).
- [24] Hopkins, T. S., Baldasserini, G., Minnett, P., Povero, P. & Zanasca, P. Icelandic Current Experiment. GIN SEA Cruise 88 - Data Report. Hydrography and Circulation. Tech. Rep. SM-260, Saclant Undersea Research Centre (1992).
- [25] Søiland, H., Prater, M. D. & Rossby, T. Rigid topographic control of currents in the Nordic Seas. *Geophys. Res. Lett.* **35** (2008).
- [26] Chafik, L. & Rossby, T. Volume, heat, and freshwater divergences in the subpolar North Atlantic suggest the Nordic Seas as key to the state of the meridional overturning circulation. *Geophys. Res. Lett.* **46**, 4799–4808 (2019).
- [27] Lozier, M. S. *et al.* A sea change in our view of overturning in the subpolar North Atlantic. *Science* **363**, 516–521 (2019).
- [28] Semper, S., Pickart, R. S., Våge, K., Torres, D. J. & McRaven, L. CTD temperature and salinity profiles along five transects in NE Iceland / Iceland-Faroe ridge. *PANGAEA*, <https://doi.pangaea.de/10.1594/PANGAEA.919516> (2020).
- [29] Semper, S., Pickart, R. S., Våge, K., Torres, D. J. & McRaven, L. Water velocity profiles from LADCP casts along five transects in NE Iceland / Iceland-Faroe ridge. *PANGAEA*, <https://doi.pangaea.de/10.1594/PANGAEA.919515> (2020).
- [30] Semper, S. *et al.* Temperature, salinity and velocities on seven transects along the continental slope north of Iceland. *PANGAEA*, <https://doi.org/10.1594/PANGAEA.903535> (2019).
- [31] Semper, S. *et al.* Water velocity profiles in the transect Slétta from LADCP from several cruises. *PANGAEA*, <https://doi.pangaea.de/10.1594/PANGAEA.919569> (2020).

-
- [32] Huang, J. *et al.* Sources and upstream pathways of the densest overflow water in the Nordic Seas. *Nat. Commun.* (in revision).
- [33] Hansen, B. & Østerhus, S. Faroe Bank Channel overflow 1995–2005. *Progr. Oceanogr.* **75**, 817–856 (2007).
- [34] Brakstad, A., Våge, K., Håvik, L. & Moore, G. W. K. Water mass transformation in the Greenland Sea during the period 1986-2016. *J. Phys. Oceanogr.* **49**, 121–141 (2019).
- [35] Moore, G. W. K., Våge, K., Pickart, R. S. & Renfrew, I. Decreasing intensity of open-ocean convection in the Greenland and Iceland seas. *Nat. Clim. Change* **5**, 877–882 (2015).
- [36] Nikolopoulos, A., Borenäs, K., Hietala, R. & Lundberg, P. Hydraulic estimates of Denmark Strait overflow. *J. Geophys. Res.* **108** (2003).
- [37] Girton, J. B., Pratt, L. J., Sutherland, D. A. & Price, J. F. Is the Faroe Bank Channel overflow hydraulically controlled? *J. Phys. Oceanogr.* **36**, 75–89 (2006).
- [38] Yang, J. & Pratt, L. J. Some dynamical constraints on upstream pathways of the Denmark Strait overflow. *J. Phys. Oceanogr.* **44**, 3033–3053 (2014).
- [39] Nøst, O. A. & Isachsen, P. E. The large-scale time-mean ocean circulation in the Nordic Seas and Arctic Ocean estimated from simplified dynamics. *J. Mar. Res.* **61**, 175–210 (2003).
- [40] de Jong, M. F., Søiland, H., Bower, A. S. & Furey, H. H. The subsurface circulation of the Iceland Sea observed with RAFOS floats. *Deep Sea Res. Part I Oceanogr. Res. Pap.* **141**, 1–10 (2018).
- [41] Chafik, L. *et al.* Discovery of an unrecognized pathway carrying overflow waters toward the Faroe Bank Channel. *Nat. Commun.* **11**, 3721 (2020).
- [42] Behrens, E., Våge, K., Harden, B., Biastoch, A. & Böning, C. W. Composition and variability of the Denmark Strait Overflow Water in a high-resolution numerical model hindcast simulation. *J. Geophys. Res. Oceans* **122**, 2830–2846 (2017).

- [43] Huang, J. *et al.* Structure and variability of the North Icelandic Jet from two years of mooring data. *J. Geophys. Res. Oceans* **124** (2019).
- [44] Hansen, B. *et al.* Transport of volume, heat, and salt towards the Arctic in the Faroe Current 1993–2013. *Ocean Sci.* **11**, 743–757 (2015).
- [45] Lique, C. & Thomas, M. D. Latitudinal shift of the Atlantic Meridional Overturning Circulation source regions under a warming climate. *Nat. Clim. Change* **8**, 1013–1020 (2018).
- [46] Våge, K., Papritz, L., Håvik, L., Spall, M. A. & Moore, G. W. K. Ocean convection linked to the recent ice edge retreat along east Greenland. *Nat. Commun.* **9** (2018).
- [47] Thurnherr, A. M. A practical assessment of the errors associated with full-depth LADCP profiles obtained using Teledyne RDI Workhorse acoustic Doppler current profilers. *J. Atmos. Ocean. Tech.* **27**, 1215–1227 (2010).
- [48] Thurnherr, A. M. How to process LADCP data with the LDEO software, `ftp://ftp.ldeo.columbia.edu/pub/LADCP/UserManuals/LDEO{ }IX.pdf` (2018).
- [49] Egbert, G. D. & Erofeeva, S. Y. Efficient inverse modeling of barotropic ocean tides. *J. Atmos. Ocean. Tech.* **19**, 183–204 (2002).
- [50] Pickart, R. S. & Smethie, W. M. Temporal evolution of the deep western boundary current where it enters the sub-tropical domain. *Deep Sea Res. Part I Oceanogr. Res. Pap.* **45**, 1053–1083 (1998).
- [51] Jochumsen, K. *et al.* Revised transport estimates of the Denmark Strait overflow. *J. Geophys. Res. Oceans* **122**, 3434–3450 (2017).
- [52] Hansen, B., Larsen, K. M. H., Kristiansen, R., Mortensen, E. & Østerhus, S. Faroe Bank Channel overflow 2012–2013. Tech. Rep. (2014).
- [53] Amante, C. & Eakins, B. ETOPO1 1 arc-minute global relief model: Procedures, data sources, and analysis. *NOAA Technical Memorandum NESDIS NGDC-24* 25, <https://www.ngdc.noaa.gov/mgg/global/relief/ETOP01/docs/ETOP01.pdf> (2009)

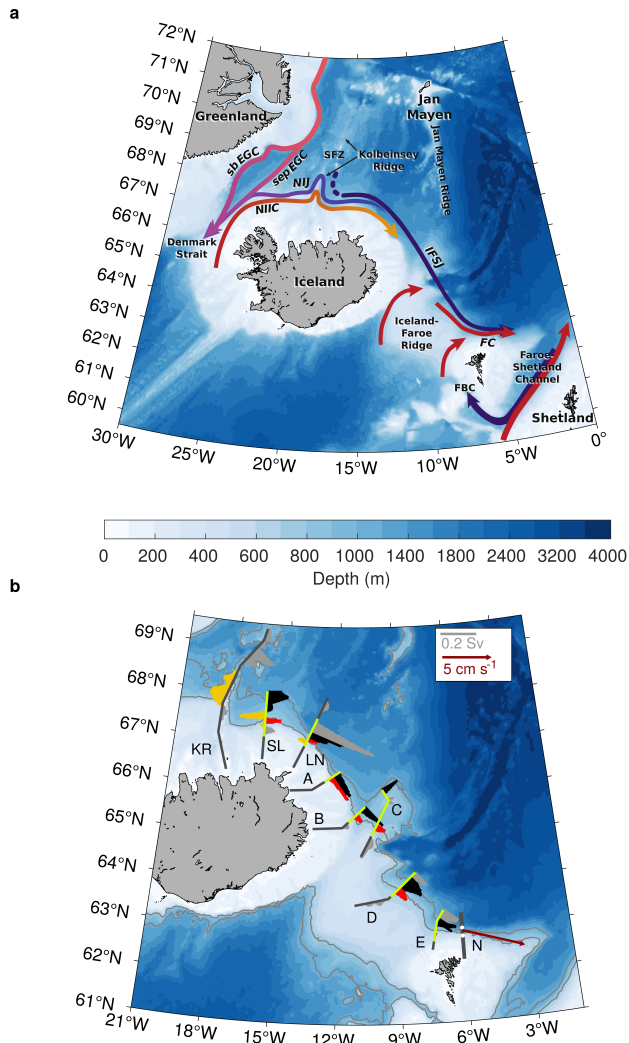


Figure 1: Bathymetry and circulation near the Greenland-Scotland Ridge.

a) Schematic pathways of the inflow of Atlantic Water (red arrows) and the outflow of dense water (purple arrows). The acronyms are: FC=Faroe Current; NIIC=North Icelandic Irminger Current; sb EGC=shelfbreak East Greenland Current; sep EGC=separated East Greenland Current; NIJ=North Icelandic Jet; IFSJ=Iceland-Faroe Slope Jet; FBC=Faroe Bank Channel; SFZ=Spar Fracture Zone. b) Depth-integrated transport of overflow water ($\sigma_{\theta} \geq 27.8 \text{ kg m}^{-3}$) per grid point across the high-resolution shipboard transects used in the study. The shallow and deep IFSJ cores are marked in red and black, respectively, the NIJ is marked in yellow, and the remaining transport in grey (see legend for scaling). The segments of the transects shown in Fig. 2 are highlighted in green. The three westernmost transect names are abbreviated as: KR=Kolbeinsey Ridge, SL=Slétta, and LN=Langanes Northeast. The mean velocity in the strongest part of the IFSJ from the year-long offshore mooring record at section N is shown by the dark red vector. Stations 4 and 5 at section N are indicated by white dots. The coloured shading in a) and b) is the bathymetry from ETOPO1⁵³; the 750 and 1100 m isobaths are highlighted in grey.

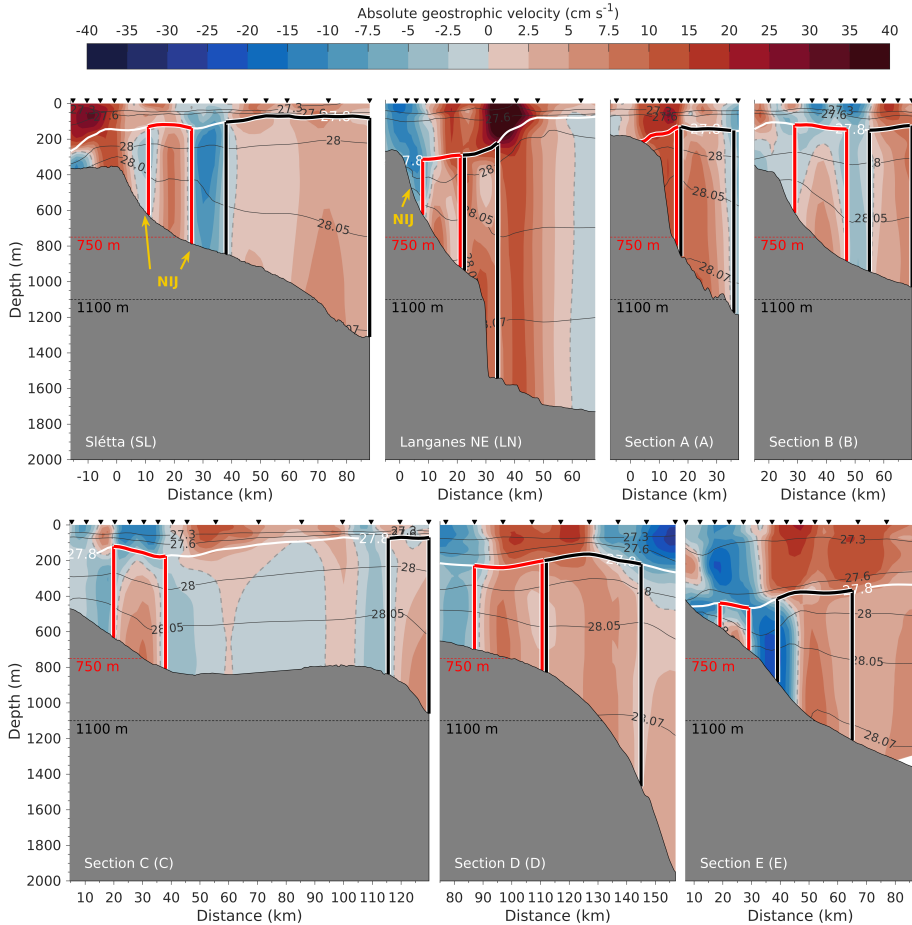


Figure 2: Vertical sections of velocity across the IFSJ. Absolutely referenced geostrophic velocity (colour) and density (thin grey lines) for the green segments of the shipboard transects in Fig. 1b. The thick white line is the 27.8 kg m^{-3} isopycnal. The black inverted triangles indicate the locations of the hydrographic profiles, which are 2.5–10 km apart, depending on the steepness of the slope. For each transect the origin (distance $y = 0$ km) was placed at the shelf break (for sections north of Iceland) or the point where the slope gradient starts to increase (for sections north of the Iceland-Faroe Slope). Positive velocities are directed toward the Faroe Islands. The red and black boxes outline the shallow and deep cores, respectively. The NIJ is indicated in yellow (cf. Fig. 1b). The abbreviated names in parentheses are used as labels in Fig. 1. The bathymetry is from the ship’s echosounder.

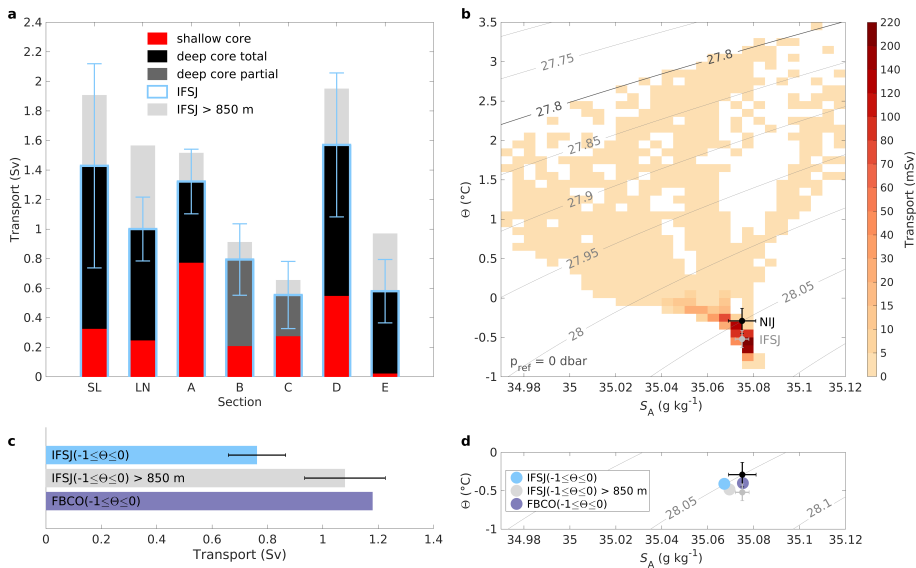


Figure 3: Transport of overflow water ($\sigma_{\theta} \geq 27.8 \text{ kg m}^{-3}$) in the IFSJ. a) Volume transport for each transect of the high-resolution shipboard survey. The estimates are broken down by core and relation to sill depth (see legend). Dark grey bars represent deep cores that were not completely bracketed by observations (Fig. 2). The error bars reflect the uncertainty of the transport from the combined instrument and processing errors scaled by the cross-sectional area of the current (see the methods section for details). b) Mean volume transport with respect to temperature and salinity properties of both cores from all transects (the red and black boxes in Fig. 2). The grey contours are density. The transport mode of the IFSJ (NIJ) is marked in grey (black); the error bars indicate one standard deviation. c) Volume transport and d) mean hydrographic properties of the IFSJ (including and excluding flow below the sill depth) and at the FBC overflow sill for temperatures between -1 and 0°C . The error bars in c) and d) are determined as in a) and b), respectively. In d) the transport modes of the IFSJ (determined from all hydrographic properties) and the NIJ from panel b) are shown in addition for reference.

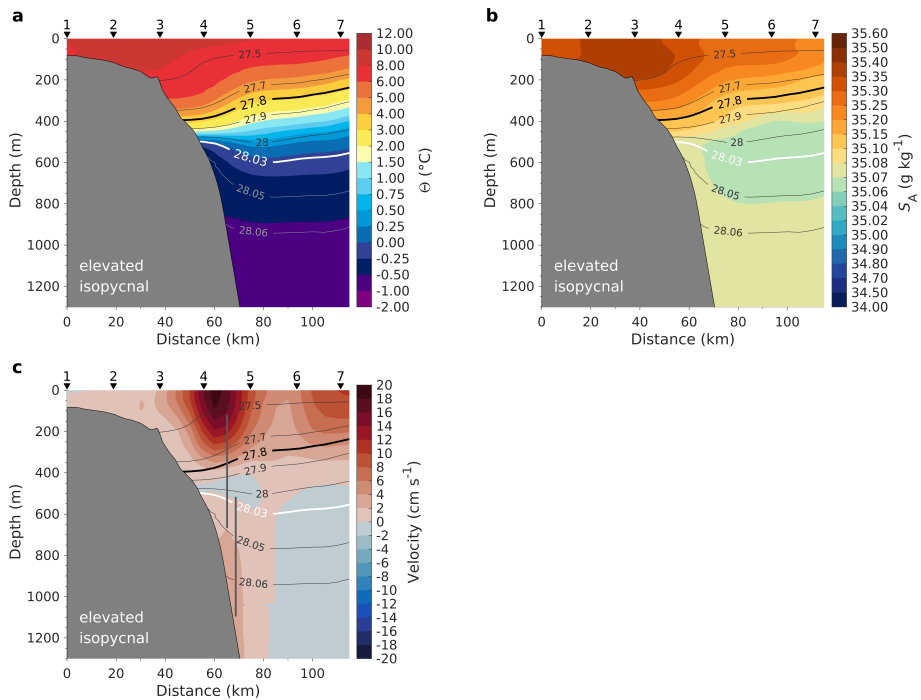


Figure 4: Composite of a subset of vertical sections north of the Faroe Islands. Mean temperature (a), salinity (b), and relative geostrophic velocity (c) for the elevated isopycnal state (see text for details). The 28.03 kg m^{-3} isopycnal used to identify this subset of sections is marked in white, and the 27.8 kg m^{-3} isopycnal, which defines the top of the overflow layer, is the thick black contour. Positive velocities relative to the level of no motion are directed eastward toward the Faroe-Shetland Channel. The station numbers are indicated along the top. The vertical grey lines in c) mark the locations and depth ranges of direct velocity measurements from moorings (Fig. 5a).

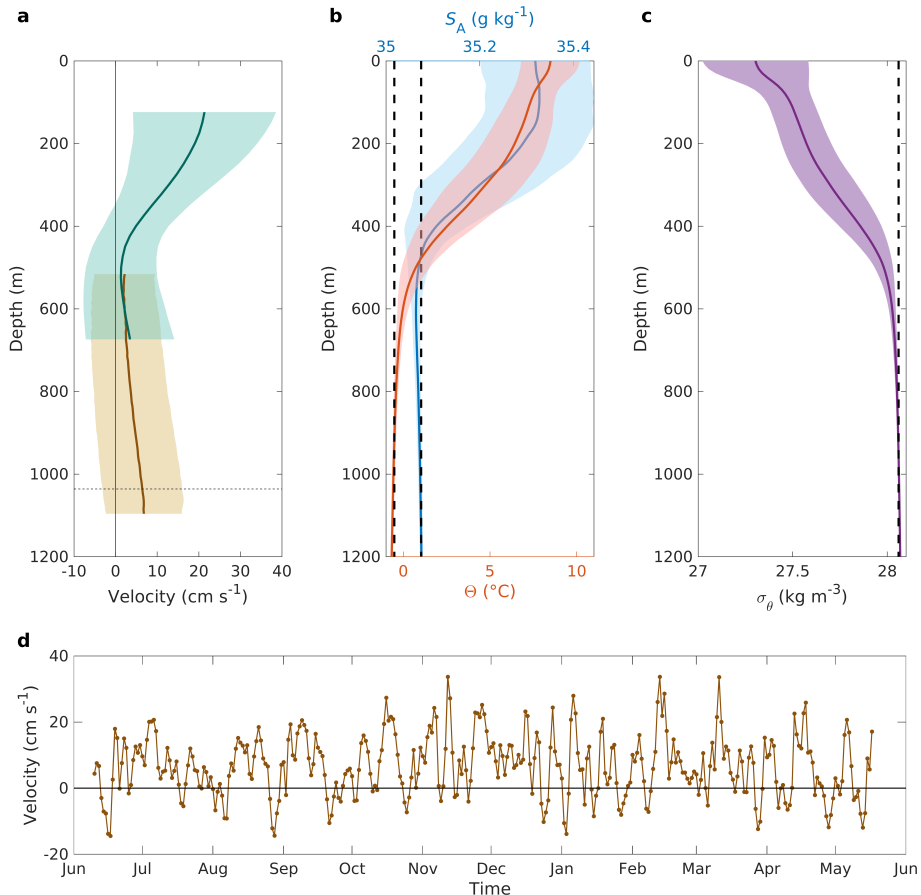


Figure 5: Year-long moored records and hydrographic profiles from section N. a) Mean along-stream velocity profiles from moorings deployed from June 2017 to May 2018 at section N at a bottom depth of 960 m (green) and 1210 m (brown; Fig. 4c). The along-stream direction is defined as 105° clockwise from true north (see methods section for details). The dashed line indicates the upper limit for the velocity depth average in d). b) and c) show mean profiles of temperature (red), salinity (blue), and density (purple) near the offshore mooring from 120 repeat occupations of section N. The properties of the IFSJ transport mode from the high-resolution transects (Fig. 3b) are marked by vertical lines. The shaded areas in a)–c) indicate one standard deviation (the standard error is very small for all profiles). d) Time series of the depth-averaged velocity in the deepest portion of the IFSJ, below the dashed line in a).

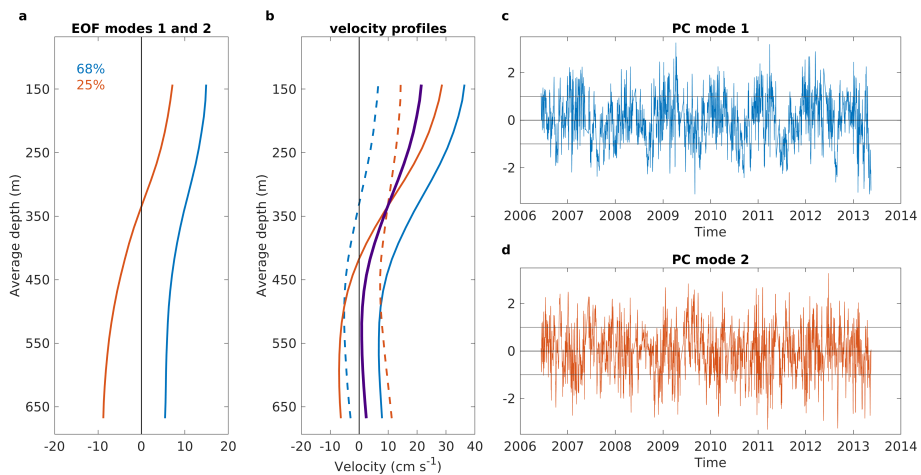


Figure 6: Dominant variability of the along-stream velocity from the in-shore moored record at section N (2006–2013; 2533 profiles). a) Empirical orthogonal function (EOF) modes 1 (blue) and 2 (red), explaining 68 and 25% of the variance, respectively. b) Mean along-stream velocity profile (thick solid purple line) and velocity profiles (blue: mode 1, red: mode 2) for times when the principal components for mode 1 and 2 are positive (solid) and negative (dashed) one standard deviation. c) and d) Principal component time series for mode 1 (PC1) and mode 2 (PC2). The units are normalised by the standard deviation.

SUPPLEMENTARY INFORMATION

The Iceland-Faroe Slope Jet: A conduit for dense water toward the Faroe Bank Channel overflow

Stefanie Semper^{*1}, Robert S. Pickart², Kjetil Våge¹, Karin Margretha Húsgarð Larsen³, Hjálmar Hátún³, and Bogi Hansen³

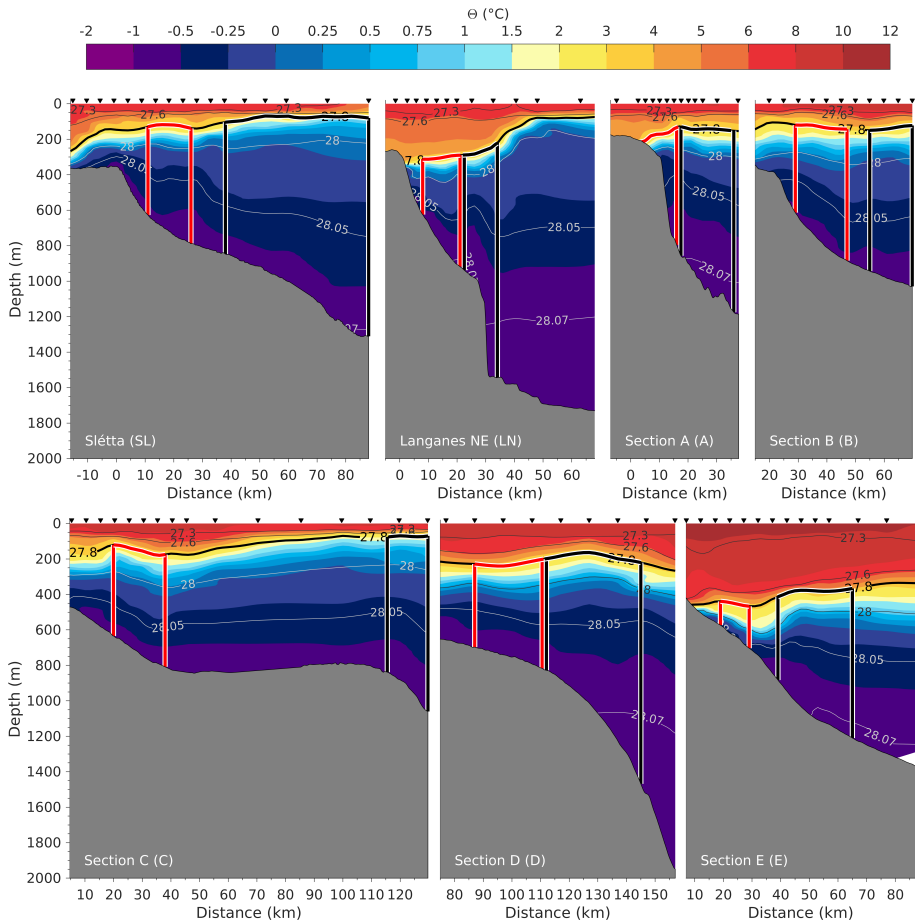
1 – Geophysical Institute, University of Bergen and Bjerknes Centre for Climate Research, Bergen, Norway.

2 – Woods Hole Oceanographic Institution, Woods Hole, Massachusetts, USA.

3 – Faroe Marine Research Institute, Tórshavn, Faroe Islands.

** Corresponding author address:* Geophysical Institute, University of Bergen and Bjerknes Centre for Climate Research, Allégaten 70, 5007 Bergen, Norway.

E-mail: stefanie.semper@uib.no



Supplementary Figure 1: Vertical sections of temperature across the IFSJ. Temperature (colour) and density (thin grey lines) for the green segments of the shipboard transects in Fig. 1b. The thick black line is the 27.8 kg m^{-3} isopycnal. The black inverted triangles indicate the locations of the stations. The red and black boxes outline the shallow and deep cores, respectively. The abbreviated names of the transects are used as labels in Fig. 1. The bathymetry is from the ship's echosounder.

Paper III

The evolution and transformation of the North Icelandic Irminger Current along the north Iceland shelf

S. Semper, K. Våge, R. S. Pickart, S. Jónsson, and H. Valdimarsson
(manuscript in preparation)

Chapter 6

Concluding discussion

The NIJ, IFSJ, and NIIC are integral components of the overturning in the Nordic Seas and the northern extremity of the AMOC. Based on a multitude of observational data sets, this thesis provides novel insight into the pathways and evolutions of these currents and thus enhances our understanding of the circulation along the Greenland-Scotland Ridge. In particular, three research questions were posed in Chapter 1:

- How does the NIJ evolve along the Iceland slope toward Denmark Strait? (Paper I)
- How does overflow water progress toward the Faroe Bank Channel? (Paper II)
- How is the NIIC modified along the north Iceland shelf? (Paper III)

These questions are addressed in the papers that constitute this thesis (Chapter 5). Since our observations are limited in time and space, definite answers are elusive, and each advancement raises new questions. In the following, I will present some of these future research questions, which have emerged from this thesis.

The importance of high-resolution observations

While the Icelandic waters have been monitored by hydrographic surveys since 1950, it took nearly 50 years for the narrow NIJ to be discovered with the advent of direct velocity measurements on the north Iceland slope (*Jónsson, 1999; Jónsson and Valdimarsson, 2004*). Densely sampled transects are crucial to resolve the hydrographic and kinematic structure of the current (Paper I). Similarly, the monitoring section N north of the Faroe Islands has been surveyed for more than three decades, and moorings recording current velocities have been in place for over 20 years, although primarily focused on the upper-layer flow (*Hansen et al., 2015*). The narrow, bottom-intensified cores of the IFSJ have previously gone unnoticed due to the coarse station spacing (Paper II). Despite the extensive costs related to high-resolution shipboard surveys, these intense observational programs are indispensable for an understanding of regional current systems that may influence the large-scale circulation – in the Nordic Seas (*Håvik et al., 2017, Papers I–II*) or elsewhere (*Pickart et al., 2005; Corlett and Pickart, 2017*). Autonomous measuring devices such as sea gliders and floats are an excellent complement and facilitate data acquisition in regions that are otherwise scarcely accessible, as during the harsh weather conditions in the western Nordic Seas in winter or under the sea ice.

The transport mode and its ramifications

The comprehensive data set used in Paper I, which comprises 13 high-resolution hydrographic/velocity surveys across the northern slope of Iceland, enabled us to robustly elucidate the properties, structure, and transport of the NIJ (Paper I). In particular, we defined the transport mode of the NIJ as the small area in hydrographic space that accounts for the bulk of the current's transport. As these properties are not modified along the NIJ's pathway, they indicate the source of these densest waters in the NIJ: Observational evidence suggests that waters with properties corresponding to the transport mode of the NIJ are regularly formed during winter in the Greenland Sea (*Huang et al.*, accepted). This agrees with *Våge et al.* (2015, in prep.) who argued for a nowadays diminished role of the Iceland Sea for the formation of the densest water in the NIJ, diverging from earlier hypotheses (*Jónsson and Valdimarsson*, 2004; *Våge et al.*, 2011).

Noticeably, the transport modes of the NIJ and the IFSJ are not significantly different (Paper II). As such, also the IFSJ appears to originate in the Greenland Sea (*Huang et al.*, accepted, Paper II). This implies that the densest waters supplying the two major overflows across the Greenland-Scotland Ridge are likely formed in the Greenland Sea, highlighting the importance of deep convection in this area (*Huang et al.*, accepted, Paper II). Changes in the location and process of dense-water formation in the Greenland Sea may influence the properties and pathways of both the NIJ and the IFSJ and may thus alter the properties and composition of the overflows. Therefore, this relation between the Denmark Strait and Faroe Bank Channel overflows needs to be explored in future observational and modelling studies.

Pathways between the Greenland and Iceland Seas

The exact pathways and transports of the dense water from the Greenland Sea to the north Iceland slope are not yet determined. *Huang et al.* (accepted) argued that the water broadly follows the Mohn, Kolbeinsey, and Jan Mayen Ridges southward (Fig. 2.2), and high-resolution hydrographic/velocity measurements from two ship-board surveys along these submarine ridges suggest that the dense water enters the Iceland Sea through several of the gaps in the ridges (A. Brakstad, personal communication, 2020). A tracer release experiment indicated that rapid export of dense water from the Greenland to the Iceland Sea is possible (*Messias et al.*, 2008). As such, identifying the exact pathways is important for determining the timescale for newly ventilated water to progress from the formation region to the overflows. The interior Iceland Sea may be considered a transit region for the densest overflow water only, as we recently have shown that it is not the main source region of either the NIJ or the IFSJ, at least in the present climate (*Våge et al.*, in prep.).

Ocean dynamics northeast of Iceland

Near the Iceland slope it remains unclear how the dense water becomes entrained into the NIJ and the IFSJ and what the dynamics of the currents' formation are. The slope northeast of Iceland is very complex due to the proximity and potential interplay of the NIIC, NIJ, and IFSJ (Papers I–III). The dense water from the Greenland Sea appears to feed both the westward-flowing NIJ and the eastward-flowing IFSJ supplying the major

overflows (Papers I–II). An understanding of the mechanisms underlying this partition requires investigations of the basin-shelf exchange of dense water and the role of topography, including the influence of the different sill depths of the overflows and upstream effects of hydraulic control. These processes may also explain why dense water banks up along the entire northern Greenland-Scotland Ridge (*Jónsson and Valdimarsson, 2004; Våge et al., 2011, Papers I–II*) and why both the NIJ and IFSJ are composed, at least at times, of two cores (*Pickart et al., 2017, Papers I–II*). High-resolution numerical models of the western Nordic Seas, along with idealised numerical models representative of the northern slope of the Greenland-Scotland Ridge that include the deep overflows, will constitute ideal tools for this analysis.

A fundamental difference between the NIJ and the IFSJ northeast of Iceland is that the NIJ emerges and increases in transport along its pathway (Paper I), while the IFSJ appears to be a fully developed current that does not vary much in transport between Iceland and the Faroe Islands (Paper II). As such, different processes are likely important for the formation of the currents. The earliest hypothesis regarding the formation of the NIJ included the NIIC as the upper limb of a local overturning circulation and water mass transformation in the Iceland Sea (*Våge et al., 2011*). This hypothesis has subsequently been questioned, in particular in terms of the supply of the densest portion of the NIJ (*Pickart et al., 2017; Ypma et al., 2019*). However, it is peculiar that the NIJ emerges exactly where the bathymetry of the Iceland slope steepens and eddies detach from the NIIC (Paper III). This indicates that the co-located disintegration of the NIIC and emergence of the NIJ northeast of Iceland may, after all, be dynamically linked. Further work is necessary to elucidate the instability processes and quantify the effect of this local diversion of heat and salt off the northeast Iceland shelf.

The East Icelandic Current

The East Icelandic Current likely also interacts with the NIIC northeast of Iceland, yet we know little about this flow. This surface-intensified current branches off the East Greenland Current and transports cold, fresh surface water and Atlantic-origin water into the Iceland Sea (*Jónsson, 2007; Macrander et al., 2014*). However, the amount of freshwater in the East Icelandic Current is very small (*Macrander et al., 2014*), so its effect on water mass transformation in the Iceland Sea is limited. The pathway of the current is unclear. Using historical hydrographic measurements, *Casanova-Masjoan et al. (2020)* suggested that the East Icelandic Current approaches the Iceland shelf break west of the Kolbeinsey Ridge and flows alongside the NIIC before the currents merge northeast of Iceland. *De Jong et al., (2018)*, however, argued based on trajectories from RAFOS floats that the East Icelandic Current passes through the Spar Fracture Zone in the Kolbeinsey Ridge, hypothesising that the flow extends to greater depths than previously assumed. This implies that the current could provide a potential barrier for the dense water progressing southward from the Greenland Sea (*de Jong et al., 2018*), but evidence to support this hypothesis is still missing. Nevertheless, the East Icelandic Current may play a role in the cooling and freshening of the NIIC (*Casanova-Masjoan et al., 2020, Paper III*). Its transport, extent, variability, and fate in the Norwegian Sea could be explored in future observational surveys employing shipboard measurements, sea gliders, or floats.

The upstream pathways of the Faroe Bank Channel overflow

The recent focus on the upstream pathways of the Faroe Bank Channel overflow has substantially advanced our knowledge about the supply of dense water to this gap in the Greenland-Scotland Ridge (*Chafik et al.*, 2020; *Huang et al.*, accepted, Paper II). With the observational evidence of the IFSJ along the slope between Iceland and the Faroe Islands (Paper II), a direct pathway of dense water toward the Faroe-Shetland Channel has been identified. While the observational analysis by *Huang et al.* (accepted) corroborated the existence of this dense-water pathway along the Iceland-Faroe Ridge, they found an additional pathway southward along the Jan Mayen Ridge (Fig. 2.2). This branch also has properties matching the densest water in the Faroe Bank Channel overflow (*Huang et al.*, accepted). Based on Lagrangian analysis from a numerical model, *Chafik et al.* (2020) suggested that some of the dense water passing north of the Faroe Islands approaches the Norwegian coast before supplying the Faroe-Shetland Channel from the east. It seems possible that this indirect pathway is the continuation of the deep flow along the Jan Mayen Ridge identified by *Huang et al.* (accepted).

However, it is important to note that these three studies only provide an initial account of the circulation pattern upstream of the Faroe Bank Channel. Extensive investigations using observations and models, comparable to the focus on the Denmark Strait overflow in recent years, are required to robustly quantify the transports and variability of these pathways and to understand their dynamics. In particular, a mooring array across the Iceland-Faroe Ridge will shed light on the structure and variability of the IFSJ, and high-resolution hydrographic/velocity surveys will be central for exploring the upstream pathways and source regions. Furthermore, it is unclear how the currents enter the Faroe-Shetland Channel. While *Chafik et al.* (2020) have demonstrated that the dense-water flow within the Faroe-Shetland Channel occurs along its eastern slope, floats entering the channel indicated high eddy activity and mixing (*Søiland et al.*, 2008). As such, future studies ought to address the entrainment of the upstream dense-water flows into the current in the Faroe-Shetland Channel, which ultimately feeds the Faroe Bank Channel overflow.

Impacts of climate change

The warming climate affects many atmospheric and oceanic processes in the Nordic Seas, and the responses of the complex coupled climate system to these changes are difficult to predict. In particular, it is crucial to better understand the air-ice-sea interaction: The wintertime sea-ice retreat in the western Nordic Seas affects the surface heat fluxes, which in turn are integral for the formation of dense water (*Moore et al.*, 2015). While convection in the interior basins weakens, new areas along the boundary currents around the Nordic Seas and parts of the Arctic Ocean that were previously insulated by sea ice are now in direct contact with the atmosphere and can be further ventilated and densified (*Moore et al.*, submitted; *Våge et al.*, 2018). This modification of the boundary currents needs to be quantified and investigated more thoroughly as it appears to be an important future process for the production of dense water affecting the composition of the overflow water.

While the properties of the overflows are changing, the volume transport of overflow water across the Greenland-Scotland Ridge has been remarkably stable over the past decades (*Hansen et al.*, 2016; *Jochumsen et al.*, 2017; *Østerhus et al.*, 2019). In

the subtropical North Atlantic, however, the AMOC has been in a reduced state since 2008 (*Smeed et al.*, 2018), which reflects the expectation of a weakening AMOC in a warming climate (*IPCC*, 2013). At 45°N the overturning strength has recently intensified, but because of the short observational time span, a lead-lag relationship to the AMOC at 26°N cannot be conclusively established, and the recovery of the subtropical AMOC is still pending (*Moat et al.*, 2020). So far, the apparent discrepancy between a stable overturning at high latitudes and a weakened circulation in the subtropical North Atlantic has not been explained.

Concluding remarks

To better understand the present overturning in the Nordic Seas and beyond and to predict its future state, a continued monitoring of the exchange flows across the Greenland-Scotland Ridge is imperative. Furthermore, observations of the upstream pathways and sources of the overflows are required, especially with respect to interannual variability and long-term trends of transports and hydrographic properties. This implies a need for internationally coordinated, interdisciplinary field campaigns obtaining joint atmospheric, physical, and biogeochemical ocean measurements following the example of the Iceland Greenland Seas Project (*Renfrew et al.*, 2019). However, a thorough understanding can only be reached by combining these observations with substantial modelling efforts encompassing the range from highly idealised to high-resolution regional and global climate models.

The three papers that constitute this thesis have, from an observational point of view, advanced our understanding of the circulation along the northern slope of the Greenland-Scotland Ridge. In particular, the main conclusions are:

- The NIJ emerges northeast of Iceland and its volume transport increases gradually toward Denmark Strait; the supply to the Denmark Strait overflow is more substantial than previously envisaged (Paper I).
- The IFSJ is a hitherto unrecognised pathway of overflow water toward the Faroe Bank Channel and accounts for approximately half of the total overflow transport through the passage (Paper II).
- The similarity of the transport modes of the NIJ and IFSJ suggests a common source, which is likely in the Greenland Sea. As such, dense water originating in the Greenland Sea supplies the two major overflows across the Greenland-Scotland Ridge (Papers I–II).
- The NIIC cools and freshens considerably along its pathway, yet the formation of overflow water on the north Iceland shelf is limited and may only sporadically supply the lighter portion of the NIJ. The NIIC's volume transport decreases significantly northeast of Iceland, where the eddy activity is enhanced, indicating a dynamical link to the emergence of the NIJ (Paper III).

Collectively, this thesis highlights the significance of the NIJ, IFSJ, and NIIC for the overturning in the Nordic Seas and their impact on the exchange between the Nordic Seas and the North Atlantic.

Bibliography

- Amante, C., and B. Eakins (2009), ETOPO1 1 arc-minute global relief model: Procedures, data sources, and analysis, *NOAA Technical Memorandum NESDIS NGDC-24*, doi:10.1594/PANGAEA.769615.
- Árthun, M., T. Eldevik, L. H. Smedsrud, Ø. Skagseth, and R. B. Ingvaldsen (2012), Quantifying the influence of Atlantic heat on Barents sea ice variability and retreat, *Journal of Climate*, 25(13), 4736–4743, doi:10.1175/JCLI-D-11-00466.1.
- Árthun, M., E. W. Kolstad, T. Eldevik, and N. S. Keenlyside (2018), Time scales and sources of European temperature variability, *Geophysical Research Letters*, 45(8), 3597–3604, doi:10.1002/2018GL077401.
- Berx, B., B. Hansen, S. Østerhus, K. M. H. Larsen, T. Sherwin, and K. Jochumsen (2013), Combining in situ measurements and altimetry to estimate volume, heat and salt transport variability through the Faroe-Shetland Channel, *Ocean Science*, 9(4), 639–654, doi:10.5194/os-9-639-2013.
- Blindheim, J., and S. Østerhus (2005), The Nordic Seas, main oceanographic features, in *The Nordic Seas: An Integrated Perspective*, vol. 158, edited by H. Drange, T. Dokken, T. Furevik, R. Gerdes, and W. Berger, pp. 11–38, AGU Geophysical Monograph.
- Bourke, R. H., R. G. Paquette, and R. F. Blythe (1992), The Jan Mayen Current of the Greenland Sea, *Journal of Geophysical Research*, 97(C5), 7241–7250, doi:10.1029/92jc00150.
- Brakstad, A., K. Våge, L. Håvik, and G. W. K. Moore (2019), Water mass transformation in the Greenland Sea during the period 1986–2016, *Journal of Physical Oceanography*, 49(1), 121–140, doi:10.1175/JPO-D-17-0273.1.
- Casanova-Masjoan, M., M. D. Pérez-Hernández, R. S. Pickart, H. Valdimarsson, S. R. Ólafsdóttir, A. Macrander, D. Grisolia-Santos, D. J. Torres, S. Jónsson, K. Våge, P. Lin, and A. Hernández-Guerra (2020), Alongstream, seasonal and interannual variability of the North Icelandic Irminger Current and East Icelandic Current around Iceland, *Journal of Geophysical Research: Oceans*, 125, e2020JC016283, doi:10.1029/2020JC016283.
- Chafik, L., and T. Rossby (2019), Volume, heat, and freshwater divergences in the subpolar North Atlantic suggest the Nordic Seas as key to the state of the meridional overturning circulation, *Geophysical Research Letters*, 46(9), 4799–4808, doi:10.1029/2019GL082110.

- Chafik, L., H. Hátún, J. Kjellson, K. M. H. Larsen, T. Rossby, and B. Berx (2020), Discovery of an unrecognized pathway carrying overflow waters toward the Faroe Bank Channel, *Nature Communications*, *11*(3721), doi:<https://doi.org/10.1038/s41467-020-17426-8>.
- Cooper, L. H. N. (1955), Deep water movements in the North Atlantic as a link between climatic changes around Iceland and biological productivity of the English Channel and Celtic Sea, *Journal of Marine Research*, *14*, 347–362.
- Corlett, W. B., and R. S. Pickart (2017), The Chukchi slope current, *Progress in Oceanography*, *153*, 50–65, doi:[10.1016/j.pocan.2017.04.005](https://doi.org/10.1016/j.pocan.2017.04.005).
- de Jong, M. F., H. Sjøiland, A. S. Bower, and H. H. Furey (2018), The subsurface circulation of the Iceland Sea observed with RAFOS floats, *Deep-Sea Research Part I: Oceanographic Research Papers*, *141*, 1–10, doi:[10.1016/j.dsr.2018.07.008](https://doi.org/10.1016/j.dsr.2018.07.008).
- de Steur, L., R. S. Pickart, D. J. Torres, and H. Valdimarsson (2015), Recent changes in the freshwater composition east of Greenland, *Geophysical Research Letters*, *42*(7), 2326–2332, doi:[10.1002/2014GL062759](https://doi.org/10.1002/2014GL062759).
- Dee, D. P., S. M. Uppala, A. J. Simmons, P. Berrisford, P. Poli, S. Kobayashi, U. Andrae, M. A. Balmaseda, G. Balsamo, P. Bauer, P. Bechtold, A. C. M. Beljaars, L. van der Berg, J. Bidlot, N. Bormann, C. Delsol, R. Dragani, M. Fuentes, A. J. Geer, L. Haimberger, S. B. Healy, H. Hersbach, E. V. Hólm, L. Isaksen, P. Kållberg, M. Köhler, M. Matricardi, A. P. McNally, B. M. Monge-Sanz, J.-J. Morcrette, B.-K. Park, C. Peubey, P. de Rosnay, C. Tavolato, J.-N. Thépaut, and F. Vitart (2011), The ERA-Interim reanalysis: configuration and performance of the data assimilation system, *Quarterly Journal of the Royal Meteorological Society*, *137*, 553–597, doi:[10.1002/qj.828](https://doi.org/10.1002/qj.828).
- Dickson, R. R., and J. Brown (1994), The production of North Atlantic Deep Water: sources, rates, and pathways, *Journal of Geophysical Research*, *99*(C6), 12319–12341, doi:[10.1029/94jc00530](https://doi.org/10.1029/94jc00530).
- Drange, H., T. Dokken, T. Furevik, R. Gerdes, W. Berger, A. Nesje, K. A. Orvik, Ø. Skagseth, I. Skjelvan, and S. Østerhus (2005), The Nordic Seas: An Overview, in *The Nordic Seas: An Integrated Perspective*, edited by H. Drange, T. Dokken, T. Furevik, R. Gerdes, and W. Berger, pp. 1–10, AGU Geophysical Monograph, doi:[10.1029/158GM02](https://doi.org/10.1029/158GM02).
- Eldevik, T., J. E. Ø. Nilsen, D. Iovino, K. A. Olsson, A. B. Sandø, and H. Drange (2009), Observed sources and variability of Nordic seas overflow, *Nature Geoscience*, *2*(6), 406–410, doi:[10.1038/ngeo518](https://doi.org/10.1038/ngeo518).
- Fogelqvist, E., J. Blindheim, T. Tanhua, S. Østerhus, E. Buch, and F. Rey (2003), Greenland-Scotland overflow studied by hydro-chemical multivariate analysis, *Deep-Sea Research Part I: Oceanographic Research Papers*, *50*, 73–102, doi:[10.1016/S0967-0637\(02\)00131-0](https://doi.org/10.1016/S0967-0637(02)00131-0).

- Gebbie, G., and P. Huybers (2010), Total matrix intercomparison: A method for determining the geometry of water-mass pathways, *Journal of Physical Oceanography*, 40(8), 1710–1728, doi:10.1175/2010JPO4272.1.
- Haine, T. W., B. Curry, R. Gerdes, E. Hansen, M. Karcher, C. Lee, B. Rudels, G. Spreen, L. de Steur, K. D. Stewart, and R. Woodgate (2015), Arctic freshwater export: Status, mechanisms, and prospects, *Global and Planetary Change*, 125, 13–35, doi:10.1016/j.gloplacha.2014.11.013.
- Hansen, B., and S. Østerhus (2000), North Atlantic-Nordic Seas exchanges, *Progress in Oceanography*, 45(2), 109–208, doi:10.1016/S0079-6611(99)00052-X.
- Hansen, B., K. M. H. Larsen, H. Hátún, R. Kristiansen, E. Mortensen, and S. Østerhus (2015), Transport of volume, heat, and salt towards the Arctic in the Faroe Current 1993–2013, *Ocean Science*, 11(5), 743–757, doi:10.5194/os-11-743-2015.
- Hansen, B., K. M. H. Larsen, H. Hátún, and S. Østerhus (2016), A stable Faroe Bank Channel overflow 1995–2015, *Ocean Science*, 12(6), 1205–1220, doi:10.5194/os-12-1205-2016.
- Harden, B., I. Renfrew, and G. N. Petersen (2011), A climatology of wintertime barrier winds off southeast Greenland, *Journal of Climate*, 24(17), 4701–4717, doi:10.1175/2011JCLI4113.1.
- Harden, B., R. S. Pickart, H. Valdimarsson, K. Våge, L. de Steur, C. Richards, F. Bahr, D. J. Torres, E. Børve, S. Jónsson, A. Macrander, S. Østerhus, L. Håvik, and T. Hattermann (2016), Upstream sources of the Denmark Strait Overflow: Observations from a high-resolution mooring array, *Deep-Sea Research Part I: Oceanographic Research Papers*, 112, 94–112, doi:10.1016/j.dsr.2016.02.007.
- Håvik, L. (2018), The East Greenland Current system north of Denmark Strait, Ph.D. thesis, University of Bergen.
- Håvik, L., R. S. Pickart, K. Våge, D. Torres, A. M. Thurnherr, A. Beszczynska-Möller, W. Walczowski, and W.-J. von Appen (2017), Evolution of the East Greenland Current from Fram Strait to Denmark Strait: Synoptic measurements from summer 2012, *Journal of Geophysical Research: Oceans*, 122(3), 1974–1994, doi:10.1002/2016JC012228.
- Helland-Hansen, B., and F. Nansen (1909), The Norwegian Sea: its physical oceanography based upon the Norwegian researches, 1900–1904, *Report on Norwegian Fishery and Marine Investigations*, 2(2), doi:10.2307/1776951.
- Hopkins, J. E., N. P. Holliday, D. Rayner, L. Houpert, I. Le Bras, F. Straneo, C. Wilson, and S. Bacon (2019), Transport variability of the Irminger Sea Deep Western Boundary Current from a mooring array, *Journal of Geophysical Research: Oceans*, 124, 3246–3278, doi:10.1029/2018JC014730.
- Hopkins, T. S., G. Baldasserini, P. Minnett, P. Povero, and P. Zanasca (1992), Icelandic Current Experiment. GIN SEA Cruise 88 - Data Report. Hydrography and Circulation, *Tech. Rep. SM-260*, Saclant Undersea Research Centre.

- Huang, J., R. S. Pickart, R. X. Huang, P. Lin, A. Brakstad, and F. Xu (accepted), Sources and upstream pathways of the densest overflow water in the Nordic Seas, *Nature Communications*.
- Huang, R. X. (2004), Ocean, Energy Flows in, *Encyclopedia of Energy*, 4, 497–509, doi:10.1016/b0-12-176480-x/00053-x.
- IOC, SCOR, and IAPSO (2010), The international thermodynamic equation of seawater - 2010: Calculation and use of thermodynamic properties, *Intergovernmental Oceanographic Commission, Manuals and Guides No. 56, UNESCO*.
- IPCC (2013), Climate Change 2013: The Physical Science Basis. Contribution of Working Group I to the Fifth Assessment Report of the Intergovernmental Panel on Climate Change, doi:10.1017/CBO9781107415324.Summary.
- Isachsen, P. E., C. Mauritzen, and H. Svendsen (2007), Dense water formation in the Nordic Seas diagnosed from sea surface buoyancy fluxes, *Deep-Sea Research Part I: Oceanographic Research Papers*, 54(1), 22–41, doi:10.1016/j.dsr.2006.09.008.
- Jeansson, E., A. Olsen, and S. Jutterström (2017), Arctic Intermediate Water in the Nordic Seas, 1991–2009, *Deep Sea Research Part I: Oceanographic Research Papers*, 128, 82–97, doi:10.1016/j.dsr.2017.08.013.
- Jochumsen, K., M. Moritz, N. Nunes, D. Quadfasel, K. M. H. Larsen, B. Hansen, H. Valdimarsson, and S. Jónsson (2017), Revised transport estimates of the Denmark Strait overflow, *Journal of Geophysical Research: Oceans*, 122(4), 3434–3450, doi:10.1002/2017JC012803.
- Johnson, H. L., P. Cessi, D. P. Marshall, F. Schloesser, and M. A. Spall (2019), Recent contributions of theory to our understanding of the Atlantic Meridional Overturning Circulation, *Journal of Geophysical Research: Oceans*, 124(8), 5376–5399, doi:10.1029/2019JC015330.
- Jónsson, S. (1999), The circulation in the northern part of the Denmark Strait and its variability, *ICES report CM-1999/L:06*.
- Jónsson, S. (2007), Volume flux and fresh water transport associated with the East Icelandic Current, *Progress in Oceanography*, 73(3-4), 231–241, doi:10.1016/j.pocean.2006.11.003.
- Jónsson, S., and H. Valdimarsson (2004), A new path for the Denmark Strait overflow water from the Iceland Sea to Denmark Strait, *Geophysical Research Letters*, 31(3), L03305, doi:10.1029/2003GL019214.
- Jónsson, S., and H. Valdimarsson (2005), The flow of Atlantic Water to the north Icelandic shelf and its relation to the drift of cod larvae, *ICES Journal of Marine Science*, 62(7), 1350–1359, doi:10.1016/j.icesjms.2005.05.003.
- Jónsson, S., and H. Valdimarsson (2012), Water mass transport variability to the north Icelandic shelf, 1994–2010, *ICES Journal of Marine Science*, 69(5), 809–815, doi:10.1093/icesjms/fst034.

- Köhl, A. (2007), Generation and stability of a quasi-permanent vortex in the Lofoten Basin, *Journal of Physical Oceanography*, 37(11), 2637–2651, doi:10.1175/2007jpo3694.1.
- Köhl, A. (2010), Variable source regions of Denmark Strait and Faroe Bank Channel overflow waters, *Tellus, Series A: Dynamic Meteorology and Oceanography*, 62(4), 551–568, doi:10.1111/j.1600-0870.2010.00454.x.
- Kuhlbrodt, T., A. Griesel, M. Montoya, A. Levermann, M. Hofmann, and S. Rahmstorf (2007), On the driving processes of the Atlantic Meridional Overturning Circulation, *Reviews of Geophysics*, 45, doi:10.1029/2004RG000166.1.INTRODUCTION.
- Langehaug, H. R., and E. Falck (2012), Changes in the properties and distribution of the intermediate and deep waters in the Fram Strait, *Progress in Oceanography*, 96(1), 57–76, doi:10.1016/j.pocean.2011.10.002.
- Latarius, K., and D. Quadfasel (2010), Seasonal to inter-annual variability of temperature and salinity in the Greenland Sea Gyre: Heat and freshwater budgets, *Tellus, Series A: Dynamic Meteorology and Oceanography*, 62(4), 497–515, doi:10.1111/j.1600-0870.2010.00453.x.
- Lehodey, P., J. Alheit, M. Barange, T. Baumgartner, G. Beaugrand, K. Drinkwater, J. M. Fromentin, S. R. Hare, G. Ottersen, R. I. Perry, C. Roy, C. D. van der Lingen, and F. Werner (2006), Climate variability, fish, and fisheries, *Journal of Climate*, 19(20), 5009–5030, doi:10.1175/JCLI3898.1.
- Lin, P., R. S. Pickart, K. Jochumsen, G. W. K. Moore, H. Valdimarsson, T. Fristedt, and L. J. Pratt (accepted), Kinematic structure and dynamics of the Denmark Strait Overflow from ship-based observations, *Journal of Physical Oceanography*, doi:10.1175/JPO-D-20-0095.1.
- Lind, S., R. B. Ingvaldsen, and T. Furevik (2018), Arctic warming hotspot in the northern Barents Sea linked to declining sea-ice import, *Nature Climate Change*, 8(7), 634–639, doi:10.1038/s41558-018-0205-y.
- Lique, C., and M. D. Thomas (2018), Latitudinal shift of the Atlantic Meridional Overturning Circulation source regions under a warming climate, *Nature Climate Change*, 8(11), 1013–1020, doi:10.1038/s41558-018-0316-5.
- Lozier, M. S., F. Li, S. Bacon, F. Bahr, A. S. Bower, S. Cunningham, M. F. de Jong, L. de Steur, B. DeYoung, J. Fischer, S. F. Gary, B. J. W. Greenan, N. P. Holliday, A. Houk, L. Houpert, M. E. Inall, W. E. Johns, H. L. Johnson, C. Johnson, J. Karstensen, G. Koman, I. A. Le Bras, X. Lin, N. Mackay, D. P. Marshall, H. Mercier, M. Oltmanns, R. S. Pickart, A. L. Ramsey, D. Rayner, F. Straneo, V. Thierry, D. J. Torres, R. G. Williams, C. Wilson, J. Yang, I. Yashayaev, and J. Zhao (2019), A sea change in our view of overturning in the subpolar North Atlantic, *Science*, 363(6426), 516–521, doi:10.1126/science.aau6592.
- Macrander, A., H. Valdimarsson, and S. Jónsson (2014), Improved transport estimate of the East Icelandic Current 2002–2012, *Journal of Geophysical Research: Oceans*, 119(6), 3407–3424, doi:10.1002/2013JC009517.

- Malmberg, S.-A. (1983), Hydrographic investigations in the Iceland and Greenland Seas in late winter 1971 – "Deep Water Project", *Jökull*, 33, 133–140.
- Malmberg, S.-A., and S. Jónsson (1997), Timing of deep convection in the Greenland and Iceland Seas, *ICES Journal of Marine Science*, 54(3), 300–309, doi:10.1006/jmsc.1997.0221.
- Marshall, J., and F. Schott (1999), Open-ocean convection: Observations, theory, and models, *Reviews of Geophysics*, 37(1), 1–64, doi:10.1029/98RG02739.
- Mastropole, D., R. S. Pickart, H. Valdimarsson, K. Våge, K. Jochumsen, and J. B. Girton (2017), On the hydrography of Denmark Strait, *Journal of Geophysical Research: Oceans*, 122, 306–321, doi:10.1002/2016JC012007.
- Mauritzen, C. (1996a), Production of dense overflow waters feeding the North Atlantic across the Greenland-Scotland Ridge. Part 1: Evidence for a revised circulation scheme, *Deep-Sea Research Part I: Oceanographic Research Papers*, 43(6), 769–806, doi:10.1016/0967-0637(96)00037-4.
- Mauritzen, C. (1996b), Production of dense overflow waters feeding the North Atlantic across the Greenland Scotland Ridge. Part 2: An inverse model, *Deep Sea Research Part I: Oceanographic Research Papers*, 43(6), 807–835, doi:10.1016/0967-0637(96)00038-6.
- Mauritzen, C., J. Price, T. Sanford, and D. J. Torres (2005), Circulation and mixing in the Faroese Channels, *Deep-Sea Research Part I: Oceanographic Research Papers*, 52(6), 883–913, doi:10.1016/j.dsr.2004.11.018.
- McCarthy, G. D., P. J. Brown, C. N. Flagg, G. Goni, L. Houpert, C. W. Hughes, R. Hummels, M. Inall, K. Jochumsen, K. M. H. Larsen, P. Lherminier, C. S. Meinen, B. I. Moat, D. Rayner, M. Rhein, A. Roessler, C. Schmid, and D. A. Smeed (2020), Sustainable Observations of the AMOC: Methodology and Technology, *Reviews of Geophysics*, 58(1), 1–34, doi:10.1029/2019RG000654.
- McKenna, C., B. Berx, and W. E. Austin (2016), The decomposition of the Faroe-Shetland Channel water masses using Parametric Optimum Multi-Parameter analysis, *Deep-Sea Research Part I: Oceanographic Research Papers*, 107, 9–21, doi:10.1016/j.dsr.2015.10.013.
- Meincke, J. (1983), The modern current regime across the Greenland-Scotland Ridge, in *Structure and Development of the Greenland-Scotland Ridge*, edited by M. H. P. Bott, S. Saxov, M. Talwani, and J. Thiede, 8 ed., pp. 637–650, NATO Conference Series (IV Marine Science), Springer, Boston, MA.
- Meincke, J., S. Jónsson, and J. H. Swift (1992), Variability of convective conditions in the Greenland Sea, *ICES Mar. Sci. Symp.*, 195, 32–39.
- Messias, M. J., A. J. Watson, T. Johannessen, K. I. C. Oliver, K. A. Olsson, E. Fogelqvist, J. Olafsson, S. Bacon, J. Balle, N. Bergman, G. Budéus, M. Danielsen, J.-C. Gascard, E. Jeansson, S. R. Olafsdottir, K. Simonsen, T. Tanhua, K. Van Scoy, and J. R. Ledwell (2008), The Greenland Sea tracer experiment 1996–2002: Horizontal

- mixing and transport of Greenland Sea Intermediate Water, *Progress in Oceanography*, 78(1), 85–105, doi:10.1016/j.pocean.2007.06.005.
- Moat, B. I., D. A. Smeed, E. Frajka-Williams, D. G. Desbruyères, C. Beaulieu, W. E. Johns, D. Rayner, A. Sanchez-Franks, M. O. Baringer, D. Volkov, L. C. Jackson, and H. L. Bryden (2020), Pending recovery in the strength of the meridional overturning circulation at 26 °N, *Ocean Science*, 16(4), 863–874, doi:10.5194/os-16-863-2020.
- Moore, G. W. K., K. Våge, R. S. Pickart, and I. A. Renfrew (2015), Decreasing intensity of open-ocean convection in the Greenland and Iceland Seas, *Nature Climate Change*, 5(9), 877–882, doi:10.1038/nclimate2688.
- Moore, G. W. K., K. Våge, I. Renfrew, and R. S. Pickart (submitted), Evolving air-sea interaction over the Nordic and Barents Seas and its impact on water mass transformation, *Nature Climate Change*.
- Nikolopoulos, A., K. Borenäs, R. Hietala, and P. Lundberg (2003), Hydraulic estimates of Denmark Strait overflow, *Journal of Geophysical Research: Oceans*, 108(3), doi:10.1029/2001jc001283.
- Nøst, O. A., and P. E. Isachsen (2003), The large-scale time-mean ocean circulation in the Nordic Seas and Arctic Ocean estimated from simplified dynamics, *Journal of Marine Research*, 61(2), 175–210, doi:10.1357/002224003322005069.
- Nurser, A. J. G., and S. Bacon (2014), The Rossby radius in the Arctic Ocean, *Ocean Science*, 10(6), 967–975, doi:10.5194/os-10-967-2014.
- Østerhus, S., and T. Gammelsrød (1999), The abyss of the Nordic Seas is warming, *Journal of Climate*, 12(11), 3297–3304, doi:10.1175/1520-0442(1999)012<3297:TAOTNS>2.0.CO;2.
- Østerhus, S., R. Woodgate, H. Valdimarsson, B. Turrell, L. de Steur, D. Quadfasel, S. M. Olsen, M. Moritz, C. M. Lee, K. M. H. Larsen, S. Jónsson, C. Johnson, K. Jochumsen, B. Hansen, B. Curry, S. Cunningham, and B. Berx (2019), Arctic Mediterranean exchanges: a consistent volume budget and trends in transports from two decades of observations, *Ocean Science*, 15(2), 379–399, doi:10.5194/os-15-379-2019.
- Pacini, A., R. S. Pickart, F. Bahr, D. J. Torres, A. L. Ramsey, J. Holte, M. Oltmanns, F. Straneo, I. A. Le Bras, G. W. K. Moore, and M. F. de Jong (2020), Mean conditions and seasonality of the West Greenland Boundary Current System near Cape Farewell, *Journal of Physical Oceanography*, 50(10), 2849–2871, doi:10.1175/JPO-D-20-0086.1.
- Papritz, L., and T. Spengler (2017), A Lagrangian climatology of wintertime cold air outbreaks in the Irminger and Nordic Seas and their role in shaping air-sea heat fluxes, *Journal of Climate*, 30(8), 2717–2737, doi:10.1175/JCLI-D-16-0605.1.
- Perkins, H., T. S. Hopkins, S.-A. Malmberg, P. M. Poulain, and A. Warn-Varnas (1998), Oceanographic conditions east of Iceland, *Journal of Geophysical Research: Oceans*, 103(C10), 21531–21542, doi:10.1029/98JC00890.

- Pickart, R. S., D. J. Torres, and P. S. Fratantoni (2005), The East Greenland Spill Jet, *Bulletin of the American Meteorological Society*, 35(6), 1037–1053, doi:10.1175/JPO2734.1.
- Pickart, R. S., M. A. Spall, D. J. Torres, K. Våge, H. Valdimarsson, C. Nobre, G. W. K. Moore, S. Jónsson, and D. Mastropole (2017), The North Icelandic Jet and its relationship to the North Icelandic Irminger Current, *Journal of Marine Research*, 75(5), 605–639, doi:10.1357/002224017822109505.
- Polyakov, I. V., A. V. Pnyushkov, M. B. Alkire, I. M. Ashik, T. M. Baumann, E. C. Carmack, I. Goszczko, J. Guthrie, V. V. Ivanov, T. Kanzow, R. Krishfield, R. Kwok, A. Sundfjord, J. Morison, R. Rember, and A. Yulin (2017), Greater role for Atlantic inflows on sea-ice loss in the Eurasian Basin of the Arctic Ocean, *Science*, 356(6335), 285–291, doi:10.1126/science.aai8204.
- Rahmstorf, S. (2006), Thermohaline Circulation, *Encyclopedia of Quaternary Science: Second Edition*, 5, doi:10.1016/B978-0-444-53643-3.00020-0.
- Renfrew, I. A., and G. W. K. Moore (1999), An extreme cold-air outbreak over the Labrador Sea: Roll vortices and air-sea interaction, *Monthly Weather Review*, 127(10), 2379–2394, doi:10.1175/1520-0493(1999)127<2379:AECAOO>2.0.CO;2.
- Renfrew, I. A., R. S. Pickart, K. Våge, G. W. K. Moore, T. J. Bracegirdle, A. D. Elvidge, E. Jeansson, T. Lachlan-Cope, L. T. McRaven, L. Papritz, J. Reuder, H. Sodemann, A. Terpstra, S. Waterman, H. Valdimarsson, A. Weiss, M. Almansi, F. Bahr, A. Brakstad, C. Barrell, J. K. Brooke, B. J. Brooks, I. M. Brooks, M. E. Brooks, E. M. Bruvik, C. Duschka, I. Fer, H. M. Golid, M. Hallerstig, I. Hessevik, J. Huang, L. Houghton, S. Jónsson, M. Jonassen, K. Jackson, K. Kvalsund, E. W. Kolstad, K. Konstali, J. Kristiansen, R. Ladkin, P. Lin, A. Macrander, A. Mitchell, H. Olafsson, A. Pacini, C. Payne, B. Palmason, M. D. Pérez-Hernández, A. K. Pettersen, G. N. Petersen, M. N. Pisareva, J. O. Pope, A. Seidl, S. Semper, D. Sergeev, S. Skjelsvik, H. Sjøiland, D. Smith, M. A. Spall, T. Spengler, A. Touzeau, G. Tupper, Y. Weng, K. D. Williams, X. Yang, and S. Zhou (2019), The Iceland Greenland Seas Project, *Bulletin of the American Meteorological Society*, 100(9), 1795–1817, doi:10.1175/bams-d-18-0217.1.
- Rosby, T., M. D. Prater, and H. Sjøiland (2009), Pathways of inflow and dispersion of warm waters in the Nordic Seas, *Journal of Geophysical Research: Oceans*, 114(4), 1–17, doi:10.1029/2008JC005073.
- Rosby, T., C. Flagg, L. Chafik, B. Harden, and H. Sjøiland (2018), A direct estimate of volume, heat, and freshwater exchange across the Greenland-Iceland-Faroe-Scotland Ridge, *Journal of Geophysical Research: Oceans*, 123(10), 7139–7153, doi:10.1029/2018JC014250.
- Rudels, B., E. Fahrbach, J. Meincke, G. Budéus, and P. Eriksson (2002), The East Greenland Current and its contribution to the Denmark Strait overflow, *ICES Journal of Marine Science*, 59(6), 1133–1154, doi:10.1006/jmsc.2002.1284.

- Rudels, B., G. Björk, J. Nilsson, P. Winsor, I. Lake, and C. Nohr (2005), The interaction between waters from the Arctic Ocean and the Nordic Seas north of Fram Strait and along the East Greenland Current: Results from the Arctic Ocean-02 Oden expedition, *Journal of Marine Systems*, 55(1-2), 1–30, doi:10.1016/j.jmarsys.2004.06.008.
- Saberi, A., T. W. N. Haine, R. Gelderloos, M. F. de Jong, H. Furey, and A. Bower (2020), Lagrangian perspective on the origins of Denmark Strait Overflow, *Journal of Physical Oceanography*, 50(8), 2393–2414, doi:10.1175/jpo-d-19-0210.1.
- Serra, N., R. H. Käse, A. Köhl, D. Stammer, and D. Quadfasel (2010), On the low-frequency phase relation between the Denmark Strait and the Faroe-Bank Channel overflows, *Tellus, Series A: Dynamic Meteorology and Oceanography*, 62(4), 530–550, doi:10.1111/j.1600-0870.2010.00445.x.
- Skjelvan, I., A. Olsen, L. G. Anderson, R. G. Bellerby, E. Falck, Y. Kasajima, C. Kivimäe, A. M. Omar, F. Rey, K. A. Olsson, T. Johannessen, and C. Heinze (2005), A review of the inorganic carbon cycle of the Nordic Seas and Barents Sea, in *The Nordic Seas: An Integrated Perspective*, edited by H. Drange, T. Dokken, T. Furevik, R. Gerdes, and W. Berger, pp. 157–175, AGU Geophysical Monograph.
- Smeed, D. A., S. A. Josey, C. Beaulieu, W. E. Johns, B. I. Moat, E. Frajka-Williams, D. Rayner, C. S. Meinen, M. O. Baringer, H. L. Bryden, and G. D. McCarthy (2018), The North Atlantic Ocean is in a state of reduced overturning, *Geophysical Research Letters*, 45(3), 1527–1533, doi:10.1002/2017GL076350.
- Søiland, H., M. D. Prater, and T. Rossby (2008), Rigid topographic control of currents in the Nordic Seas, *Geophysical Research Letters*, 35(L18607), doi:10.1029/2008GL034846.
- Somavilla, R. (2019), Draining and upwelling of Greenland Sea Deep Waters, *Journal of Geophysical Research: Oceans*, 124(4), 2842–2860, doi:10.1029/2018JC014249.
- Stefánsson, U., and J. Ólafsson (1991), Nutrients and fertility of Icelandic waters, *Rit Fiskideildar*, 7, 1–56.
- Strass, V. H., E. Fahrbach, U. Schauer, and L. Sellmann (1993), Formation of Denmark Strait overflow water by mixing in the East Greenland Current, *Journal of Geophysical Research*, 98(C4), 6907–6919, doi:10.1029/92JC02732.
- Swift, J. H., and K. Aagaard (1981), Seasonal transitions and water mass formation in the Iceland and Greenland Seas, *Deep Sea Research*, 28A(10), 1107–1129.
- Swift, J. H., K. Aagaard, and S.-A. Malmberg (1980), The contribution of the Denmark Strait overflow to the deep North Atlantic, *Deep Sea Research Part A, Oceanographic Research Papers*, 27(1), 29–42, doi:10.1016/0198-0149(80)90070-9.
- Tanhua, T., K. Bulsiewicz, and M. Rhein (2005), Spreading of overflow water from the Greenland to the Labrador Sea, *Geophysical Research Letters*, 32(10), doi:10.1029/2005GL022700.

- Tsubouchi, T., K. Våge, B. Hansen, K. M. H. Larsen, and S. Østerhus (accepted), Increased ocean heat transport into the Arctic Mediterranean over the period 1993–2016, *Nature Climate Change*.
- Turrell, W. R., G. Slessor, R. D. Adams, R. Payne, and P. A. Gillibrand (1999), Decadal variability in the composition of Faroe Shetland Channel bottom water, *Deep-Sea Research Part I: Oceanographic Research Papers*, 46, 1–25, doi:10.1016/S0967-0637(98)00067-3.
- Våge, K., R. S. Pickart, M. A. Spall, H. Valdimarsson, S. Jónsson, D. J. Torres, S. Østerhus, and T. Eldevik (2011), Significant role of the North Icelandic Jet in the formation of Denmark Strait overflow water, *Nature Geoscience*, 4(10), 723–727, doi:10.1038/ngeo1234.
- Våge, K., R. S. Pickart, M. A. Spall, G. W. K. Moore, H. Valdimarsson, D. J. Torres, S. Y. Erofeeva, and J. E. Ø. Nilsen (2013), Revised circulation scheme north of the Denmark Strait, *Deep-Sea Research Part I: Oceanographic Research Papers*, 79, 20–39, doi:10.1016/j.dsr.2013.05.007.
- Våge, K., G. W. K. Moore, S. Jónsson, and H. Valdimarsson (2015), Water mass transformation in the Iceland Sea, *Deep-Sea Research Part I: Oceanographic Research Papers*, 101, 98–109, doi:10.1016/j.dsr.2015.04.001.
- Våge, K., L. Papritz, L. Håvik, M. A. Spall, and G. W. K. Moore (2018), Ocean convection linked to the recent ice edge retreat along east Greenland, *Nature Communications*, 9(1), doi:10.1038/s41467-018-03468-6.
- Våge, K., S. Semper, H. Valdimarsson, S. Jónsson, G. W. K. Moore, and R. S. Pickart (in prep.), Four decades of dense water formation in the Iceland Sea.
- Ypma, S. L., N. Brüggemann, S. Georgiou, P. Spence, H. A. Dijkstra, J. D. Pietrzak, and C. A. Katsman (2019), Pathways and watermass transformation of Atlantic Water entering the Nordic Seas through Denmark Strait in two high resolution ocean models, *Deep-Sea Research Part I: Oceanographic Research Papers*, 145, 59–72, doi:10.1016/j.dsr.2019.02.002.



Graphic design: Communication Division, UIB / Print: Skjipes Kommunikasjon AS



uib.no

ISBN: 9788230862018 (print)
9788230843277 (PDF)